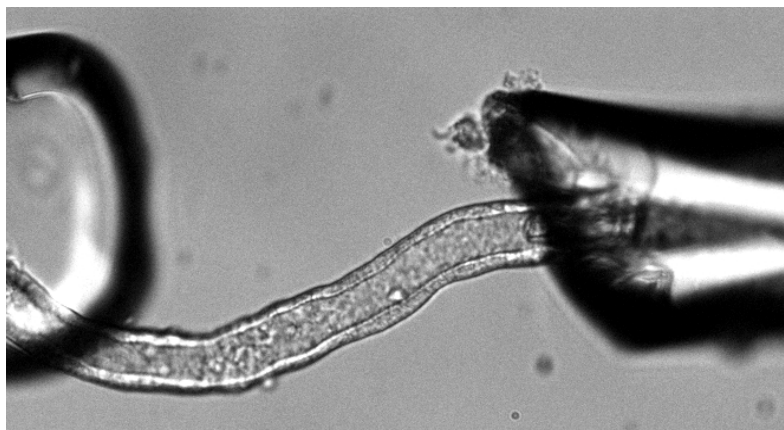


Regulation of the tight junction permeabilities in the TAL



Dissertation
zur Erlangung des Doktorgrades
der Mathematisch-Naturwissenschaftlichen Fakultät
der Christian-Albrechts-Universität zu Kiel
vorgelegt von
Allein Plain Reyes
Kiel, 2015

“Choose a job you love,
and you will never have to work a day in your life”

Confucius

Reviewer: Prof. Dr. Markus Bleich
2nd reviewer: Prof. Dr. Eric Beitz
Committee chair: Prof. Dr. Gernot Friedrichs
Committee member: Prof. Dr. Frank Melzner
Oral examination: 18. 12. 2015
Approved for print: 18. 12. 2015

List of Abbreviations

aTL	ascending Thin Limb
AVP	Arginine vasopressin
CaSR	Calcium Sensing Receptor
CD	Collecting Duct
Cld	Claudin
CLD	Claudin gene
CNT	Connecting Tubule
DCT	Distal Convolutd Tubule
dKO	Double knock-out for Cld10 and Cld16
DMSO	Dimethyl sulfoxide
dTL	descending Thin Limb
DTT	Dithiothreitol
FHHNC	Familial Hypomagnesemia with Hypercalciuria and Nephrocalcinosis
HDAC	Histone deacetylase
HEPES	4-(2-Hydroxyethyl)piperazine-1-ethanesulfonic acid
11 β -HSD2	11 β -hydroxysteroid dehydrogenase type 2
I_{sc}	Equivalent short circuit current
miR	micro RNA
MR	Mineralocorticoid receptor
NKCC2	Na ⁺ -K ⁺ -2Cl ⁻ cotransporter
PT	Proximal Tubule
PTH	Parathyroid hormone
ROMK	Renal outer medullary potassium channel
R_{te}	Transepithelial resistance
SAHA	Suberanolhydroxamic acid
SDS	Sodium dodecyl sulfate
TAL	Thick Ascending Limb
TBS	Tris-buffered saline
Tween (20)	Polysorbate 20
V_{te}	Transepithelial voltage
WR	Water-restricted
WL	Water-loaded
WT	Wild-type

List of Figures

Figure 1:	Nephron structure, showing a superficial and a juxtamedullary nephron and the kidney regions.....	16
Figure 2:	Transport of ions in the TAL and generation of the lumen positive potential.....	20
Figure 3:	Tight junction proteome.....	23
Figure 4:	Expression pattern of the mineralocorticoid receptor (MR), aquaporin 2 (AQP2), and the epithelial sodium channel (ENaC) in DCT, CNT, and CD.....	27
Figure 5:	PTH action over small intestine, kidney and bone.....	28
Figure 6:	Graphic representation of a mouse kidney and a kidney slice.....	36
Figure 7:	Graphic representation of the customized forceps.....	37
Figure 8:	Experimental setup to measure transepithelial voltages.....	41
Figure 9:	Original recording of the transepithelial voltage in a TAL for a mouse on high calcium diet.....	51
Figure 10:	Original paired AVP stimulation trace record.....	52
Figure 11:	Schematic experimental protocol with low chloride perfusion and bath.....	54
Figure 12:	Transepithelial voltage (V_{te}) of mechanically and enzymatically dissected TAL.....	61
Figure 13:	Transepithelial resistance (R_{te}) and equivalent short circuit current (I_{sc}) of mechanically and enzymatically dissected TAL.....	61
Figure 14:	Paracellular properties of mechanically and enzymatically dissected TAL.....	62
Figure 15:	Renal fractional excretion of calcium (left axis) and phosphates (right axis) of mice from low- Ca^{2+} , control, and high- Ca^{2+} diet groups.....	64
Figure 16:	Transepithelial electrical properties determined on isolated and microperfused TAL of mice at low- Ca^{2+} , control or high- Ca^{2+} diet.....	65
Figure 17:	Ex vivo paracellular transport properties of microperfused TAL from the calcium diet groups after inhibition of NKCC2.....	66
Figure 18:	Transepithelial electrical properties determined on isolated and microperfused TAL of mice at control, low- Mg^{2+} , or high- Mg^{2+} diet.....	68
Figure 19:	Ex vivo paracellular transport properties of microperfused TAL from the magnesium diet groups, after inhibition of NKCC2.....	69
Figure 20:	Properties of ex vivo perfused TAL tubules from wild-type mice after a four hour treatment with vehicle (left column) or SAHA (right column).....	71
Figure 21:	Urine osmolality of mice kept on water-loaded (WL) or water-restricted (WR) conditions for 5 days.....	72
Figure 22:	Transepithelial transport properties of mTAL from mice kept on water-loaded (WL) or water-restricted (WR) conditions.....	72
Figure 23:	Expression of <i>Cldn10</i> , <i>Cldn16</i> , <i>Cldn19</i> , and NKCC2 in TAL from mice under water-loaded (WL) or water-restricted (WR) conditions.....	73
Figure 24:	Paracellular transport properties of mTAL of mice on water-restricted (WR) and water-loaded (WL) conditions.....	73
Figure 25:	Transepithelial transport increases in presence of AVP.....	74
Figure 26:	Selectivity for cations in freshly isolated mTAL after stimulation with AVP.....	74
Figure 27:	Transepithelial transport parameters in the TAL of wild-type (WT) mice and mineralocorticoid receptor-deficient ($MR^{AQP2Cre}$) mice.....	75

Figure 28:	<i>Paracellular permeabilities to Na⁺, Cl⁻, Mg²⁺, and Ca²⁺ (P_x) in TAL of mineralocorticoid receptor-deficient mice (MR^{AQP2Cre}) and litter-mate wild-type animals (WT).....</i>	76
Figure 29:	<i>Response to one hour incubation with vehicle (Veh) or cyclosporin A (CsA) in TAL from wild-type mice (WT) or SOLRA^{-/-} mice.....</i>	78
Figure 30:	<i>Transepithelial transport of cortical and medullary TAL in CLd10, Cld16, and Cld10/Cld16 knock-out mouse models (c10KO, c16KO, and dKO).....</i>	80
Figure 31:	<i>Sodium-chloride permeability ratios of cortical and medullary TAL from Cld10 and Cld16 knock-out, and double knock-out mice.....</i>	80
Figure 32:	<i>Absolute permeabilities to sodium, chloride, magnesium, and calcium of cortical and medullary TALs from Cld10 and Cld16 knock-out, and double knock-out mice.....</i>	81
Figure 33:	<i>Epigenetic regulation of CLD14 expression.....</i>	92
Figure 34:	<i>Proposed endogenous mechanism of SORLA as inhibitor of calcineurin A (CnAβ).....</i>	98

List of Tables

<i>Table 1:</i>	<i>Modified physiological Ringer-like solutions.....</i>	<i>39</i>
<i>Table 2:</i>	<i>Composition of the two parts of the SDS-PAGE.....</i>	<i>46</i>
<i>Table 3:</i>	<i>Solutions related to the Western blotting procedure.....</i>	<i>47</i>
<i>Table 4:</i>	<i>Primary and secondary antibodies used in the Western blots.....</i>	<i>48</i>
<i>Table 5:</i>	<i>Calcium and magnesium diets composition.....</i>	<i>49</i>
<i>Table 6:</i>	<i>Metabolic parameters of mice on the calcium diets.....</i>	<i>63</i>
<i>Table 7:</i>	<i>Metabolic parameters of mice on the magnesium diets.....</i>	<i>67</i>

Contents

List of Abbreviations.....iii

List of Figures.....iv

List of Tables.....vi

Contents.....vii

1. Summary.....10

2. Zusammenfassung.....12

3. Introduction.....14

 3.1. The nephron.....15

 3.2. The thick ascending limb of the Henle's loop.....18

 3.2.1. TAL properties: active transcellular transport and a lumen positive potential.....19

 3.2.2. Paracellular transport.....21

 3.3. Regulation of the ion transport in the TAL.....24

 3.3.1. Na⁺ reabsorption.....24

 3.3.2. Control of Ca²⁺ and Mg²⁺ homeostasis.....27

 3.3.3. NKCC2 phosphorylation and dephosphorylation.....29

 3.3.4. Inhibition of histone deacetylase with suberanilohydroxamic acid (SAHA) affects Cld14 expression.....30

4. Aims of the thesis.....32

 4.1. Establishment of a simplified equation for the calculation of absolute permeabilities.....32

 4.2. Optimization of enzyme assisted tubule dissection for measurements in isolated perfused TAL from old mice.....32

 4.3. Measurements of the effects of calcium modified diets.....32

 4.4. Measurements of the effects of magnesium modified diets.....33

 4.5. Assessment of epigenetic regulation of Cld14 expression.....33

4.6. Measurement of the tight junction permeability regulation in the TAL by AVP	33
4.7. Measurement of the influence of high plasma aldosterone on TAL ion transport.....	34
4.8. Inhibition of the deactivation of NKCC2 by treatment with the calcineurin (CnA β) inhibitor cyclosporin A.....	34
4.9. Characterization of the TAL transport properties in Cld10/Cld16 double knock-out mice.....	34
5. Materials and Methods.....	36
5.1. Tubule isolation techniques.....	36
5.2. Blood and urine collection and analysis.....	37
5.3. Experimental solutions.....	38
5.4. Tubule perfusion.....	40
5.5. Equations for the calculation of transepithelial and paracellular parameters	41
5.6. Western blot.....	45
5.7. Food for the diets.....	48
5.8. Animals and experimental design used for the studies performed in this thesis.....	49
5.8.1. Calcium and magnesium diets.....	49
5.8.2. AVP stimulation.....	50
5.8.3. Cld10 KO, Cld16 KO, and Cld10/16 double KO.....	52
5.8.4. Treatment with suberanilohydroxamic acid (SAHA).....	53
5.8.5. Sorting-protein-related receptor knock-out mice.....	53
5.8.6. Mineralocorticoid receptor-deficient mice.....	54
5.8.7. Quality criteria.....	54
5.9. Ethical approval.....	55
5.10. Statistics.....	55
6. Results.....	57

6.1. Simplified equation for the calculation of absolute paracellular permeabilities	57
6.2. Electrophysiological properties of enzymatically prepared TAL from mice of different ages.....	60
6.3. Effects of high and low divalent cation diets on the TAL.....	62
6.3.1. Control of Ca ²⁺ and Mg ²⁺ reabsorption in thick ascending limb of Henle's loop in consequence of dietary Ca ²⁺	63
6.3.2. Dietary Mg ²⁺ does not trigger regulation in the paracellular transport properties of the TAL.....	66
6.4. Inhibition of histone deacetylase with suberanilohydroxamic acid (SAHA) increases the paracellular cation conductance in the TAL.....	69
6.5. Regulation by arginine vasopressin of the tight junction's permeability in the TAL.....	71
6.6. A constitutive high plasma aldosterone mouse model, had unaltered transport rates in the TAL compared to wild-type animals.....	75
6.7. Inhibition of the deactivation of NKCC2 by treatment with the calcineurin inhibitor cyclosporin A.....	76
6.8. Characterization of the TAL transport properties in Cld10/Cld16 double knock-out mice.....	78
7. Discussion.....	82
7.1. Methodological discussion.....	82
7.2. Influence of dietary intake of divalent cations on the TAL.....	84
7.3. Regulation by hormones and second messengers.....	91
7.4. Knock-out models.....	96
8. Conclusions.....	103
Publications related to the thesis.....	106
Acknowledgments.....	107
Erklärung.....	108
References.....	109

1. Summary

The thick ascending limb of Henle's loop (TAL) is one of the key places in the nephron for the reabsorption of divalent cations. This reabsorption occurs entirely through the cation selective paracellular pathway, driven by the lumen-positive transepithelial voltage present in this renal tubule. The transepithelial voltage is indirectly created by the active transcellular transport. It is known that the transcellular transport is regulated at several points, but the regulation at the paracellular pathway hasn't been widely studied. It is not until recently with the discovery of the claudin family of proteins and their properties that regulation in the paracellular pathway has come into focus.

To functionally study how the reabsorption of divalent cations can be regulated, TALs were dissected and microperfused *ex vivo*. The recording of transepithelial voltages (V_{te}), transepithelial resistances (R_{te}), and diffusion voltages allowed the calculation of equivalent short circuit currents (I_{sc}), permeability ratios, and absolute paracellular permeabilities to ions (P_x) in the TAL.

TALs from mice on high dietary calcium intake reached lower values of V_{te} , P_{Mg} and P_{Ca} than TALs from the control group, indicating clearly that a regulatory process has taken place. Low calcium intake for 8 days had no verifiable effects in the TAL of those mice. The same experiments with low and high magnesium daily intake did not produce any effect in the TAL, even though the animals had altered their metabolic parameters.

To further characterize the mechanisms of regulation of TAL tight-junction properties, mice were treated with suberanilohydroxamic acid (SAHA). SAHA inhibits histone deacetylase, causing in the TAL a reduction in claudin 14 membrane expression. TALs from treated mice had lower R_{te} and higher P_{Na} than TALs from control animals.

Another possible regulatory pathway was studied by inducing a systemic increase in arginine vasopressin (AVP) via water restriction or by directly stimulating isolated TALs with AVP. TALs

from water-restricted mice had lower R_{te} , with higher V_{te} , I_{sc} , and P_{Na} than tubules from water-loaded mice. Acute *ex vivo* stimulation of TALs with AVP, showed that AVP could increase V_{te} , and the paracellular selectivity for cations. Therefore, water restriction and AVP increase paracellular selectivity and permeability for cations in the TAL.

TALs from a high aldosterone mouse model were also studied. The TAL theoretically could be enlisted in the compensatory actions of the nephron when the collecting duct is not responding to aldosterone. However, no effects were observed in TAL of those mice in the electrophysiological parameters analyzed.

Transgenic knock-out mouse models were used to characterize the functionality of the tight-junction in the TAL when claudin 10, claudin 16, or both claudins simultaneously were absent. The results suggest that both claudins are complementary, and their deficiency largely affects the paracellular permeability to cations.

Using another transgenic mouse model, deficient for the intracellular sortilin-related receptor (SORLA), it was functionally observed that calcineurin $A\beta$ (CnA β) might be involved in the deactivation of NKCC2 cotransporter. Inhibitors of CnA β increase the activity of NKCC2 in TAL from wild-type mice, but not in TAL from SORLA knock-out mice.

In summary, the data presented here are a further step in characterizing the paracellular pathway in the TAL and its regulation as a physiologically relevant mechanism in ion homeostasis.

2. Zusammenfassung

Der dicke aufsteigende Ast der Henle-Schleife (TAL) spielt eine Schlüsselrolle für die Reabsorption divalenter Kationen im Nephron. Diese Reabsorption erfolgt ausschließlich über den Kationen-selektiven parazellulären Weg und wird durch die in der TAL vorherrschende Lumen-positive transepitheliale Potentialdifferenz getrieben. Diese Potentialdifferenz wird indirekt durch den aktiven transzellulären Transport generiert. Es ist bekannt, dass der transzelluläre Transport auf unterschiedliche Arten reguliert wird. Im Gegensatz dazu ist die Regulation des parazellulären Weges weitgehend unerforscht. Erst in den letzten Jahren ist die Regulation des parazellulären Weges in den Fokus gerückt, gemeinsam mit der Entdeckung und zunehmenden Erforschung der Claudin-Familie.

Um die Regulation der Reabsorption divalenter Kationen funktionell zu untersuchen, wurden TAL-Segmente disseziert und *ex vivo* mikroperfundiert. Die Messung des transepithelialen Potentials (V_{te}), des transepithelialen Widerstandes (R_{te}) und von Diffusionspotentialen ermöglichte die Berechnung des äquivalenten Kurzschlussstroms (I_{sc}) sowie von Permeabilitäts-Quotienten und absoluten parazellulären Ionen-Permeabilitäten (P_x) in der TAL.

TAL-Segmente von Mäusen mit hoher diätetischer Kalzium-Aufnahme zeigten niedrigere Werte für V_{te} , P_{Mg} und P_{Ca} als TAL von Mäusen der Kontrollgruppe. Dies deutete klar auf einen regulatorischen Prozess hin. Im Gegensatz dazu hatte die Aufnahme von wenig Kalzium über acht Tage keinen Effekt auf die TAL der Mäuse. Analoge Experimente mit niedriger oder hoher täglicher Magnesium-Aufnahme zeigten ebenfalls keinerlei Effekte in der TAL, obwohl die metabolischen Parameter durch die Diät verändert waren.

Um die Regulationsmechanismen der Tight junction-Eigenschaften in der TAL näher zu analysieren, wurden Mäuse mit SAHA (Vorinostat, N-Hydroxy-N'-phenyloctandiamid) behandelt. SAHA inhibiert die Histon-Deacetylase und verursachte so eine Reduktion der Membran-

Expression von Claudin-14 in der TAL. TAL-Segmente von entsprechend behandelten Mäusen wiesen geringere R_{te} - und höhere P_{Na} -Werte auf als TAL aus Kontrolltieren.

Um einen weiteren regulatorischen Weg zu untersuchen, wurde ein systemischer Anstieg von Arginin-Vasopressin (AVP) entweder durch diätische Wasser-Restriktion oder durch direkte Stimulation isolierter TAL mit AVP induziert. TAL-Segmente von Wasser-restringierten Mäusen zeigten geringere R_{te} mit Anstieg in V_{te} , I_{sc} und P_{Na} als TAL von Mäusen mit hoher Wasser-Aufnahme. Die direkte Stimulation von TAL mit AVP führte zu einer Erhöhung von V_{te} und der parazellulären Ionenselektivität. Insgesamt erhöhten Wasser-Restriktion und AVP-Anstieg die parazelluläre Selektivität und Permeabilität für Kationen in der TAL.

Weiterhin wurden TAL-Segmente von einem Hoch-Aldosteron-Mausmodell untersucht. Hierbei sollte analysiert werden, inwieweit die TAL an einer Kompensation des Nephrons beteiligt ist, wenn das Sammelrohr nicht auf Aldosteron reagiert. Im Hinblick auf die analysierten elektrophysiologischen Parameter konnten keine Effekte in der TAL beobachtet werden.

In einem weiteren Ansatz wurden transgene Mausmodelle benutzt, um die Funktion der TAL bei Abwesenheit von entweder Claudin-10 oder Claudin-16 oder bei kombinierter Abwesenheit beider Claudine zu charakterisieren. Die Ergebnisse legen nahe, dass beide Claudine sich komplementär verhalten und dass ihre Abwesenheit die parazelluläre Permeabilität gegenüber Kationen in hohem Maß beeinflusst.

In einem weiteren Mausmodell, defizient für den intrazellulären Sortilin-ähnlichen Rezeptor (SORLA), zeigte sich, dass Calcineurin A β (CnA β) an der Deaktivierung des Cotransporters NKCC2 beteiligt ist. Inhibitoren von CnA β steigerten die Aktivität von NKCC2 in der TAL von Wildtyp-Mäusen, nicht aber von SORLA Knock-out-Mäusen.

Zusammenfassend stellen die hier präsentierten Daten einen weiteren Schritt in der Charakterisierung des parazellulären Weges in der TAL sowie seiner Regulation als physiologisch relevanten Mechanismus in der Ionenhomöostase dar.

3. Introduction

The kidney is responsible among other multiple functions for the maintenance of the body's extracellular liquid composition. But it does not do it alone; it is actually a full interplay with other organs like bones, intestine, and skin, where hormones and sensing receptors have control on the fine tuning. Keeping a tight control in the extracellular liquid composition is vital, since our cells need this constant surrounding medium to function at their best. The kidney's structural unit, the nephron, filtrates blood in the glomerulus allowing around a 50% of virtually protein free plasma to pass, carrying with it waste products but also important small soluble substances like electrolytes, glucose or amino acids. Along the nephron this tubular fluid changes its composition. The tubules reabsorb most of the glucose and amino acids filtered, and the precise amounts of electrolytes needed at each moment. They also secrete substances like NH_4^+ , urea, uric acid, creatinine, H^+ , K^+ , or drugs into the lumen. At the same time, the urine needs to be concentrated, as no non-aquatic animal can afford to waste the huge amounts of liquid filtered through the glomerulus. This way, during the process of urine formation from the first filtrate, the nephron has not only to reabsorb all the electrolytes and nutrients needed, but it also has to reabsorb water to concentrate the urine.

In terms of composition the process can plainly be summarized as:

Urinary excretion = Glomerular filtration – Tubular reabsorption + Tubular secretion

The present dissertation will focus on the reabsorption of ions in the thick ascending limb of Henle's loop, more particularly on the reabsorption of divalent cations throughout the tight junction in this tubular segment. In the following sections I give a brief overview over the nephron functionality and its regulation to place in context the goals of this work.

3.1. The nephron

The nephron is formed by the glomerulus and a sequence of tubules that begin right after the glomerulus and finish by joining with other nephrons in the collecting duct (Figure 1). These tubules have very different properties and are organized functionally and spatially to maximize the efficiency of those processes of reabsorption, secretion, and concentration of the urine. The reabsorption in these tubules takes place either using the transcellular or the paracellular pathways. The transcellular pathway uses actively the cell machinery of transporters, co-transporters, ion channels, and pumps to move ions, other solutes, and water across the cells in the tubular wall. The paracellular transport takes place through the tight junctions, and makes use of osmotic forces and electrochemical gradients to move water and ions.

The first tubular segment is the proximal tubule (PT). Almost all filtered organic solutes, and around two-thirds of all the salts are reabsorbed in the PT. About one-third of the reabsorbed salts and water go transcellular, and the other two-thirds paracellular. Particularly, about 65 % of the Ca^{2+} , and 25 % of the Mg^{2+} is reabsorbed paracellularly here. The very high transcellular transport activity in the PT is supported by a very active metabolism, a high number of mitochondria and the presence of a brush border. The tubule is at first convoluted, which makes its cortical part longer, and then it turns straight as it runs into the kidney medulla, beginning this way the loop of Henle.

The loop of Henle consists of four different segments: the straight section of the PT, the descending thin limb (dTl), the ascending thin limb (aTl) and the thick ascending limb (TAL), forming a highly specialized structure. Making its way down into the medulla, the dTl goes after the straight section of the PT, and is after a loop followed by the aTl. The thin tubules, in contrast to the PT, exhibit considerably less metabolic activity and almost no active transport. The descending segment is highly permeable to water (20% of all the water reabsorbed in the nephron is due to this segment) but has very low permeability to ions like Na^+ or Cl^- . In contrast, both ascending segments of the loop, the aTl and the TAL, are virtually impermeable to water. These properties are critical for the concentration of urine. The TAL is again characterized by a

very active metabolism. It actively transports around 25% of the filtered amounts of Na^+ , Cl^- , and K^+ . The TAL is a very important segment for the reabsorption of Ca^{2+} and Mg^{2+} . Under standard conditions, 25% of the filtered Ca^{2+} and up to 70% of the Mg^{2+} are reabsorbed paracellularly in this segment. After the TAL touches the glomerulus in the macula densa, the nephron structure is again at the same spatial level of the convoluted part of its PT. Here, starting at the macula densa, the distal convoluted tubule (DCT), the connecting tubule (CNT), and later the collecting ducts are the subsequent structures.

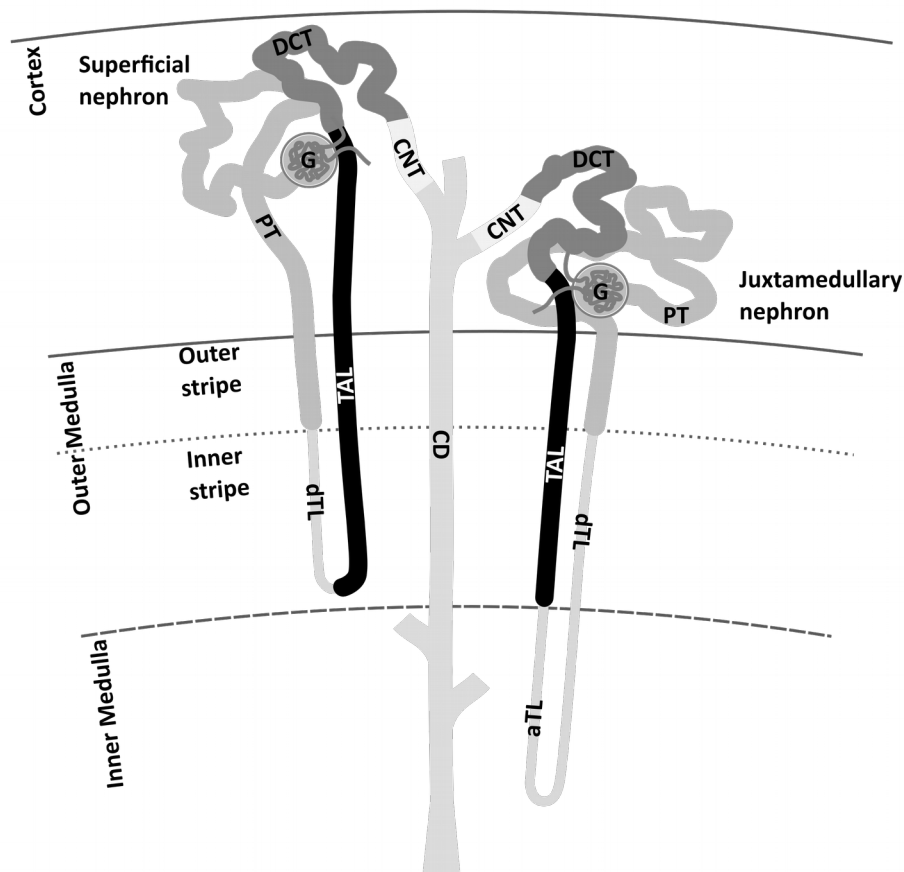


Figure 1: Nephron structure, showing a superficial and a juxtamedullary nephron and the kidney regions. The kidney schematic cross sectional view is divided in four regions: cortex, outer and inner stripes of outer medulla, and inner medulla (IM). Depicted nephron structures are denoted as: G, glomerulus; PT, proximal tubule; dTL, descending thin limb; aTL, ascending thin limb; TAL, thick ascending limb; DCT, distal convoluted tubule; CNT, connecting tubule; CD, collecting duct.

The fine tuning for ion and water reabsorption takes place tightly controlled by hormones in the late portion of the nephron. The DCT has very similar properties to the TAL, meaning that both are virtually impermeable to water and urea, and actively transport Na^+ , and Cl^- from the lumen to renal interstitial fluid. Immediately after the DCT is the CNT, which connects with the cortical CD. These distal segments have very similar functionality and are characterized by their cell heterogeneity. The connecting tubules are formed by connecting tubule cells and intercalated cells; while the cortical collecting ducts are formed by principal cells and intercalated cells. Two subtypes of intercalated cells have been identified: α -intercalated cells and β -intercalated cells. Alpha-intercalated cells secrete H^+ and reabsorb K^+ , whereas β -intercalated cells secrete HCO_3^- . In general, principal cells reabsorb water, Na^+ , Cl^- from the lumen and secrete K^+ . In the initial collecting duct, the principal cells represent about two thirds of the cells. That ratio increases further down into the medulla, reaching almost 100% of principal cells in the inner medullary collecting duct. However, the segment is still involved in the transport of electrolytes and water, tightly controlled by hormones. The connecting tubules and the collecting ducts are virtually impermeable to water without the presence of arginine vasopressin (AVP).

There are two kinds of nephrons: superficial nephrons and juxtamedullary nephrons (Figure 1). Superficial nephrons have short loops of Henle, which penetrate only the most external part of the medulla, dividing it into two clearly distinct regions: outer medulla and inner medulla. It has been estimated that 85% of the nephrons belong to this type. In contrast, the juxtamedullary nephrons have long loops that reach deep into the inner medulla, and their glomeruli are located in the cortex next to the onset of the outer medulla. These nephrons are very important for urine concentration; together with the *vasa recta* vascular system they perform a countercurrent multiplier mechanism that creates a longitudinal concentration gradient in the kidney's medullary interstitium.

It is this gradient, actively sustained by the TAL's reabsorption of NaCl , that provides the osmotic force to concentrate the urine via the water reabsorption, first in the dTLs and finally in the collecting ducts.

The combination of the properties of the nephron segments and their spatial organization is fundamental to the kidneys' ability to excrete wastes, reabsorb nutrients, keep the acid-base balance, and maintain the extracellular liquid composition and the plasma volume at very controlled levels. This system can be challenged by many factors. Physiological stimuli such as blood pressure, dietary intake of salts, nutrients, and amount of water consumption trigger the system's readjustment via direct sensing or hormonal display. Likewise, some genetic defects affect the correct functioning of these highly regulated mechanisms.

3.2. The thick ascending limb of the Henle's loop

The watertight thick ascending limb of the Henle's loop (TAL) is relevant for the reabsorption of divalent cations, sodium, chloride, and potassium. Its active transport is responsible for providing the substrate to induce the osmotic gradient in the kidney medulla, which is used for the concentration of urine and for the movement of other ions and urea, and has a critical role in the extracellular fluid volume homeostasis. This makes it an interesting target for the study of potential regulatory mechanisms responding to different stimulations. In the last years the number of data supporting the understanding of the molecular physiology of the TAL increased. Examples of this are the presence in its basolateral side of the calcium sensing receptor and the signaling cascades it triggers; the TAL's proven capability to react to hormones like AVP to increase its transcellular transport capability; or the recent data on the complex net of proteins that build the TAL's tight junctions, where modifications or regulation can change the paracellular properties.

In the present dissertation I am going to focus on the TAL properties, and for that account the following section is dedicated to the key elements that are necessary to understand this work.

3.2.1. TAL properties: active transcellular transport and a lumen positive potential

Anatomy

The TAL is a uniform tubule which reaches from the bottom of the outer medulla to the cortex. TAL of juxtamedullary nephrons barely enter in the kidney cortex, whereas TAL of superficial nephrons can reach deep into the cortex. The TAL, in general, is impermeable to water, has a high metabolic activity to reabsorb Na^+ and Cl^- transcellularly, and provides a paracellular pathway highly selective to cations. Medullary TAL (mTAL) or cortical TAL (cTAL) are the segments of TAL that are clearly located in those regions. The basic molecular machinery and the type of cells in mTAL and cTAL are so far described as the same, but their properties show some variation. The different environments that those segments face might result in regulatory adjustments that change the paracellular permeabilities or the ability to generate the driving forces for reabsorption.

Transcellular transport and the generation of the lumen positive potential

TAL cells are highly polarized to ensure the conduction of transport. Located on the basolateral membrane, the sodium-potassium pump ($\text{Na}^+\text{-K}^+$ ATPase) creates a Na^+ gradient between the inside of the cell and the lumen (Figure 2). This is the motor for the transport of Na^+ , Cl^- , and K^+ from the lumen to the cell. For this movement of ions essentially only one cotransporter is used in the TAL: the renal NKCC2 cotransporter. The transport via NKCC2 is a non-electrogenic process with a stoichiometry of 1 K^+ and 2 Cl^- for each Na^+ . Cl^- -channels of the ClC family (ClC-Kb) located in the basolateral membrane guarantee the continuous transport of Cl^- to the interstitium. In contrast, K^+ can be transported in two directions: towards the basolateral side of the membrane via the $\text{K}^+\text{-Cl}^-$ cotransporter KCC4, or reversely to the luminal side using ROMK channels. In this way, the return of K^+ to the TAL lumen assures the adequate functioning of the NKCC2 cotransporter, but also creates a charge unbalance, causing in part the typical lumen-positive potential in this tubular segment. This lumen-positive potential is the driving force for the reabsorption of divalent cations via the paracellular pathway. At the same time, the highly cation

selective property of the TAL's paracellular pathway relies on the particular composition of proteins from the claudin family present in the TAL tight junction.

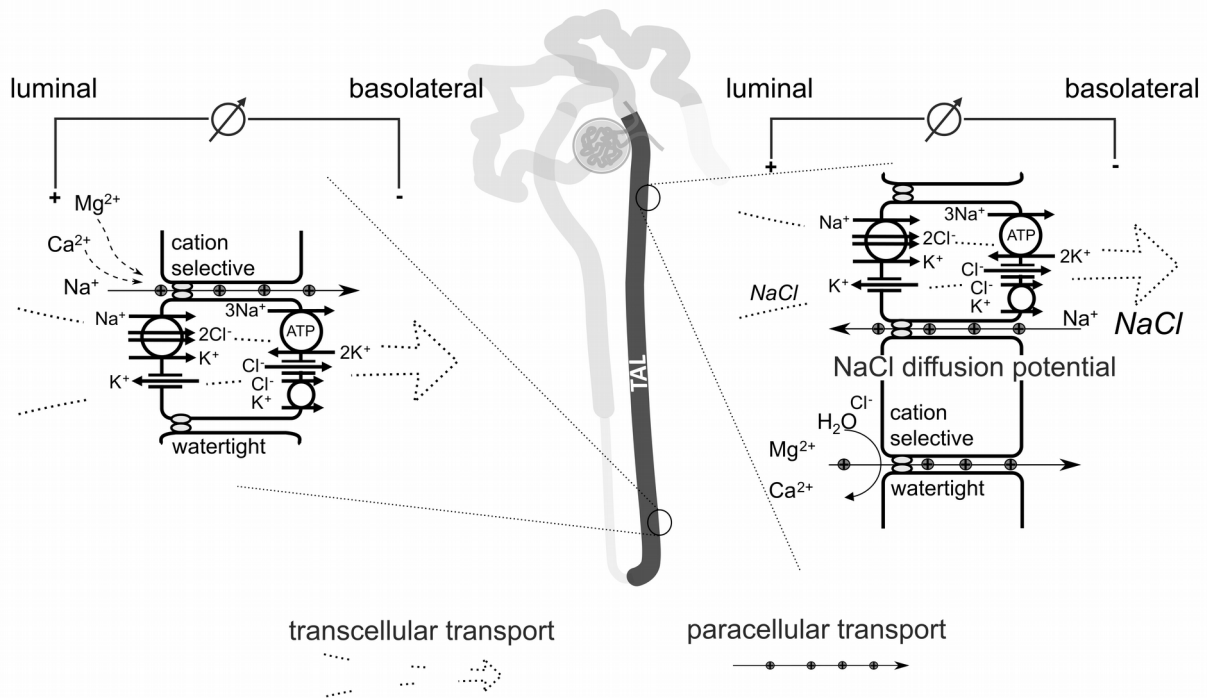


Figure 2: Transport of ions in the TAL and generation of the lumen positive potential.

NKCC2 and ROMK are depicted in the luminal cellular membrane. The $\text{Na}^+\text{-K}^+$ ATPase, Cl^- -channel, and $\text{K}^+\text{-Cl}^-$ cotransporter can be seen in the basolateral cellular membrane. The active transport in the early TAL (left) generates a lumen positive potential of around 5 mV due to the return of K^+ to the luminal side via ROMK. The difference in NaCl -concentration between luminal and basolateral sides of the membrane in the late TAL (right) induce a Na^+ diffusion potential that increase the lumen positive potential to values in the proximity of 30 mV. The lumen positive potential favors the paracellular reabsorption of divalent cations.

The lumen-positive potential in the TAL can be canceled by the presence of loop diuretics, such as furosemide, ethacrynic acid, and bumetanide. The presence of furosemide disrupts the NaCl transport by blocking NKCC2 functionality. If this happens an immediate drop from around 8 mV to almost 0 is observed in the transepithelial voltage, reducing also the paracellular driving forces.

3.2.2. Paracellular transport

Whereas the entire Cl^- reabsorption in the TAL takes place transcellularly, only about half of the Na^+ reabsorption takes place this way. Nevertheless, in total the reabsorption of both ions has a ratio of 1. Due to the stoichiometry of 1 Na^+ /1 K^+ /2 Cl^- of the NKCC2 luminal cotransporter, the remaining Na^+ has to be transported via the paracellular pathway.

The pathway through the tight junctions of the TAL is cation-selective. The ratio between the permeability to Na^+ and the permeability to Cl^- ($P_{\text{Na}}/P_{\text{Cl}}$) as an indicator of selectivity exceeds 1, usually with values between 2 and 5. The paracellular resistance in the TAL is higher than in the proximal tubules, but it is still relatively low. Nevertheless, one of the most distinctive characteristics of the TAL is its very low water permeability. In total, its capacity of ion transport and its extremely low water permeability permit the TAL not only to generate, but also to sustain high NaCl gradients of up to 120 mM between the lumen and the interstitium.

The driving forces for the substantial paracellular reabsorption of divalent cations that takes place in the TAL are the lumen-positive potential and the high osmolality gradients sustained by the tubular membrane. At the beginning of the TAL, the osmolalities are high and similar to each other at both sides of the membrane. At this point lumen-positive potentials of around 8 mV are generated by the transcellular mechanisms previously described. Downstream, at the distal portion of the TAL, the situation is completely different: here the active transport and the water tightness of the wall have reduced the luminal fluid osmolality extensively. Under these conditions, the lumen-positive potential is mainly generated as a diffusion voltage by the 'back-leak' of Na^+ ions into the lumen, reaching values of around 30 mV. Because of this, the electrical component of the electrochemical gradient for Mg^{2+} and Ca^{2+} is increased and enhances their paracellular reabsorption at this portion of the tubule (Bleich *et al.*, 2012).

Claudins in the TAL

The protein composition of the tight junctions varies along the nephron, resulting in completely different paracellular properties in the different segments. Many proteins interact in a very

complex cluster of membrane proteins, and together with the cytoskeleton, they define the amount of tight junction stripes, conferring tightness and stiffness to the tight junction (Figure 3). Among those, the claudin family of proteins modulates the tight junction's permeability (Günzel & Fromm, 2012; Günzel & Yu, 2013). Around 27 different claudins have been identified, but not all are expressed simultaneously in every epithelial tissue. Each segment of the nephron is characterized by a specific set of claudins. Regulation or modification of the claudin composition can change the properties of a tubular segment. In the mouse TAL, claudins 3, 10b, 11, 14, 16, and 19 are co-expressed, with claudin 16 (Cld16) and claudin 19 (Cld19) being exclusively expressed in the TAL.

Mutations of some claudin genes have been linked to kidney diseases. Namely, mutations in human Cld16 and Cld19 have been associated with the Familial Hypomagnesemia with Hypercalciuria and Nephrocalcinosis (FHHNC) (Simon *et al.*, 1999; Konrad *et al.*, 2006; Hou & Goodenough, 2010). When expressed individually in the anion selective LLC-PK1 cell line, Cld16 and also Cld19 change the cell line properties to almost non-selective: Cld16 appears to increase Na⁺ permeability without affecting the permeability to Cl⁻, while conversely Cld19 decreases Cl⁻ permeability without affecting the permeability to cations (Gong *et al.*, 2012). However, when co-expressed, they physically interact and endow the tight junction with a high selectivity for cations. It has been shown that claudin 14 (Cld14) interacts with Cld16, but not with Cld19, strongly reducing the cation selectivity of Cld16, and of Cld16-Cld19-complex (Gong *et al.*, 2012). Cld14 promoter activity was found in the mouse kidney exclusively in the TAL, but only very little expression of Cld14 is present in wild-type mice under normal dietary conditions. Cld14 expression is suppressed constitutively by microRNA (miR-9 and miR-374) in the TAL (Gong *et al.*, 2012, 2014), and is up-regulated in high extracellular Ca²⁺ conditions, sensed by the calcium-sensing-receptor (CaSR) (see below) (Gong *et al.*, 2012, 2014; Dimke *et al.*, 2013). Thus, Cld14 functions as a modulator of the cation selectivity in the TAL's tight junction. Mimicking the human FHHNC, both Cld16 knock-down and Cld19 knock-out mice presented hypermagnesuria,

hypercalciuria, with hypomagnesemia, although no signs of nephrocalcinosis. Taken together, these three claudins play an essential role in the reabsorption of divalent cations by the TAL.

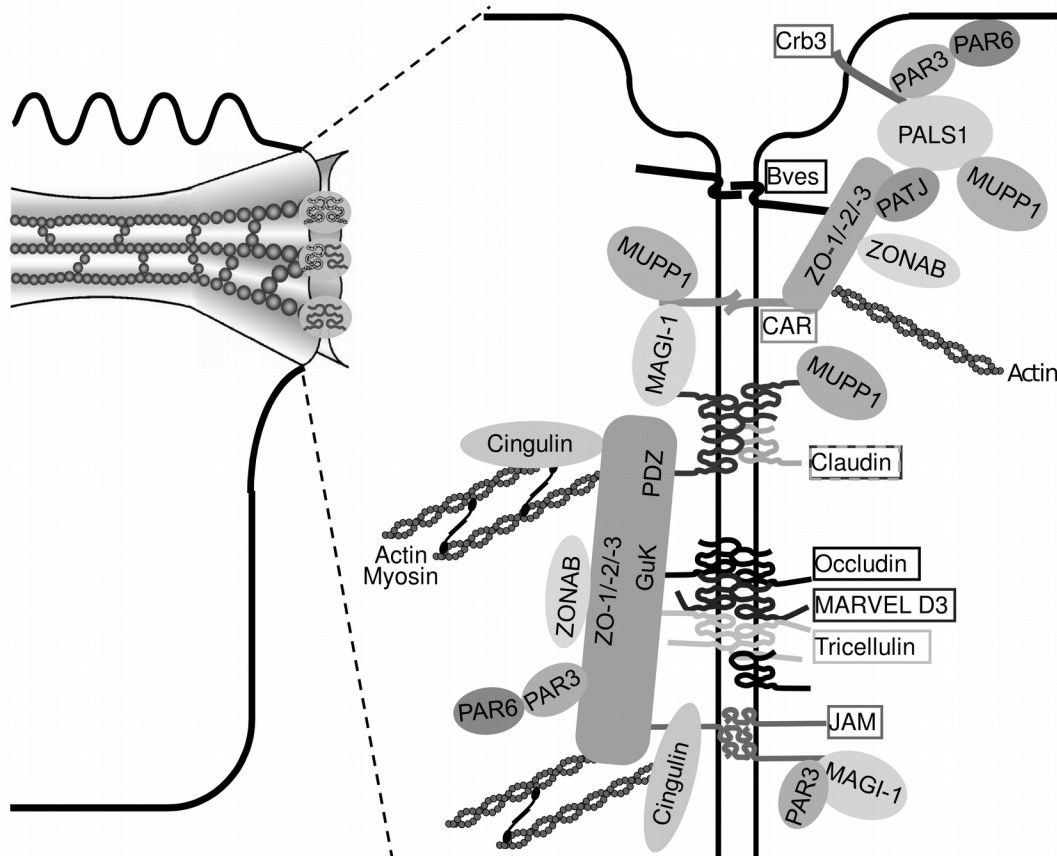


Figure 3: Tight junction proteome.

The figure illustrates the complexity of the tight-junction. Modified from Günzel&Fromm, 2012.

Claudin 10 (Cld10), on the other hand, plays a different role. There are two main isoforms of Cld10: Cld10a and Cld10b. In the mouse kidney Cld10a is preferentially expressed in the cortex while Cld10b appears to be more common in the medulla (Van Itallie *et al.*, 2006; Günzel *et al.*, 2009). Cld10b is highly expressed in the TAL with very little to no presence of Cld10a (Breiderhoff *et al.*, 2012). Experiments with Cld10b knock-out mice have demonstrated that Cld10 determines in part the paracellular permeability to Na^+ (P_{Na}) in the TAL: a reduction in P_{Na}

was shown in isolated perfused TAL from Cld10b knock-out mice, together with an increase in permeability to Ca^{2+} and Mg^{2+} (Breiderhoff *et al.*, 2012).

3.3. Regulation of the ion transport in the TAL

The main goal of the present work is to challenge the different regulatory pathways that control the water and ion reabsorption in the kidney, looking for new insights in the regulation of the TAL transport of ions. In the following sections, I give a brief introduction to some key points fundamental to the presented research.

In the TAL, it is known that the transepithelial transport of NaCl is regulated by multiple hormones. An increase of NaCl transport via increase of intracellular cAMP is the common signaling pathway for hormones like vasopressin, parathyroid hormone (PTH), glucagon, calcitonin, as well as β -adrenergic stimulation. Conversely, extracellular Ca^{2+} and prostaglandin E_2 have a negative effect on the NaCl transport in the TAL. Little is known about how the paracellular pathway of this segment is regulated, but phosphorylation, membrane trafficking and protein expression might be involved.

3.3.1. Na^+ reabsorption

Water and sodium reabsorption in the kidney are link together in many aspects, and the watertight TAL plays a key role. The loop diuretics effect serves here as an example: Loop diuretics block the capability of the TAL to reabsorb NaCl (indirectly preventing reabsorption of divalent cations due to the loss of driving force), and thereby reduce the osmotic gradient between the tubular lumen and the interstitium. Under these circumstances, the hormone-controlled water reabsorption in the collecting duct will be impaired, thus resulting in water loss. Under normal conditions (in the absence of loop diuretics), some of the hormones involved in water-salt control also have an effect on the TAL; for example vasopressin (Mutig *et al.*, 2007),

atrial natriuretic peptide (Ares *et al.*, 2011), and angiotensin II (Lerolle, 2004). In this study, I will focus on the general effects of arginine vasopressin and aldosterone in the TAL.

Arginine vasopressin

One of the most studied activators of the TAL's transepithelial transport is the hormone arginine vasopressin (AVP), also known as anti diuretic hormone. Its secretion is increased in the hypothalamus when plasma osmolality increases or when blood pressure or blood volume decreases. AVP acts in the kidney via the V_2 basolateral membrane receptor mainly to promote water reabsorption. In the principal cells of the CNT and the CD, AVP induces incorporation of aquaporin 2 in the apical membrane by promoting exocytosis of intracellular vesicles. Aquaporin 2 is a water channel that raises the water permeability of those tubules. In contrast, in the TAL, AVP leads to increase of the NaCl transport by stimulating the $\text{Na}^+\text{-K}^+$ ATPase and the net NKCC2 and ROMK activities (Giebisch, 2001; Rieg *et al.*, 2013; Mount, 2014).

AVP up-regulates NKCC2 by influencing its protein expression and its membrane trafficking, as well as affecting directly its activity by phosphorylation (Giménez & Forbush, 2003; Mutig *et al.*, 2007; Rieg *et al.*, 2013). AVP also increases the number of NKCC2 proteins in the membrane by promoting exocytosis of intracellular vesicles via intracellular signaling cascades activating adenylyl-cyclase VI, leading to a higher transport rate (Rieg *et al.*, 2013; Mount, 2014). These cascades also stimulate the transport activity of the already present membrane-bound NKCC2 by phosphorylating some N-terminal threonines and serines residues, involving SPAK/OSR1 kinases (see below). This activity strongly depends on the chloride concentration, with saturation concentrations that adjusts to Michaelis-Menten kinetics (Greger *et al.*, 1983b).

Based on the fact that AVP activates the transcellular transport in the TAL, and the importance of the paracellular pathway for the reabsorption of Na^+ and divalent cations, I hypothesize that the tight junctions in the TAL are regulated by AVP to increase paracellular permeabilities to cations. In the present work, I will present results that strongly indicate the existence of regulatory effects of AVP in the TAL's paracellular pathway.

Aldosterone

The Na⁺ and water reabsorption in the kidney have another key modulator: aldosterone. Aldosterone is secreted in the *zona glomerulosa* of the adrenal gland as a response to multiple stimuli, controlled by the renin-angiotensin-aldosterone-system (RAAS). Low Na⁺ intake causes an increase in aldosterone and angiotensin II levels. This stimulates the reabsorption of Na⁺ between the DCT and the CD. On the contrary, high Na⁺ intake reduces their secretion, resulting in the waste of large amounts of Na⁺ by the kidneys. Nevertheless, due to the interplay with AVP the kidney is able to either excrete highly concentrated urine with almost no waste of Na⁺, or to excrete large amounts of dilute urine without altering Na⁺ excretion.

Aldosterone binds to the nuclear mineralocorticoid receptor (MR). It activates the Na⁺ transport by stimulating the sodium-chloride cotransporter (NCC) in the DCT, and causes membrane expression of the amiloride-sensitive epithelial sodium channel (ENaC) in the distal portion of the DCT, in the CNT and CD (Figure 4) (Guyton & Hall, 2005; Ronzaud *et al.*, 2007). At the same time, it also activates and up-regulates the basolateral Na⁺-K⁺ pump (Salyer *et al.*, 2013). This way, aldosterone stimulates Na⁺ and water reabsorption.

The MR can be also stimulated by glucocorticoids such as cortisol. In the aldosterone target tissue, the presence of the enzyme 11 β -hydroxysteroid dehydrogenase type 2 (11 β -HSD2) catalyzes the interconversion of cortisol to the inactive form of cortisone, protecting the MR. So far, any activity of aldosterone in the TAL is unknown, but messenger RNA for MR have been reported to be expressed in mouse TAL (Ackermann *et al.*, 2010). Even though the TAL has not been classically considered to be a target for aldosterone, other studies report the presence of some 11 β -HSD2 in the TAL (Farman & Bocchi, 2000), indicating a possible co-expression. Taking also into account that aldosterone has functions in other kind of cells and tissues (like intercalated cells of the cortical collecting tubules, in the gut, or in salivary and sweat glands), and that in the TAL transcellular and paracellular transport of Na⁺ is used to create the driving forces for the reabsorption of divalent cations, systemic high aldosterone may affect the paracellular reabsorption to cations in the TAL.

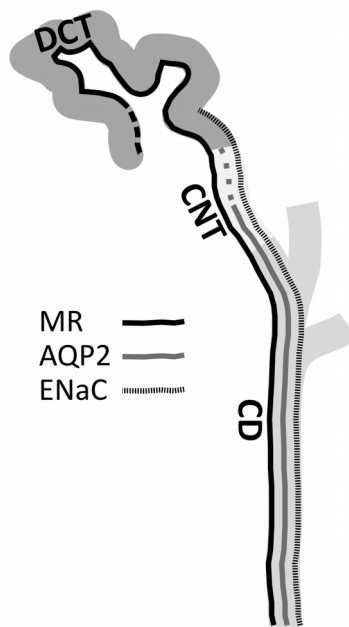


Figure 4: Expression pattern of the mineralocorticoid receptor (MR), aquaporin 2 (AQP2), and the epithelial sodium channel (ENaC) in DCT, CNT, and CD.

3.3.2. Control of Ca^{2+} and Mg^{2+} homeostasis

The regulation of calcium, magnesium, and phosphate plasma levels is tightly bound together and involves the interaction between gastrointestinal tract, bone, and kidney. About 99% of all calcium present in the body is stored in bones and can act as a source of calcium when extracellular calcium decreases. Ca^{2+} has to be controlled at a low but stable concentration in the extracellular fluids, and even lower in the cytoplasm, given its crucial role in intracellular signalling. The extracellular calcium homeostasis is controlled by an elaborated hormonal system with parathyroid hormone (PTH) as the main player (Figure 5), and additionally involving vitamin D3, calcitonin, and FGF23. Decrease in plasma Ca^{2+} stimulates the secretion of the PTH; conversely, an increase in the concentration of plasma Ca^{2+} inhibits the parathyroid gland via the calcium-sensing receptor (CaSR). With regards to magnesium, more than half of the total amount of the body is also stored in the bones, and the rest in intracellular compartments, with less than 1% present in the extracellular fluids. The concentration of cytosolic Mg^{2+} is very similar to the concentration in the extracellular space. The plasma values of Mg^{2+} highly depend on the

renal tubular reabsorption, yet bone and intestine influx and efflux have an important role. In general, glomeruli filter 50% of the plasma Ca^{2+} and Mg^{2+} . However, only 5 to 10% of the filtered Mg^{2+} is excreted in urine in normal conditions, and only around 1% of the filtered Ca^{2+} is found in the final urine. The regulatory mechanisms of Mg^{2+} excretion are not yet fully understood. It might mimic that of Ca^{2+} , as extracellular Mg^{2+} is also able to activate CaSR, although to a lesser extent than Ca^{2+} (Riccardi & Brown, 2010). Further, loss of function mutations in CaSR, some claudins, or NKCC2 affect in high scale not only Ca^{2+} but also Mg^{2+} balance (Günzel & Yu, 2009; Hou & Goodenough, 2010; Li *et al.*, 2011).

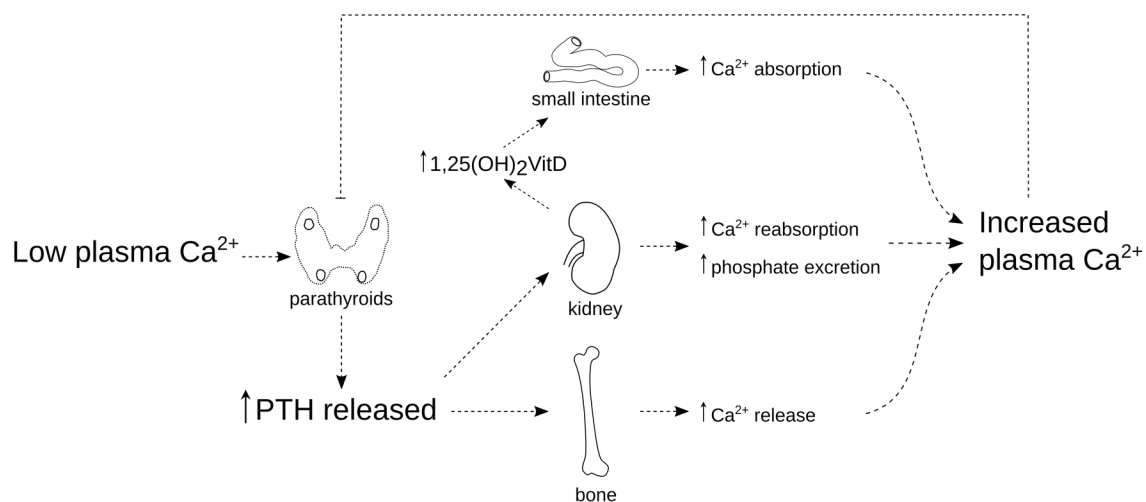


Figure 5: PTH action over small intestine, kidney and bone.

PTH, parathyroid hormone. 1,25(OH)₂VitD: 1,25-dihydroxycholecalciferol.

In the TAL, CaSR is present in the basolateral membrane. It couples with an inhibitory G protein that has an effect opposite to the stimulation induced by vasopressin. Increases in intracellular Ca^{2+} , due to the activation of CaSR, regulate the production of cAMP, either directly by inhibiting the adenylyl cyclase VI, or indirectly by activation of protein kinase C, or by other means like calmodulin or the generation of AA metabolites with a negative effect in the transport of NaCl (Halls *et al.*, 2010; Mount, 2014).

Transgenic mouse models as well as cell culture models have proven helpful for elucidating claudin function and regulation. However, the physiological responses of the tubular segments

to dietary changes are not yet fully understood. Here I present two studies analysing the effects of low and high Ca^{2+} , as well as Mg^{2+} dietary intake on driving force, permeability, and selectivity for paracellular Ca^{2+} and Mg^{2+} absorption.

3.3.3. NKCC2 phosphorylation and dephosphorylation

The NKCC2 cotransporter is an integral plasma membrane protein with 12 transmembrane segments. C-terminus and N-terminus are located at the cytoplasmic side of the plasma membrane. Phosphorylation in conserved serine and threonine sites in the N-terminus increases the transport activity of NKCC2 (Giménez & Forbush, 2003, 2005; Ponce-Coria *et al.*, 2008; Richardson *et al.*, 2011). Phosphorylation of threonine residues T96 and T101 has been linked to SPAK (Ste20/SPS1-related proline-alanine rich kinase) and OSR1 (oxidative stress-responsive kinase). The sortilin-related receptor, L(DLR class) A repeats containing (SORLA), an intracellular receptor involved in sorting and trafficking of proteins, is essential for SPAK activity (Reiche *et al.*, 2010; Borschewski *et al.*, 2015). Several studies propose kinase cascades as a mechanism for enhancing NKCC2 activity, but little is known about the corresponding phosphatases that might reverse this process. The protein phosphatase calcineurin, a calcium-dependent serine-threonine phosphatase, is known to be active in the kidney and it has been recently proposed as possible phosphatase acting on NKCC2. Calcineurin inhibitors like cyclosporin or tacrolimus are widely used as immunosuppressants to prevent acute transplant rejection, but they cause hypertension, related to water and salt retention. Treatments with calcineurin inhibitors in mice have been linked to an increase in the phosphorylation and activity of the renal thiazide-sensitive Na^+ - Cl^- cotransporter (NCC) in DCT.

Calcineurin A β (CnA β), which is locally expressed in the TAL but not present in the DCT, was recently shown to interact with NKCC2 (Borschewski *et al.*, 2015). Furthermore, they presented that CnA β from rat kidney lysate interacts with conserved threonine residuals in the NKCC2 when they are phosphorylated, but not in the trials mimicking dephosphorylation. In the same work it was shown that CnA β inhibitor cyclosporin A (CsA) increased substantially the phosphorylation of NKCC2 at the SPAK/OSR1-dependent threonines T96, and T101, with no

significant changes in the phosphorylation activity of SPAK/OSR1-kinases induced by CsA. Those results, strongly suggest that CnA β may be involved in NKCC2 dephosphorylation. In addition, CnA β was seen to interact with SORLA's intracellular tail, an indication that cellular trafficking of CnA β could also depend on the referred receptor. Taking all these into account, inhibitors of calcineurin in the TAL could raise as well the abundance in phospho-NKCC2 (pNKCC2) and therefore its activity.

In summary, phosphorylation of NKCC2 by SPAK/OSR1 increments the cotransporter activity; the protein phosphatase CnA β appears to interact with pNKCC2; and SORLA might be, at least partly, involved in the trafficking of the enzymes involved in both processes, very likely favoring SPAK actions and inhibiting CnA β . The absence of this receptor caused by selective mutation would therefore result in decreased levels of NKCC2 phosphorylation, partly in the absence of SPAK in its right place, and partly in an increased calcineurin abundance and activity.

3.3.4. Inhibition of histone deacetylase with suberanilohydroxamic acid (SAHA) affects Cld14 expression

As previously mentioned recent data have evidenced an epigenetic regulatory path for the Cld14 expression, and Cld14 is known as a modulator of the paracellular permeability in the TAL (Gong *et al.*, 2012, 2014). The interaction of Cld14 with Cld16 and the Cld16-Cld19 complex reduces the selectivity for cations of the paracellular pathway in the TAL.

Extracellular Ca²⁺ down-regulates the expression of two micro RNAs (miR), miR-9 and miR-374, via the CaSR. When these micro RNAs are present, they target the 3'-UTR of CLD14 mRNA and repress its stability and translation, causing Cld14's very low normal expression. The regulatory mechanism of these miR partly involves histone deacetylase (HDAC). Active HDAC, which is stimulated by the CaSR, causes histones to wrap the DNA more tightly by deacetylation, thus impeding the transcription of nearby genes. In line with this, the expression of miR9 and miR374 was shown to be up regulated in the presence of the HDAC inhibitor suberanilohydroxamic acid (SAHA). It was also observed that the administration of SAHA affects the Ca²⁺ and Mg²⁺ excretion

in mice: reduced fractional excretions compared to vehicle treated animals together with increased plasma levels of Mg^{2+} indicated that SAHA induced an increase of reabsorption of divalent cations in the kidney.

In other words: extracellular Ca^{2+} triggers CaSR to stimulate HDAC. HDAC tightens to the DNA histones that are located near the genes coding for miR9 and miR374, therefore reducing their expression. This results in a reduction or lack of miR9 and miR374, causing a stabilization of mRNA from the CLD14 gene which then is again free to move and be translated into a Cld14 protein. Therefore, the presence of Cld14 is increased in the tight junction where it interacts with Cld16 and the Cld16-Cld19 complex reducing the cation selectivity of this tight junction. As a result, the excretion of Ca^{2+} and Mg^{2+} increases. SAHA inhibits HDAC.

4. Aims of the thesis

4.1. Establishment of a simplified equation for the calculation of absolute permeabilities

The calculation of the absolute permeability to an ion across the TAL was not clearly established in literature. Before presenting the experimental results, I will address this problem in the first result chapter and introduce a simplified equation based on Kimizuka & Koketsu (1964) that will allow for an easy calculation of the absolute paracellular permeabilities to Na^+ , Cl^- , Mg^{2+} and Ca^{2+} .

4.2. Optimization of enzyme assisted tubule dissection for measurements in isolated perfused TAL from old mice

Mechanical dissection and sorting of TAL or any other nephron segment present two major problems: first, it is a very difficult task, if not almost impossible, to collect enough material for protein or RNA studies; and second, with age the connective tissue in the kidney increases, making the mechanical dissecting method impracticable in kidneys from mice older than 12 weeks. In this result section, I will introduce an enzymatic technique that not only allows a fast and efficient way of collecting hundreds of almost any of the nephron's tubular segments for protein and RNA analysis, but also to perfuse and measure the transport properties of TAL from old mice.

The availability of this technique allows us to test the hypothesis that age affects the ability of reabsorbing cations in the TAL. Here, I present results of the analyses of TAL properties from mice that are a few weeks old, mice of around half a year, and mice older than one year.

4.3. Measurements of the effects of calcium modified diets

The TAL plays an important role in calcium homeostasis. Here I study how the paracellular pathway is regulated in the TAL when physiological conditions are challenged. Mice received low and high Ca^{2+} -diets to study the transport properties of freshly enzymatically isolated TAL. I

hypothesize that systemic regulatory mechanisms triggered in those mice by the changes in the Ca^{2+} dietary intake include regulatory modifications in the paracellular pathway for Ca^{2+} reabsorption in the TAL.

4.4. Measurements of the effects of magnesium modified diets

Taking into account that the TAL is the main site for reabsorption of Mg^{2+} in the kidney, and according to the arguments outlined above, mice received low and high magnesium diets, followed by measurements of transepithelial transport, ion selectivity, and paracellular permeabilities in freshly enzymatically isolated TAL. Here I propose that variations in the Mg^{2+} -intake affect the driving forces and the permeabilities to Mg^{2+} in the TAL tight junction.

4.5. Assessment of epigenetic regulation of Cld14 expression

As mentioned, the reabsorption of Ca^{2+} and Mg^{2+} through the paracellular pathway in the TAL is negatively modulated, in part by the expression of Cld14. The Cld14 expression is regulated by inhibitory miR, and it has been shown that the presence of HDAC inhibitor SAHA up-regulates the expression of those miR. Because acute inoculation with SAHA reduces Ca^{2+} and Mg^{2+} fractional excretions, the transport properties of mechanically dissected TAL from mice exposed to SAHA were measured to corroborate that the paracellular pathway for divalent cations has been up-regulated.

This work is part of a scientific paper published in collaboration with Prof. Dr. Jianghui Hou's group (Gong *et al.*, 2014).

4.6. Measurement of the tight junction permeability regulation in the TAL by AVP

AVP increases water intake in the CNT and CD, and also stimulates Na^+ reabsorption in the TAL, the CNT and the CD. Based on this, I hypothesize that AVP might also have an effect in the paracellular reabsorptive properties for divalent cations in the TAL. This would reduce the

chances of precipitation of calcium and magnesium salts in the lumen during the subsequent extreme concentration of urine.

4.7. Measurement of the influence of high plasma aldosterone on TAL ion transport

Considering the potential co-expression of MR and 11 β -HSD2 in the TAL and the importance of aldosterone for water and volume balance, I postulate that aldosterone has some effect on the regulation of ion reabsorption in the TAL. To evaluate this hypothesis I measured transcellular and paracellular transport properties of TAL from old mice with systemic high aldosterone. These genetically modified mouse model (MR^{AQP2Cre}) lack the MR selectively in those cells that express aquaporin 2 and therefore show extremely elevated aldosterone concentrations.

4.8. Inhibition of the deactivation of NKCC2 by treatment with the calcineurin (CnA β) inhibitor cyclosporin A

The SORLA intracellular receptor is known to play an important role in trafficking of the kinases involved in NKCC2-activation. Further, it might also play a role in the intracellular migration of CnA β , which in turn might act as a phosphatase on NKCC2. Considering these premises, I studied the transcellular transport of TAL from wild-type mice and SORLA knock-out mice (SORLA^{-/-} mice) stimulated with cyclosporin A, with the intention to functionally evaluate the proposed role of CnA β as a phosphatase involved in the dephosphorylation of NKCC2.

This work is part of a scientific paper published in collaboration with Dr. Kerim Mutig (Borschewski *et al.*, 2015)

4.9. Characterization of the TAL transport properties in Cld10/Cld16 double knock-out mice

With the intention to add further insights into the observed phenotypical differences in Cld16-KO and Cld10-KO mice, I studied the transport properties of TAL from a Cld16/Cld10 double knock-out mouse model in collaboration with Dr. Tilman Breiderhoff. We hypothesize that

conditional Cld10 deletion in Cld16-KO mice can rescue the hypermagnesuria and hypercalciuria. On the other hand, we do not expect the hypermagnesemia present in the Cld10KO model to break out in the dKO because of the absence of Cld16.

5. Materials and Methods

5.1. Tubule isolation techniques

Enzymatically assisted kidney tubule isolation

A 1 mg/ml solution of collagenase type II (PAN 10-0141, PAN-Biotech, Germany) was used to disrupt the kidney connecting tissue to easily isolate kidney tubules by sorting. The mice were placed in a surgery setup under inhalational anaesthesia (3-5% isoflurane). At this point, 0.6-1 ml of collagenase solution was infused fast and carefully into the renal artery. This enzyme solution was previously heated to 41°C, so that the solution was around 37°C while perfusing the mouse. Immediately after, both kidneys were collected and decapsulated.

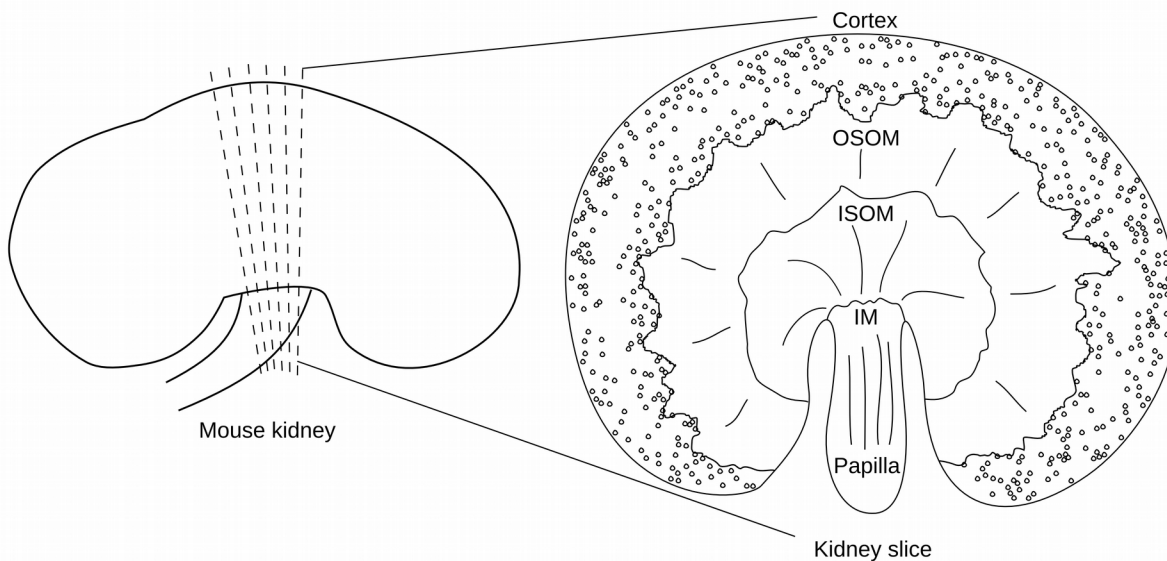


Figure 6: Graphic representation of a mouse kidney and a kidney slice.

The cortex, outer and inner stripe of outer medulla (OSOM and ISOM), inner medulla (IM), and papilla are depicted in the kidney slice.

4-6 thin transversal slices of less than 0.5 mm were cut out of each kidney (Figure 6) and placed in a 2ml Eppendorf vial in 1-1.4 ml preheated at 37°C collagenase II solution. Using a Thermomixer *comfort* (22331, Eppendorf AG, Hamburg, Germany) at 850 rpm the sample was shaken at 37°C for 10 minutes initially. The supernatant, around 1ml of solution with hundreds

of dispersed tubules, was then transferred to an ice-cold 1 ml sorting solution (see below for the composition of the sorting solution). The original vial was refilled with 1 ml of incubation solution (see below for the composition of the incubation solution) preheated at 37°C and placed again into the thermomixer for another 5 minutes. The procedure was repeated every 5 minutes to collect 3 to 4 more batches.

Mechanical kidney tubule isolation

Mice were euthanized by cervical dislocation and quickly beheaded, to let blood flow out. Kidneys taken from beheaded mice were decapsulated and sliced as thin as possible in a similar way as described before. The slices were kept in ice-cold sorting solution. The dissection of the tubule of interest was made mechanically under a stereo-microscope using customized forceps for the task (Figure 7). This technique allows an accurate spatial location of the isolated tubule along the corticomedullary axis (Figure 6).

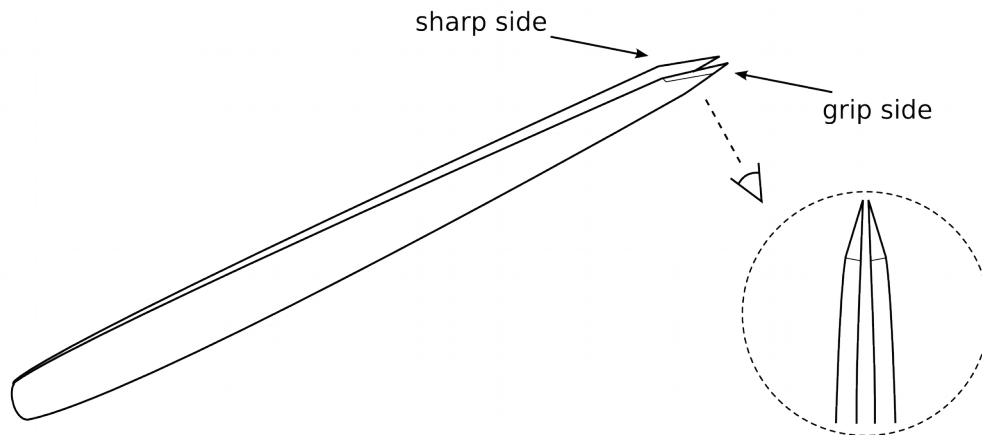


Figure 7: Graphic representation of the customized forceps.

The sharp side is used for cutting the tissue, while the grip side is used for grab and pull the tubules. Two of them were used at a time.

5.2. Blood and urine collection and analysis

Up to 1ml of blood was taken directly from vena cava inferior with the syringe needle coated internally with Na-heparine (Heparin-Natrium-25000-ratiopharm, Ratiopharm® GmbH, Ulm,

Deutschland). The puncture was performed with a 22G x ¾ needle (Henke Sass Wolf GmbH, Tuttlingen, Deutschland). Blood was then centrifuged at 13000 rpm in a Heraeus Biofuge^{VITO} laboratory centrifuge for 3 minutes and serum was then carefully collected. Spot urine was collected with a 27G x 1½ needle (Henke Sass Wolf GmbH, Tuttlingen, Deutschland) directly from bladder. Serum and urine samples were analysed for electrolytes and creatinine concentrations at the Institute of Clinical Chemistry, UKSH Kiel, Germany.

The fractional excretion of electrolyte x was calculated as the percentage of the clearance of electrolyte with respect to the glomerular filtration rate, which was estimated by the clearance of creatinine:

$$FE_x = \frac{C_x}{C_{Crea}} \cdot 100 \quad (1), \text{ where clearance (C) is}$$

$$C_x = \frac{U_x \cdot U_{flow}}{Pl_x} \quad (2)$$

where U_x and Pl_x are the urine and plasma concentrations of x, and U_{flow} is the urine flow rate.

This way, the fractional excretion of electrolyte x was calculated using the equation:

$$FE_x = \frac{U_x \cdot Pl_{Crea}}{Pl_x \cdot U_{Crea}} \cdot 100 \quad (3)$$

5.3. Experimental solutions

Incubation solution

The incubation solution was made adding 35.5 mg of glycine (3908.2, Carl Roth GmbH +Co, Karlsruhe, Germany), 4.8 mg of trypsin inhibitor (1001702226, SIGMA-ALDRICH Chemie GmbH, USA), and 2.5 mg of DNase I (1128432001, Roch Diagnostics GmbH, Mannheim, Germany) to 100 ml of a glucose free physiological Ringer-like solution (Table 1 A).

Sorting solution

The sorting solution was made adding 25 mg of albumin to 50 ml of incubation solution. Albumin would stick to the surface of the container avoiding the loss of tubules on it.

The solutions used for the electrophysiological experiments (Table 1 C, D, E, F) were modifications of the control solution (Table 1 B). They were designed to have the same osmolality but different concentrations of ions to allow the calculation of paracellular permeability ratios and absolute permeabilities to Na^+ , Cl^- , Mg^{2+} , and Ca^{2+} . The control solution was used to record transepithelial voltages and calculate the transepithelial resistance and equivalent short circuit current as transepithelial transport parameters.

Table 1: Modified physiological Ringer-like solutions

	Molar mass (g/mol)	A (mM)	B (mM)	C (mM)	D (mM)	E (mM)	F (mM)
NaCl	58.44	140.0	145.0	30.0	-	-	28.0
Na_2SO_4	142.04	-	-	-	-	-	62.0
KCl	74.56	-	-	-	3.6	3.6	-
HEPES	238.3	-	-	-	3.0	3.0	-
KH_2PO_4	136.09	0.4	0.4	0.4	-	-	0.4
$\text{K}_2\text{HPO}_4 \times 3 \text{H}_2\text{O}$	228.23	1.6	1.6	1.6	-	-	1.6
$\text{MgSO}_4 \times 7 \text{H}_2\text{O}$	246.48	1.0	-	-	-	-	-
$\text{MgCl}_2 \times 6 \text{H}_2\text{O}$	203.3	-	1.0	1.0	72.5	-	1.0
$\text{CaCl}_2 \times 2 \text{H}_2\text{O}$	147.02	-	-	-	-	72.5	-
Na-Acetate $\times 3 \text{H}_2\text{O}$	136.08	10.0	-	-	-	-	-
α -Ketoglutarate	146.1	1.0	-	-	-	-	-
Ca-Gluconate $\times 1 \text{H}_2\text{O}$	448.4	1.3	1.3	1.3	1.3	-	1.6
Glucose	180.16	-	5.0	5.0	5.0	5.0	5.0
Manitol	182.17	-	-	230.0	71.0	75.0	230.0

A, basal buffer solution. B, control solution. C, low sodium-chloride solution. D, high magnesium solution with no sodium. E, high calcium solution with no sodium. F, low chloride solution.

HEPES, 4-(2-Hydroxyethyl)piperazine-1-ethanesulfonic acid

5.4. Tubule perfusion

Freshly isolated TAL were microperfused to measure transepithelial voltages using a system of concentric pipettes designed for *in vitro* perfusion of isolated renal tubules (Greger & Hampel, 1981). The experimental setup (Figure 8) permits to hold both extremes of the tubule with a holding and a constriction pipette. Both were carefully made by heating and pulling glass capillaries (Sodalime glasscapillaries, Hilgenberg, 1409679). The perfusion was performed with an elongated double barreled glass capillary (Theta-Bo-glasscapillaries, Hilgenberg, 1402401) as perfusion pipette. One barrel was used for fluid exchange and transepithelial voltage measurement. The inside of this barrel was connected via an agar bridge (1 M KCL, 5% AGAR) to a 1 M KCl reservoir where a silver-chloride electrode, Ag/AgCl (RC-3, World Precision Instruments, Inc., USA) served as measurement electrode. On the other side, as reference electrode, another silver-chloride electrode was connected to the bath through another 1M KCl reservoir/ KCl-Agar bridge construction (Figure 8). Both electrodes were connected to an amplifier, and this one to a Flatbed Recorder Type BD12 (Kipp&Zonen B.V., Delft, Neederland), through which the voltage across the TAL membrane was recorded on paper. The other barrel of the perfusion pipette was use to inject a current of 13.0 nA for 1 second every 8 seconds (Figure 9). Given the solutions conductance, the tubule length and the tubule inner diameter, the voltage deflection in the chart trace induced by this current injection was used to calculate the transepithelial resistance using the cable equation (Greger, 1981). The perfusion flow was controlled by a constant pressure supplied by a pressure unit build in the electric workshop of our institute. The tubules were continuously superfused on the bath side driven by gravity. The solution running in the bath could be changed according to the needs of the experiment as well as the luminal solution via the fluid exchange pipette. All the voltages measured were corrected for liquid junction potentials.

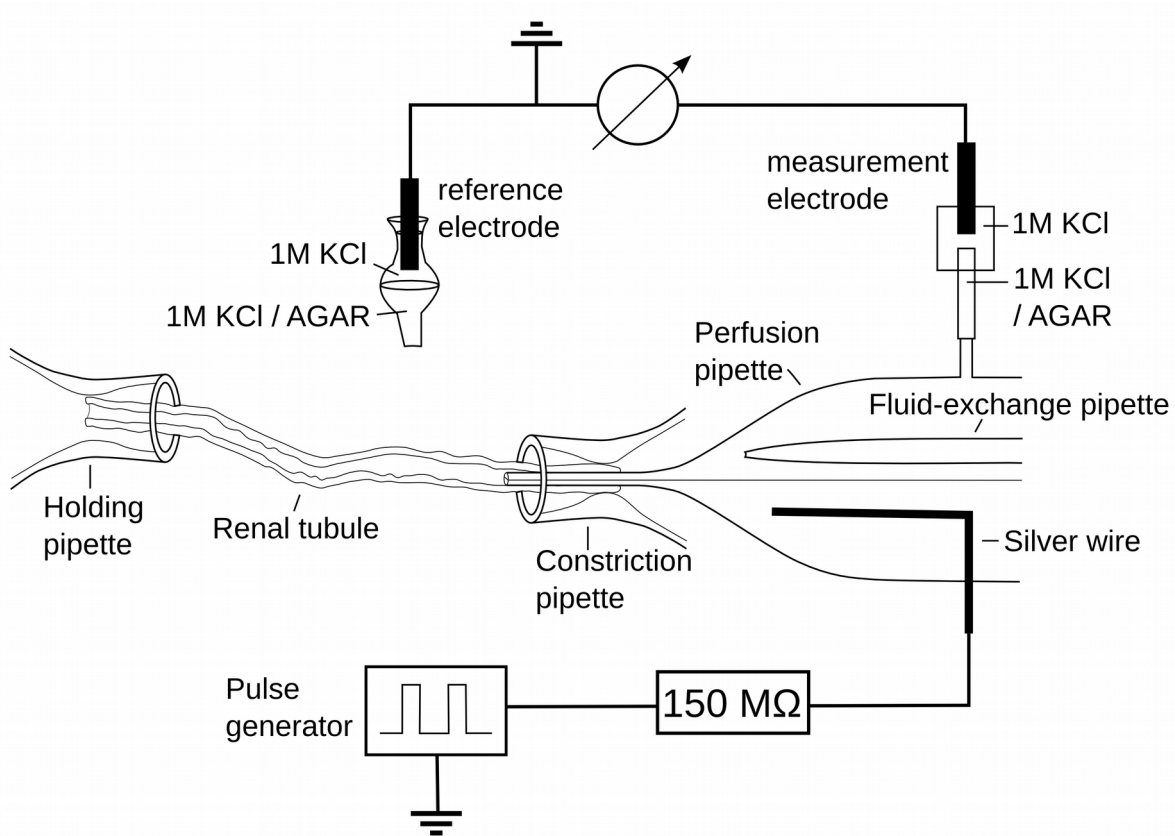


Figure 8: Experimental setup to measure transepithelial voltages.

The injection of a known current allows the calculation of transepithelial resistance. The system is formed by several glass pipettes shaped to hold and perfuse renal tubules, and to permit fluid exchange.

5.5. Equations for the calculation of transepithelial and paracellular parameters

Transepithelial resistance

The transepithelial resistance (R_{te}) was calculated using the cable equation as previously described (Greger, 1981):

$$R_{te} = 2 \sqrt{\pi \varrho \lambda^3 \frac{\Delta V_{te}}{I_o} \tanh\left(\frac{L}{\lambda}\right)} \quad (4)$$

ϱ is the resistivity of the used solution ($\Omega \cdot \text{cm}$). ΔV_{te} is the induced voltage deflection near the perfusion side due to the current injection (I_o). L is the tubule length, and λ is the length

constant. For this calculation, λ was estimated using the mathematical expression presented by Greger (1981) for when the tubule segment is at least 3 times longer than λ :

$$\lambda = \frac{\Delta V_{te} \pi r_m^2}{I_o Q} \quad (5)$$

This way λ became also a selection criterium, the TAL had to be 3 times longer than their calculated value for the length constant for being considered in the analysis.

Equivalent short circuit current

The equivalent short circuit current is the highest current that can exist in an electrical system under short-circuit conditions. In the transepithelial electrical system it implies the current needed to sustain the transepithelial voltage registered, and is a direct indicator of the transepithelial transport across the membrane. It was calculated by the expression:

$$I_{sc} = \frac{V_{te}}{R_{te}} \quad (6)$$

Sodium-chloride permeability ratio

The Goldman-Hodgkin-Katz (GHK) voltage equation for monovalent positive (C^+) and negative (A^-) ion species (Goldman, 1943; Hodgkin & Katz, 1949) was the starting point for the calculation of the sodium-chloride permeability ratio:

$$E_m = \frac{RT}{F} \ln \left(\frac{\sum_{i=1}^n P_{C_i} [C^+]_{out} + \sum_{j=1}^m P_{A_j} [A^-]_{in}}{\sum_{i=1}^n P_{C_i} [C^+]_{in} + \sum_{j=1}^m P_{A_j} [A^-]_{out}} \right); \quad E_m = E_{in} - E_{out} \quad (7)$$

where R is the gas constant, F Faraday constant, and T the absolute temperature in Kelvin.

The diffusion voltage generated by basolateral application of low sodium-chloride solution, after luminal furosemide then has the following form, since the activity of other ions apart from Na^+ and Cl^- is negligible:

$$E_m = \frac{RT}{F} \ln \left(\frac{P_{Na} [Na^+]_{bl} + P_{Cl} [Cl^-]_{ap}}{P_{Na} [Na^+]_{ap} + P_{Cl} [Cl^-]_{bl}} \right) \quad (8)$$

Equation (8) can be transformed to calculate the sodium-chloride permeability ratio out of the direct measurement of the transepithelial potential (E_m) generated by diffusion of Na^+ and Cl^- (diffusion voltage):

$$\frac{P_{Na}}{P_{Cl}} = \frac{[Cl^-]_{ap} - e^u [Cl^-]_{bl}}{e^u [Na^+]_{ap} + [Na^+]_{bl}}; \quad u = \frac{FE_m}{RT} \quad (9)$$

All the measurements were performed at $\sim 37^\circ\text{C}$ (~ 310 K).

Divalent cation-sodium permeability ratio

The use of high calcium and high magnesium solutions on the basolateral side, with control solution plus furosemide running in the TAL lumen, generates a bi-ionic diffusion voltage that permits calculation of the calcium and magnesium paracellular permeability ratio with sodium. The GHK voltage equation cannot be used here as it is a particular solution for monovalent ion species. Therefore we used the ion fluxes approach.

In steady state the sum of the currents of all ions through a membrane is equal to 0:

$$0 = \sum_{i=1}^n I_i \quad (10)$$

The experimental solutions were made in a way that only the activity of Na^+ , Cl^- , and Ca^{2+} or Mg^{2+} (X) was appreciable (more than 3 ions is not helpful with this approach):

$$0 = I_{Na} + I_{Cl} + I_X \quad (11)$$

The individual current of an ion x is defined by the GHK flux equation (Goldman, 1943; Hodgkin & Katz, 1949), where Z is its valence, and P its absolute permeability:

$$I_x = P_x Z_x^2 E_m \frac{F^2}{RT} \frac{[X]_{in} - [X]_{out} e^{-Z_x u}}{1 - e^{-Z_x u}}; \quad u = \frac{FE_m}{RT}; \quad E_m = E_{in} - E_{out} \quad (12)$$

Given x as a divalent cation (i.e. Ca^{2+} or Mg^{2+} for the interest of this dissertation), it is possible to substitute equation (12) in (11) for Na^+ , Cl^- , and X^{2+} , and isolate P_x/P_{Na} :

$$\frac{P_x}{P_{Na}} = \left(\frac{P_{Na}}{P_{Cl}} \right)^{-1} \frac{(e^u + 1)([Cl^-]_{ap} - e^u [Cl^-]_{bl}) - (e^u + 1)(e^u [Na^+]_{ap} - [Na^+]_{bl})}{4(e^{2u} [X^{2+}]_{ap} - [X^{2+}]_{bl})} \quad (13)$$

For this calculation is necessary to have done first a diffusion voltage step to calculate P_{Na}/P_{Cl} .

Absolute paracellular permeabilities for Na^+ , Cl^- , Mg^{2+} , and Ca^{2+}

As presented in results (see 4.1) it is possible to calculate the absolute paracellular permeability to Na^+ in the TAL using the “simplified Kimizuka-Koketsu equation” (Van Itallie *et al.*, 2001; Günzel *et al.*, 2009):

$$P_{Na} = G_r \frac{RT}{F^2} \frac{1}{[NaCl]_{ctrl} \left(1 + \frac{P_{Cl}}{P_{Na}} \right)} \quad (14)$$

The absolute permeability to Cl^- was obtained multiplying the result of equation (14) by the reverse of the result of equation (9):

$$P_{Cl} = P_{Na} \left(\frac{P_{Na}}{P_{Cl}} \right)^{-1} \quad (15)$$

Likewise, absolute permeabilities for Ca^{2+} and Mg^{2+} were calculated multiplying the results of equation (13) for Ca^{2+} and Mg^{2+} by P_{Na} :

$$P_x = P_{Na} \frac{P_x}{P_{Na}} \quad (16)$$

5.6. Western blot

Gels

The separation of proteins by electrophoresis was performed using continuous polyacrylamide gels loaded with sodium dodecyl sulfate (SDS-PAGE) to maintain polypeptides in a denatured state. The gel have two different portions: the resolution gel, to separate the proteins by size, and the stacking gel built on top of the resolution gel to concentrate the proteins. The stacking gels were made using 6.5% polyacrylamide for Cld10 and Cld19, and 4% polyacrylamide for Cld16 and NKCC2 (Table 2). The resolving gels were made using 15% polyacrylamide for Cld10 and Cld19, and 8% for Cld16 and NKCC2 (Table 2).

Collection of samples

The samples for Western blotting were collected from enzymatically assisted isolated TAL. Approximately 50 TALs were sorted for every sample and stored at -80°C in 15-20 µl sorting solution + 5 µl of 5x Laemmli (Table 3). The amount of material in each sample was controlled by number of tubules and by visual estimation of total volume. A picture taken of the first sample containing exactly 50 TALs of an average of 350-400 µm of length was used as standard, and all subsequent samples were compared to it. This was done as a way to have a similar amount of material per sample, as with those little amounts of tissue a total protein determination was unrealizable.

Immunoblotting and bands detection

All the aliquots were incubated at 56°C for 30 minutes in an Eppendorf ThermoStat 5320 dry block heater, and later centrifuged briefly (3 consecutive spin down shocks) in a bench centrifuge (SPROUT™, HEATROW Scientific® LLC, Illinois, USA), before being loaded into the wells of an electrophoresis gel aside with 5µl of protein marker (Page Ruler Prestained Protein Ladder, #26619, Thermo-Scientific, Germany). The electrophoresis and the posterior transfer step were executed in a Bio-Rad Mini PROTEAN® Tetra System (Bio-Rad Laboratories GmbH, Munich, Germany). The gel was already positioned in the holder and placed into the chamber

containing 1L of electrophoresis buffer (Table 3). The electrophoresis was then run at 100 V for approximately 1h.

Table 2: Composition of the two parts of the SDS-PAGE.

	Resolving gel (2 gels)		Stacking gel (2 gels)	
	8%	15%	4%	6.5%
Acrylamid (40%)	4.0 ml	7.5 ml	1.0 ml	1.63 ml
Resolving gel buffer 4x (Table 3)	5.0 ml	5.0 ml	-	-
Stacking gel buffer 4x (Table 3)	-	-	2.5 ml	2.5 ml
Deionised H ₂ O	6.0 ml	7.30 ml	6.4 ml	5.77 ml
Ammonium persulfate (APS)	150.0 µl	150.0 µl	75.0 µl	75.0 µl
Tetramethylethyldiamine (TEMED)	60.0 µl	60.0 µl	30.0 µl	30.0 µl

The proteins were transferred to a Bio-Rad nitrocellulose membrane (0.45 µm pore size). The nitrocellulose membrane and 4 pieces of paper filter were first cut to a similar size of the gel and soaked in transfer buffer (Table 3) for 15 minutes. The gel was carefully recovered and the stacking gel discarded. To transfer the proteins, the resolving gel was placed next to the nitrocellulose membrane, covered at both sides with 2 paper filters, in a Bio-Rad transfer holder and put back into the chamber with 1L of transfer buffer and a cool-pack stored previously at -80°C. A voltage of 100 V was applied across the sandwich for 1h, with the anode on the side of the nitrocellulose membrane. For the transfer the Bio-Rad system was placed on ice to avoid overheating.

The nitrocellulose membrane was then placed in 5% (w/v) skimmed powdered milk in TBS-Tween on a horizontal shaker at 30 rpm for 1h to block the remaining protein binding sites of the membrane. It was washed subsequently 3 times with TBS-Tween (Table 3) for 10 minutes. After this procedure, the primary antibody (Table 4) was added and incubated overnight at 4°C on a horizontal shaker at 30 rpm.

Table 3: Solutions related to the Western blotting procedure.

	Laemmli (5x)	Resolving gel buffer (4x)	Stacking gel buffer (4x)	Electro- phoresis buffer	Tansfer buffer	TBS-Tween
Tris	300 mM	1.5 M	0.5 M	30 mM	20 mM	80 mM
NaCl	-	-	-	-	-	150 mM
DTT	500 mM	-	-	-	-	-
SDS	10% (w/v)	0.4% (w/v)	0.4% (w/v)	0.1% (w/v)	-	-
Bromophenol blue	Until it is colored	-	-	-	-	-
Glycerol (100%)	50% (v/v)	-	-	-	-	-
Glycine	-	-	-	200 mM	192 mM	-
Methanol (100%)	-	-	-	-	20% (v/v)	-
Tween 20	-	-	-	-	-	0.05% (v/v)
pH	6.8	8.8	6.8	-	-	7.6

TBS, Tris-buffered saline; DTT, dithiothreitol; SDS, sodium dodecyl sulfate; Tween 20, polysorbate 20.

The next day the nitrocellulose membrane was washed again 3 times in TBS-Tween for 10 minutes before adding the secondary antibody (Table 4). The membrane was incubated for 1h with the secondary antibody, always shaking at 30 rpm. After washing 4 times with TBS-Tween for 10 minutes the membrane was ready for detection.

The detection was done in a Bio-Rad ChemiDoc MP system. The membrane was carefully covered with the Amersham ECL Select™ Western Blotting reagent for sensitive band detection. Images of the membrane were taken using the chemiluminescent and the colorimetric protocols of acquisition of the Image Lab 5.0 (Bio-Rad Laboratories), to have the protein bands and the marker respectively.

After detection of the bands of the protein of interest (Cld10, Cld16, Cld19, and NKCC2) the nitrocellulose membrane was recovered, washed for three more times in TBS-Tween and incubated overnight with the anti-β-Actin primary antibody. The entire procedure was then

repeated to obtain β -Actin bands as loading control. The bands were analyzed with Image Lab 5.0 (Bio-Rad Laboratories). Each band intensity from the protein of interest normalized to the corresponding β -Actin band in the same sample.

Table 4: Primary and secondary antibodies used in the Western blots.

Primary antibody	Origin	Concentration (in 1% (w/v) BSA in TBS-T)	Producer
anti-Claudin 10	Mouse	1:1000	Thermo Scientific GmbH, Schwerte, Germany, #415100
anti-Claudin 16	Rabbit	1:2000	gift from Dr Jianghui Hou, Washington University, St. Louis
anti-Claudin 19	Rabbit	1:2000	gift from Dr Jianghui Hou, Washington University, St. Louis
anti-NKCC2	Guinea Pig	1:10000	gift from Dr Kerim Mutig, Charité, Berlin
anti- β -Actin	Rabbit	1:1000	Cell Signaling Technology Inc., Danvers, USA, # 4967
Secondary antibody			
anti-Mouse IgG HRP	Sheep	1:10000	GE Healthcare Europe GmbH, Freiburg, Germany, NA 931
Anti-Guinea Pig IgG HRP	Donkey	1:10000	DIANOVA GmbH, Hamburg, Germany, 706-035-148
anti-Rabbit IgG HRP	Goat	1:50000	DIANOVA GmbH, Hamburg, Germany, 111-035-144

HRP, Horseradish Peroxidase-Conjugated Antibody.

5.7. Food for the diets

Mineral adjusted diets were bought from SSNIFF (SSNIFF Spezialdiäten GmbH, Germany) for the calcium and magnesium diets. The food, coming in pellet form, contained 0.90% of calcium and 0.23% of magnesium for the control diet. The high calcium and high magnesium diets were 5 times higher in calcium and magnesium respectively, with the low diets having less than 0.06% of calcium and less than 0.03% magnesium (Table 5).

Table 5: Calcium and magnesium diets composition

Diet:	Control	High calcium	Low calcium	High magnesium	Low magnesium
Calcium	0.90%	5.00%	<0.06%	0.90%	0.90%
Phosphates	0.60%	0.60%	0.60%	0.60%	0.60%
Magnesium	0.23%	0.23%	0.23%	1.10%	<0.03%
Sodium	0.20%	0.20%	0.20%	0.20%	0.20%
Chloride	0.35%	0.35%	0.35%	1.10%	0.35%

SSNIFF pulverized control food was used for the water-load and water restricted diets. The diets were designed using as basis the daily food and water intake preferences for the C57BL/6J mouse strain of approximately 5g of food and 7.8 ml of water per 30g body weight (Bachmanov *et al.*, 2002). Water containing 1% of Agar and pulverized food were mixed to make a jelly food. For the water-load diet 3 times the preferred water intake was used. The water-restricted diet was made to fit the daily requirement proportion of water and food.

5.8. Animals and experimental design used for the studies performed in this thesis

5.8.1. Calcium and magnesium diets

The divalent cations diet experiments were completed on 5 to 8-week-old young female C57BL/6J mice breed in the Viktor-Hensen animal house of the University of Kiel. The animals were fed *ad libitum* with the required diets and housed under a 12 hours light cycle at room temperature and standard humidity. After 8 days, non-recovery experiments were performed and both kidneys were then taken for micro-dissection, using the enzymatically assisted procedure described before. The calcium diet experiments with control, low, and high-calcium diets extended for a term of 3 weeks, where 8 to 11 mice per diet group were randomly used. Later, the magnesium diet experiments including control, low, and high-magnesium diets were carried out in a lapse time of 2 weeks, using 8 animals per diet group.

From each animal weight and length from nose to the beginning of the tail was recorded at the final day, and blood serum sample, spot urine, tail tip, and kidney portions were collected and stored at -80°C . Kidney portions were deep frozen in liquid nitrogen before storage at -80°C . Serum and urine were analyzed for electrolytes and creatinine concentrations, and fractional excretions were calculated. Tail tip and kidney portions were kept for any possible further examination.

Experimental protocol

Enzymatically suspended TAL were microperfused with control solution in a running bath of control solution. Once steady, and if the tubule fulfilled the quality criteria for the experiment (see below), the luminal fluid was exchanged by control solution containing furosemide ($50\ \mu\text{M}$). After the transepithelial voltage stabilized at almost $0\ \text{mV}$ the bath solution was changed to low sodium-chloride solution to measure the respective diffusion voltage. The interest here is the biophysical response of the intercellular junction to evaluate the paracellular properties of the TAL, and not the possible readjustment of the cell membrane to the new situation. Later, after a recovery step with control solution, the tubules were challenged with high-magnesium solution followed by high-calcium solution for about 2 minutes each, before restoring to control solution and rinse out of furosemide. Figure 9 shows an original trace made with this protocol.

5.8.2. AVP stimulation

Water-restricted, and water-loaded mice

8 to 10-week-old C57BL/6J mice breed in the Viktor-Hensen animal house of the University of Kiel were fed for 5 days with water-restricted diet or with water-loaded diet. The animals were weighed every day to control they were growing normally, and the corresponding amount of jelly-food plus 5-10% was added to the cage. 12 animals from each group were used for electrophysiological measurements of transepithelial transport and paracellular properties. Mechanically dissected TALs were microperfused using the same protocol as described before for the calcium and magnesium diets (Figure 9). Another 12 animals per diet were used to

collect TALs for Western blot as described before. Urine osmolality was determined by the freezing-point method in a cryoscopic osmometer OSMOMAT 30 (Gonotec GmbH, Germany).

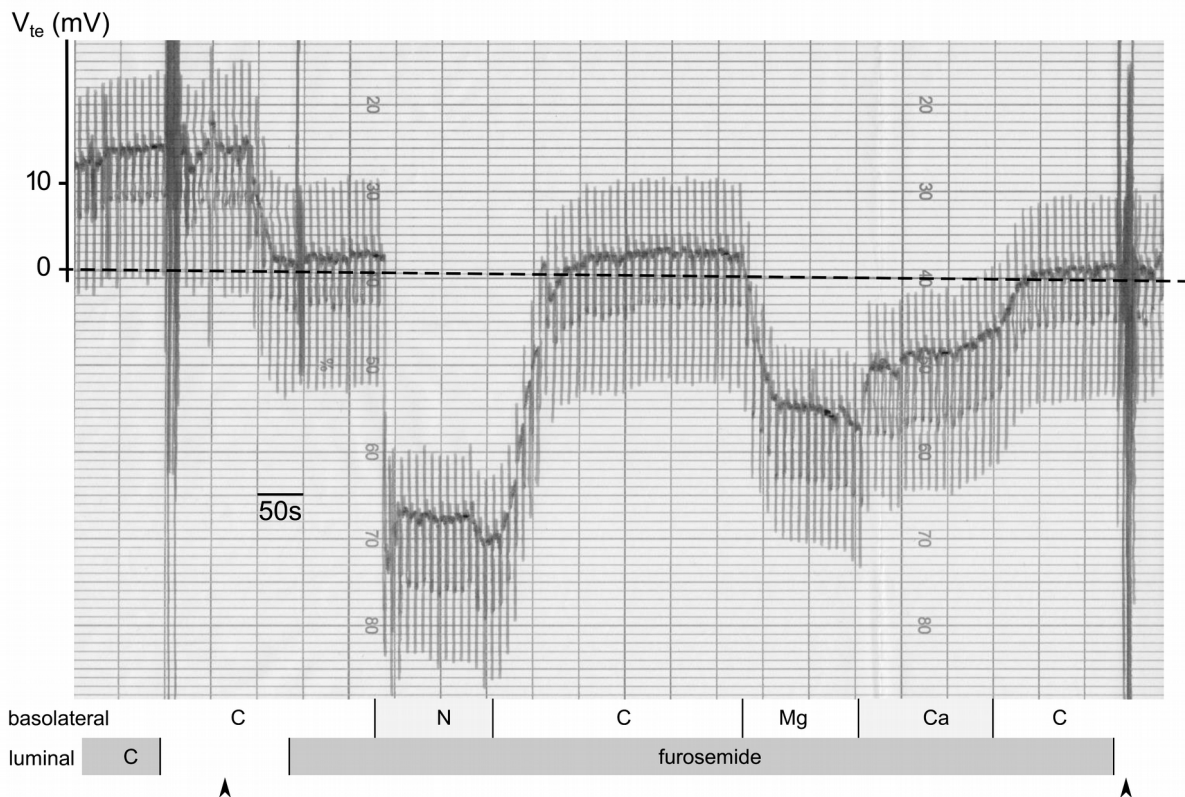


Figure 9: Original recording of the transepithelial voltage in a TAL for a mouse on high calcium diet. The figure illustrates the operational protocol during the experiment. C, control solution; N, low sodium-chloride solution; Mg, high magnesium solution; Ca, high calcium solution; furosemide, 50 μ M furosemide in control solution. The arrow heads indicate luminal fluid exchange. The dashed line is the zero line following a slightly negative baseline shift.

Acute AVP stimulation

TALs from SV129/BL6 mixed background mice of 5 to 10 weeks old were mechanically dissected for microperfusion and acute stimulation with AVP. These experiments were performed in Aarhus, Denmark, as a collaboration with Prof. Dr. Jens Leipziger from the Department of Biomedicine, Physiology and Biophysics of the Aarhus University. The animals were bred in the animal facility of the department in Aarhus.

Microperfused TALs were equilibrated under control conditions for approximately 6 minutes before luminal fluid was exchanged from control to furosemide (50 μ M) solution. A diffusion voltage was then generated by basolateral change of control to low sodium-chloride solution. After that, the conditions were step wise recovered to the starting point: low sodium-chloride was first rinsed with control solution in the basolateral side, and then furosemide was rinsed with control solution from the luminal side. The tubules were let to recover for 5 to 6 minutes and then a new solution containing 10 nM AVP (94836, SIGMA-ALDRICH Co. LLC, USA) in control solution was run at the basolateral side for 12 minutes. Only those tubules that were steady were stimulated with AVP. After the stimulation time, the tubules were again perfused with furosemide solution and a diffusion voltage induction was performed to compare pre and post-stimulation effect. Figure 10 shows an original record of one of these experiments.

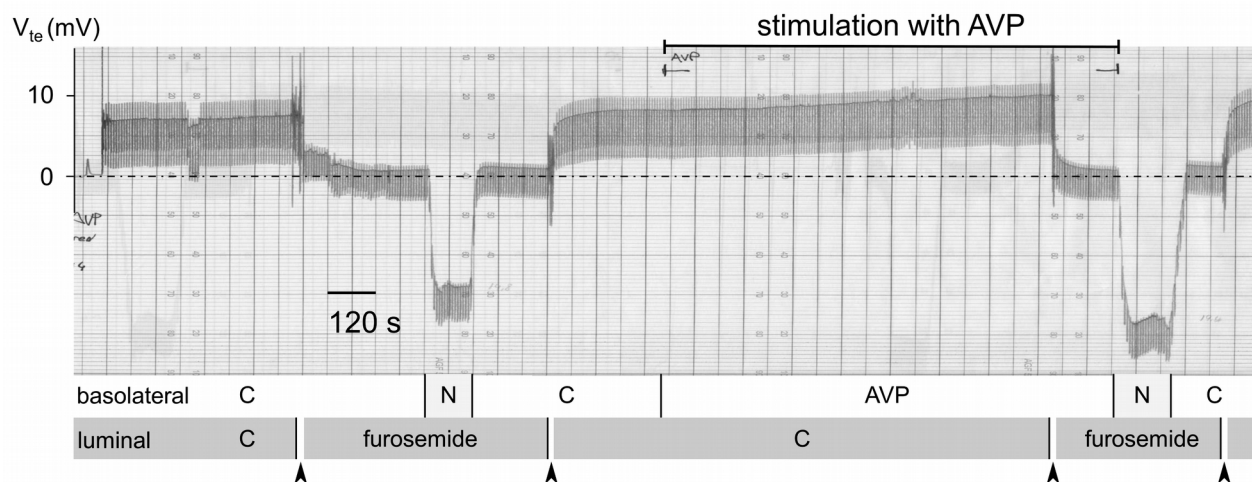


Figure 10: Original paired AVP stimulation trace record.

C, control solution; N, low sodium-chloride solution; AVP, 10 nM AVP in control solution; furosemide, 50 μ M furosemide in control solution. Arrow heads indicate luminal fluid exchange. The dashed line is the zero line.

5.8.3. Cld10 KO, Cld16 KO, and Cld10/16 double KO

The Cld10/16 double KO mouse model was generated by Dr. Tilman Breiderhoff crossbreeding the Cld16KO mouse model and the Cld10 kidney specific conditional knock-out mouse model previously described (Will *et al.*, 2010; Breiderhoff *et al.*, 2012). C57BL/6J mice homozygous for

the floxed *Cldn10* allele and ksp-Cre positive (*Cldn10^{fl/fl} Cre⁺*, here Cld10KO) were bred with C57BL/6J mice homozygous for the deleted *Cld16* allele (*Cld16^{-/-}*, here Cld16KO). The resulting double heterozygous mice were then inbred to generate *Cld16^{-/-} Cldn10^{fl/fl} Cre⁺* animals (dKO).

TALs from 7 to 9-week-old mice were dissected mechanically for microperfusion. The experiments were performed following the same protocol as with the calcium and magnesium diets (Figure 9) for the calculation of the transepithelial and paracellular properties.

5.8.4. Treatment with suberanilohydroxamic acid (SAHA)

Young 7 to 10-week-old C57BL/6J mice were treated by gavage with a 0.05% (w/v) preparation of suberanilohydroxamic acid (SAHA) (sc-220139, Santa Cruz Biotechnology®, Inc.) in 0.9% saline solution. The animals received 0.1 mg of SAHA per 20g body weight (5mg/kg-200µl). Four hours later, no-recovery experiments were performed. TALs were mechanically dissected for microperfusion. The experimental protocol used to estimate the transepithelial and paracellular properties of microperfused TALs was the same as the one described before for the calcium and magnesium diets (Figure 9).

5.8.5. Sorting-protein-related receptor knock-out mice

Sorting-protein-related receptor knock-out BALB/c mice (*SORLA^{-/-}*) (Reiche *et al.*, 2010) were provided by Dr. Mutig. Age and sex matched wild-type Balb/c mice were ordered from Charles River for being used as control. Freshly mechanically isolated TALs were microperfused (time 0h). Additionally enzymatically isolated TAL were measured after incubation for 1 hour in incubation solution with cyclosporin A (5 nM) or vehicle (0.006% DMSO).

The tubules were first perfused with control solution in a control solution running bath. Then basolateral solution was changed to low chloride solution (Table 1, F), and finally luminal solution was also exchanged to low chloride solution (Figure 11).

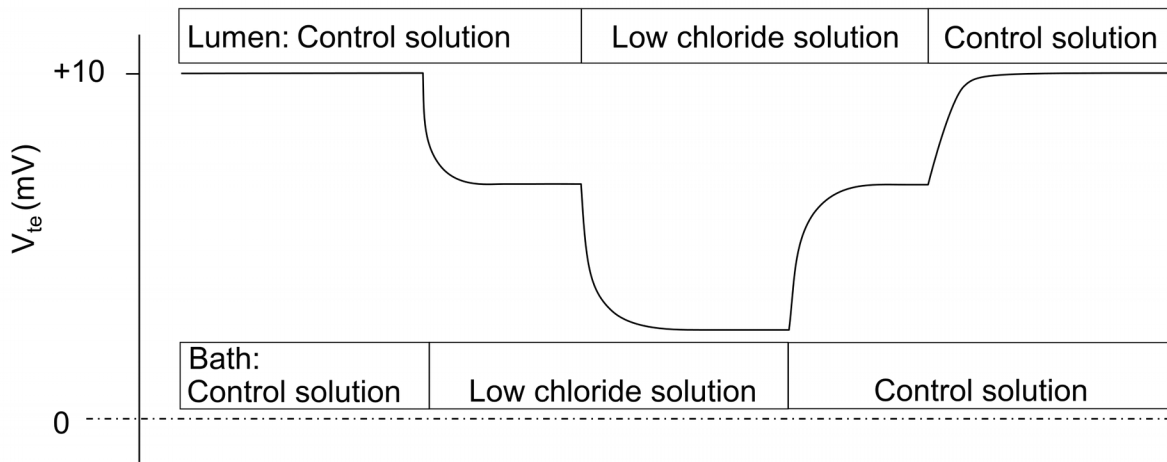


Figure 11: Schematic experimental protocol with low chloride perfusion and bath.

5.8.6. Mineralocorticoid receptor-deficient mice

Ronzaud *et al.* (2007) generated the mineralocorticoid receptor (MR) deficient mouse model with a mixed genetic background of FVB/N and C57Bl/6. Those animals were engineered to have a conditional MR allele (MR^{lox}), and Cre recombinase knock-in under the control of the AQP2 promoter. $MR^{lox/lox}$ AQP2Cre ($MR^{AQP2Cre}$) mice were deficient for MR in those cells that expressed AQP2.

Males $MR^{lox/lox}$ AQP2^{Cre/WT} ($MR^{AQP2Cre}$) and females $MR^{lox/lox}$ AQP2^{WT/WT} mice (control mice) were mated in the Viktor-Hensen animal facility to produce new $MR^{AQP2Cre}$ and control mice. Mice were tailed at birth and genotyping was performed to identify the $MR^{AQP2Cre}$ mice. TAL from old 52 to 58-week-old mice were obtained enzymatically for microperfusion. The experiments were performed following the same protocol as the one mentioned before for calcium and magnesium diets (Figure 9).

5.8.7. Quality criteria

The electrophysiological measurements in a perfused isolated TAL were conducted only when:

- there were no obvious leaks in the tubule. At least, not close to the perfusion pipette extreme. In case of an observable leak in the tubule, the length was measured from the tip of the perfusion pipette until the leak.
- the tubules were completely open at the free end.
- the perfused tubule was not deformed by pressure during perfusion.
- the transepithelial voltage was steady.

If the previous criteria were fulfilled, the results were considered for the analysis when:

- the tubular length was longer than 3 times λ (shorter tubules would compromise the accuracy of the measurements).
- there were no drastic changes in diameter during the experiment nor over-perfusion (diameters around 10 μm were usually the common values).
- the calculated transepithelial resistance was in between 2.5 and 40 $\Omega\cdot\text{cm}^2$.
- the initial transepithelial voltage was higher than 5 mV (lower V_{te} would be an indication of a damaged tubule).
- the absolute value of the diffusion voltage was lower than 35 mV.
- the tubule responded to furosemide treatment: an obvious reduction in V_{te} and I_{sc} .

5.9. Ethical approval

All experiments were performed in accordance with the German law on animal protection and approved by the local authorities.

5.10. Statistics

The Shapiro-Wilk's normality test was used to assess whether normality premise could be rejected from our data. Homoscedasticity was evaluated using Levene's test.

When comparing directly two samples for the null hypothesis that both come from the same population, Student's t-test of mean comparison was used if normality and homogeneity of variance could be assumed. When normality or homoscedasticity premises were rejected, and transformation of the data proved useless, the nonparametric Mann-Whitney-Wilcoxon rank-sum test was used instead. Paired t-test or paired Wilcoxon test were performed when analyzing the AVP paired experiments.

Kruskal-Wallis method or ANOVA were used when normality and homoscedasticity were not rejected, for testing differences between three or more samples. As post-hoc when differences were revealed Dunn's test and paired-wise Student's test were used, respectively. For both alternatives post-hoc the Holm-Bonferroni correction for multiple comparisons was used.

Student's t-test for directly comparing two samples was done in Microsoft Excel 2010. All the other methods here described were executed in R, version 3.1.0, using the interface RStudio 0.98.1103.

6. Results

6.1. Simplified equation for the calculation of absolute paracellular permeabilities

In the present dissertation the calculation of electrophysiological variables is the main tool to evaluate the transport of ions across the TAL membrane. To calculate absolute ion permeabilities we used the so-called “simplified Kimizuka-Koketsu equation”. This equation, although already cited in the literature, was impossible to be tracked back to its development. It is not explicitly documented in Kimizuka-Koketsu’s original paper (Kimizuka & Koketsu, 1964). Cross-citations or at most citations of Kimizuka-Koketsu (1964) are all citations available in the literature applying the equation (Van Itallie *et al.*, 2001; Kahle *et al.*, 2004; Hou *et al.*, 2005, 2008; Günzel & Yu, 2009; Yu *et al.*, 2009; Günzel *et al.*, 2009; Englund *et al.*, 2012; Gong *et al.*, 2012; Dimke *et al.*, 2013). For that reason, I redeveloped the “simplified Kimizuka-Koketsu equation” based on the formulations presented in Kimizuka-Koketsu (1964).

Kimizuka-Koketsu (1964) make use of the definitions of ion flux and chemical potential based on the thermodynamics of irreversible processes to establish the basis of their development. They attempt in that work to obtain simple mathematical statements for the calculation of the ion flux, membrane potential and membrane conductance in cell membranes. It is not my intention to repeat here their formalisms, were they obtain equations similar to those previously presented by Goldman, Hodgkin, Katz, and Ussing among others. It is important to mention that their solutions cannot be applied directly to the transepithelial movement of ions for the estimation of the absolute permeability, if precalculated ion fluxes values are not available. Nevertheless, Kimizuka-Koketsu (1964) obtained an interesting solution for the membrane conductance. They define membrane conductance in resting state as the geometrical mean of the *in* and *outflow* conductance, a definition differing from the constant field theory:

$$G_r = (G_{+r} * G_{-r})^{1/2} \quad (17)$$

In this equation r refers to the resting state, and + and – refer to the outward and inward currents respectively.

In general, their solutions for G_+ and G_- obtained by deriving the total current with $G=(G_+*G_-)^{1/2}$, and assuming ions valences of 1 for simplicity, were:

$$G_+ = \frac{F^2}{RT} \sum_{c,a} \left(P_c C_{ci} e^{\frac{\eta_{ci}}{2RT}} + P_a C_{ao} e^{\frac{\eta_{ai}}{2RT}} \right) \quad (18)$$

$$G_- = \frac{F^2}{RT} \sum_{c,a} \left(P_c C_{co} e^{\frac{\eta_{ci}}{2RT}} + P_a C_{ai} e^{\frac{\eta_{ai}}{2RT}} \right) \quad (19)$$

where c and a refer to the cations and the anions, and o and i to outside and inside, respectively. $\eta_{\alpha i}$ (α including all ion species) is the energy of interaction, P_{α} , the membrane permeability to ion α , C_{α} , the concentration, R , the gas constant, F , Faraday constant, and T the absolute temperature in Kelvin.

Under the assumption that for all free ions $\eta_{\alpha i} = 0$ in equations (18) and (19) (i.e., specific interactions will only occur in the membrane) the voltage equation presented by Kimizuka & Koketsu (1964) would be reduced to the same equation presented by Goldman (1943) and by Hodgkin & Katz (1949) (see Materials and methods). On this conditions, G_{+r} and G_{-r} in steady state equal:

$$G_{+r} = \frac{F^2}{RT} \sum_{c,a} (P_c C_{ci} + P_a C_{ao}) \quad (20)$$

$$G_{-r} = \frac{F^2}{RT} \sum_{c,a} (P_c C_{co} + P_a C_{ai}) \quad (21)$$

By creating experimental conditions where only Na^+ and Cl^- are relevant at both sides of the membrane, equations (20) and (21) can be written as:

$$G_{+r} = \frac{F^2}{RT} (P_{Na} [Na^+]_i + P_{Cl} [Cl^-]_o) \quad (22)$$

$$G_{-r} = \frac{F^2}{RT} (P_{Na} [Na^+]_o + P_{Cl} [Cl^-]_i) \quad (23)$$

Replacing equation (22) and (23) in (17) and isolating P_{Na} leads to:

$$G_r = \sqrt{\left(\frac{F^2}{RT}\right)^2 (P_{Na} [Na^+]_i + P_{Cl} [Cl^-]_o)(P_{Na} [Na^+]_o + P_{Cl} [Cl^-]_i)}$$

$$G_r = P_{Na} \frac{F^2}{RT} \sqrt{\left([Na^+]_i + \frac{P_{Cl}}{P_{Na}} [Cl^-]_o\right)\left([Na^+]_o + \frac{P_{Cl}}{P_{Na}} [Cl^-]_i\right)}$$

$$P_{Na} = G_r \frac{RT}{F^2} \frac{1}{\sqrt{\left([Na^+]_i + \frac{P_{Cl}}{P_{Na}} [Cl^-]_o\right)\left([Na^+]_o + \frac{P_{Cl}}{P_{Na}} [Cl^-]_i\right)}} \quad (24)$$

If the same NaCl solution is present at both sides of the membrane while calculating G_r :

$$[Na^+]_i = [Na^+]_o = [Na^+]_{ctrl}$$

$$[Cl^-]_i = [Cl^-]_o = [Cl^-]_{ctrl}$$

Equation (6) can be reduced to:

$$P_{Na} = G_r \frac{RT}{F^2} \frac{1}{[Na^+]_{ctrl} + \frac{P_{Cl}}{P_{Na}} [Cl^-]_{ctrl}} \quad (25)$$

Finally, taking in account that in this solution sodium and chloride activities are very similar to each other, it is possible simplify equation (25) even more:

$$[Na^+]_{ctrl} \simeq [Cl^-]_{ctrl} = [NaCl]_{ctrl}$$

$$P_{Na} = G_r \frac{RT}{F^2} \frac{1}{[NaCl]_{ctrl} \left(1 + \frac{P_{Cl}}{P_{Na}}\right)} \quad (26)$$

Equation (26) is the “simplified Kimizuka-Koketsu equation” applied to the calculation of absolute permeability to Na⁺ in this work.

Methodological note: all the ion “concentrations” represented in this section should be considered as ion activities; which is consistent with the no interaction assumption.

6.2. Electrophysiological properties of enzymatically prepared TAL from mice of different ages

The properties of freshly enzymatically dissected TAL at different groups of age were analyzed in a pilot study. Three groups were formed using C57BL/6J mice: a young group representing ages between 6 and 13 weeks old, a second group including mice being 20 to 34 weeks old, and a third group including older mice born 66 to 77 weeks before the experiments. The electrophysiological properties of 24, 13, and 17 TAL from these animals, respectively, were studied by micro-perfusion. A fourth group with data obtained from additional experiments in which TALs were mechanically dissected from C57BL/6J mice (n = 38) was included for comparison. Measurements were done following the same protocol as outlined above. The animals from the mechanically dissected group are in the same age range than those included in the young group.

Interestingly, the transepithelial voltage (V_{te}) generated by the TAL cells, our primary direct measurement and one of the components that drive the paracellular reabsorption, was higher in the TAL from the middle-aged group than V_{te} in tubules from younger and older mice (Figure 12). Not differences among age groups concerning the transepithelial resistance (R_{te}) or the calculated equivalent short circuit current (I_{sc}) were observed (Figure 13).

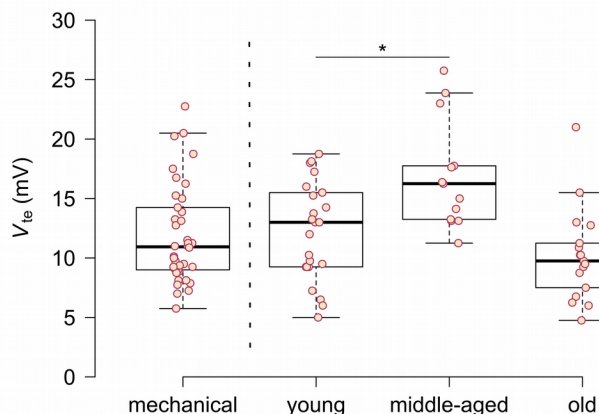


Figure 12: Transepithelial voltage (V_{te}) of mechanically and enzymatically dissected TAL.

The figure shows data from enzymatically dissected TAL from young (young, $n = 24$), adult (middle-aged, $n = 13$), and old mice (old, $n = 17$), or mechanically dissected tubules ($n = 38$) from young mice. *, $p < 0.05$

The paracellular properties also appear not to change with age in this trial. No obvious differences were observed among the age groups in terms of TAL ion selectivity, expressed as the ratio of the permeability to Na^+ and the permeability to Cl^- ($P_{\text{Na}}/P_{\text{Cl}}$), or absolute paracellular permeabilities to Na^+ (P_{Na}) or Cl^- (P_{Cl}) (Figure 14).

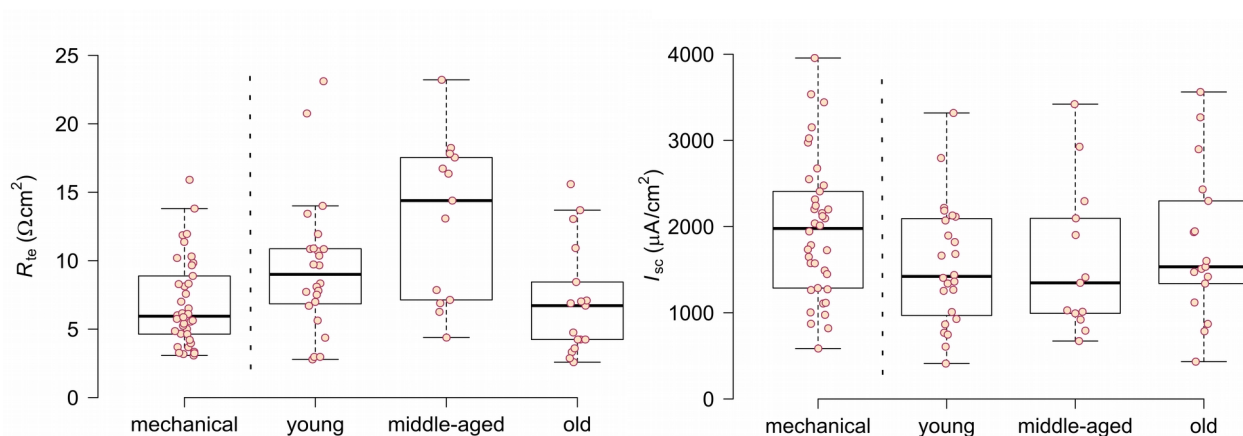


Figure 13: Transepithelial resistance (R_{te}) and equivalent short circuit current (I_{sc}) of mechanically and enzymatically dissected TAL.

The figure shows data from enzymatically dissected TAL from young (young, $n = 24$), adults (middle-aged, $n = 13$), and old mice (old, $n = 17$), or mechanically dissected tubules ($n = 38$) from young mice. $p < 0.05$

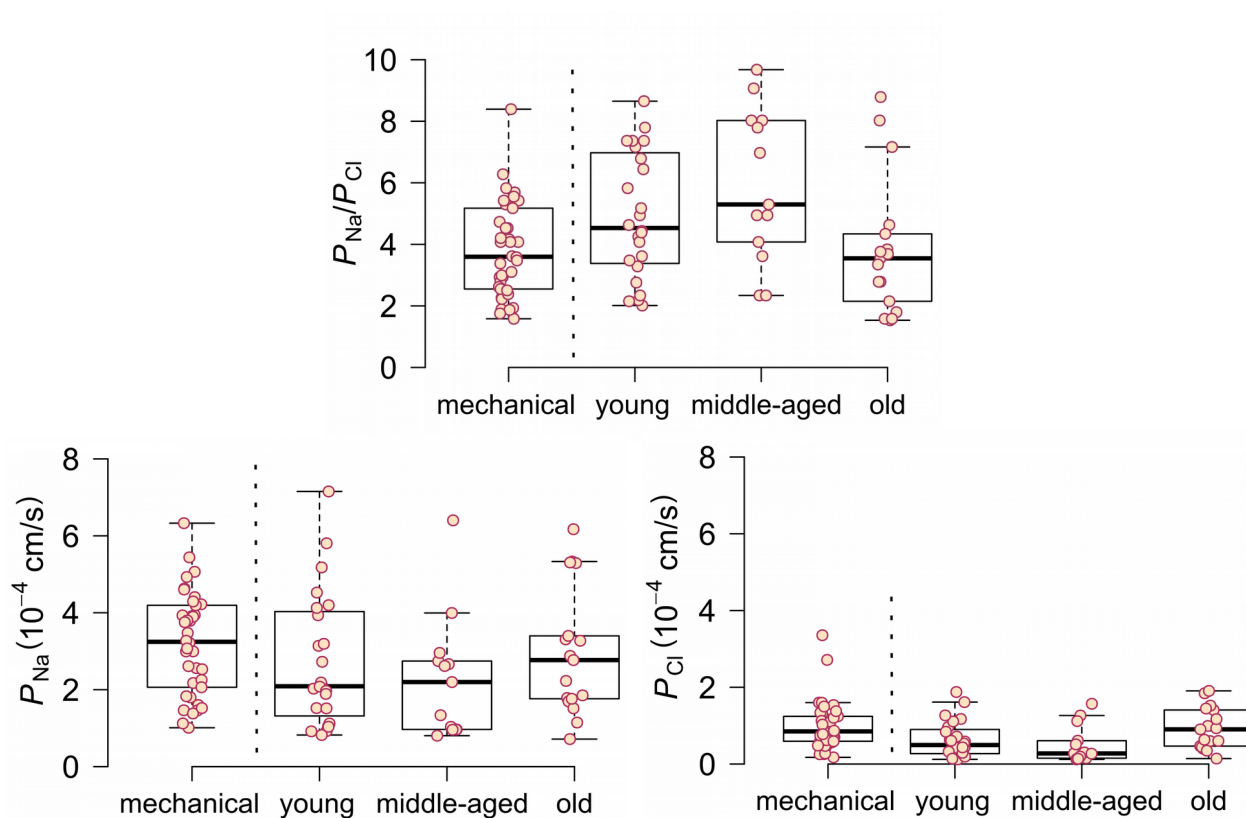


Figure 14: Paracellular properties of mechanically and enzymatically dissected TAL.

The figure shows data from enzymatically dissected TAL from young (young, $n = 24$), adults (middle-aged, $n = 13$), and old mice (old, $n = 17$), or mechanically dissected tubules ($n = 38$) from young mice. $p < 0.05$

6.3. Effects of high and low divalent cation diets on the TAL

In two different approaches groups of young C57BL/6J mice received calcium or magnesium diets to test the physiological effect of changes in the daily intake of divalent cations on the paracellular reabsorption in the TAL. The electrophysiological data from the calcium-diet study are published in *Pflügers Archiv – European Journal of Physiology*, together with qPCR and immunohistochemical data obtained in parallel in our research group.

6.3.1. Control of Ca^{2+} and Mg^{2+} reabsorption in thick ascending limb of Henle's loop in consequence of dietary Ca^{2+}

Elevated plasma Ca^{2+} concentration during high- Ca^{2+} diet

All diets were tolerated well. After 8 days on diet, weight and length of mice were registered and the body mass index was calculated. No significant differences were found regarding any of these indicators among the different groups (Table 6).

Table 6: Metabolic parameters of mice on the calcium diets.

	low- Ca^{2+} diet	control diet	high- Ca^{2+} diet
<i>body parameters</i>			
body weight, g	17.4 ± 0.3	17.8 ± 0.3	18.2 ± 0.6
body length, cm	8.6 ± 0.1	8.8 ± 0.1	8.9 ± 0.1
body mass index, kg/m^2	2.33 ± 0.03	2.31 ± 0.04	2.32 ± 0.03
<i>blood parameters</i>			
Na^+ , mM	155 ± 4	153 ± 1	151 ± 1
K^+ , mM	4.4 ± 0.1	4.2 ± 0.1	4.5 ± 0.1
Cl^- , mM	113 ± 2	109.6 ± 0.7	107.1 ± 0.4 *
Ca^{2+} , mM	2.22 ± 0.02	2.20 ± 0.02	2.41 ± 0.04 *
Mg^{2+} , mM	1.01 ± 0.06	0.97 ± 0.02	0.99 ± 0.03
phosphate, mM	2.4 ± 0.2	2.7 ± 0.2	2.9 ± 0.3
urea, mM	9.6 ± 0.8	11.1 ± 0.9	9.7 ± 0.6
creatinine, μM	9.4 ± 0.4	9.5 ± 0.5	9.4 ± 0.5
hematocrit, %	44 ± 1	44 ± 2	46 ± 1
<i>urine parameters</i>			
FE_{Na} , %	0.7 ± 0.2	0.4 ± 0.1	0.36 ± 0.06
FE_{K} , %	20 ± 3	27 ± 6	17 ± 1
FE_{Cl} , %	0.6 ± 0.2	0.5 ± 0.1	0.40 ± 0.05
FE_{Ca} , %	0.34 ± 0.02	0.6 ± 0.2	2.0 ± 0.4 *
FE_{Mg} , %	19 ± 2	19 ± 2	15 ± 1
$\text{FE}_{\text{phosphate}}$, %	36 ± 5 *	19 ± 4	6 ± 1 *
FE_{urea} , %	49 ± 4	50 ± 6	46 ± 2

n = 5-8; *, p < 0.05

The low- Ca^{2+} diet did not affect blood parameters and the mice managed to maintain a normal Ca^{2+} concentration in plasma (Table 6). The renal function parameters reflected the physiological reaction on Ca^{2+} depletion. During low- Ca^{2+} diet fractional P_i excretion was markedly increased and Ca^{2+} excretion tended to be lower compared to control group (Table 6).

Compared to Ca^{2+} -restricted animals, mice on high- Ca^{2+} diet exhibited a contrary response with respect to renal Ca^{2+} and P_i excretion. Fractional Ca^{2+} excretion increased more than threefold and P_i excretion was reduced to one third (Table 6, Figure 15). Still, the plasma Ca^{2+} level was clearly elevated (Table 6), and a slight decrease in plasma Cl^- was observed. Renal handling of Na^+ , Cl^- and K^+ was not affected as shown by the fractional excretion values.

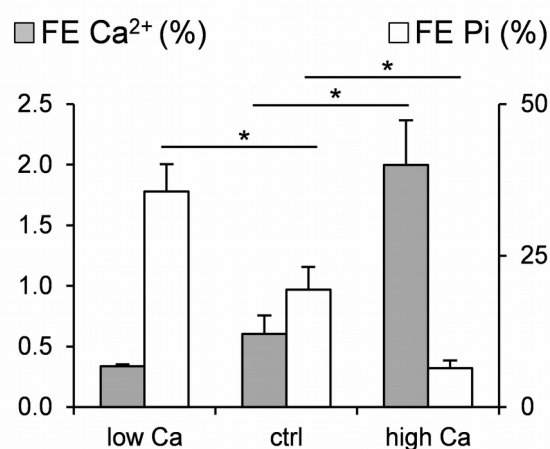


Figure 15: Renal fractional excretion of calcium (left axis) and phosphates (right axis) of mice from low- Ca^{2+} , control, and high- Ca^{2+} diet groups. $n = 5-8$; *, $p < 0.05$

High- Ca^{2+} diet decreased transepithelial voltage and permeabilities to Ca^{2+} and Mg^{2+} in perfused TAL

TAL isolated from all groups revealed distinct lumen-positive transepithelial voltages. Tubules of the low- Ca^{2+} diet group did not show significantly different voltages compared to the control group. On the contrary, high dietary Ca^{2+} led to a considerable reduction of the transepithelial voltage (Figure 16 A), indicating a reduction in the forces that drive the paracellular reabsorption of cations in the TAL. Equivalent short circuit current (I_{sc}), that mainly reflects the net NaCl transport, and transepithelial resistance (R_{te}) did not significantly differ among dietary groups,

but a tendency to decrease with increasing calcium intake is appreciable for the I_{sc} (Figure 16 B, C).

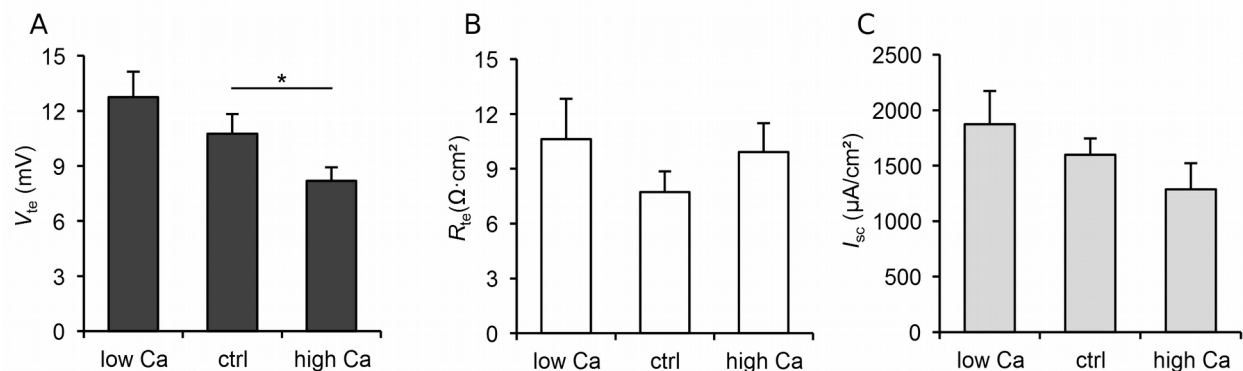


Figure 16: Transepithelial electrical properties determined on isolated and microperfused TAL of mice at low- Ca^{2+} , control or high- Ca^{2+} diet.

A) Transepithelial voltage (V_{te}). B) Transepithelial resistance (R_{te}). C) Equivalent short circuit current (I_{sc}). $n = 17-23$; *, $p < 0.05$

Subsequently, the paracellular ion permeabilities of perfused TAL were determined through measurements of diffusion potentials after inhibiting the NKCC2 activity by luminal exposure to furosemide (Figure 17). TAL obtained from all dietary groups proved to be strongly cation-selective, with permeability ratios of Na^+ and Cl^- ($P_{\text{Na}}/P_{\text{Cl}}$) exceeding a mean value of 4. No significant differences between TAL from mice from the low- Ca^{2+} diet and controls were observed. Conversely, TAL from mice on high- Ca^{2+} diet reacted also by regulating the paracellular properties. In those tubules a slight but yet significant reduction in the NaCl dilution potential (Figure 17 A) was observed, reflecting a reduced $P_{\text{Na}}/P_{\text{Cl}}$ value (Figure 17 B). The high- Ca^{2+} conditions revealed no effect on TAL's absolute paracellular permeabilities to Na^+ or Cl^- , albeit P_{Na} tended to be slightly decreased. In contrast, high dietary intake of Ca^{2+} led to strongly reduced paracellular permeabilities to Mg^{2+} and Ca^{2+} compared to the control group (Figure 17 C). Other results obtained in parallel studies conducted by our research group showed that in the high- Ca^{2+} diet group the expression of Cld10b and Cld14 increased in the TAL tight junctions.

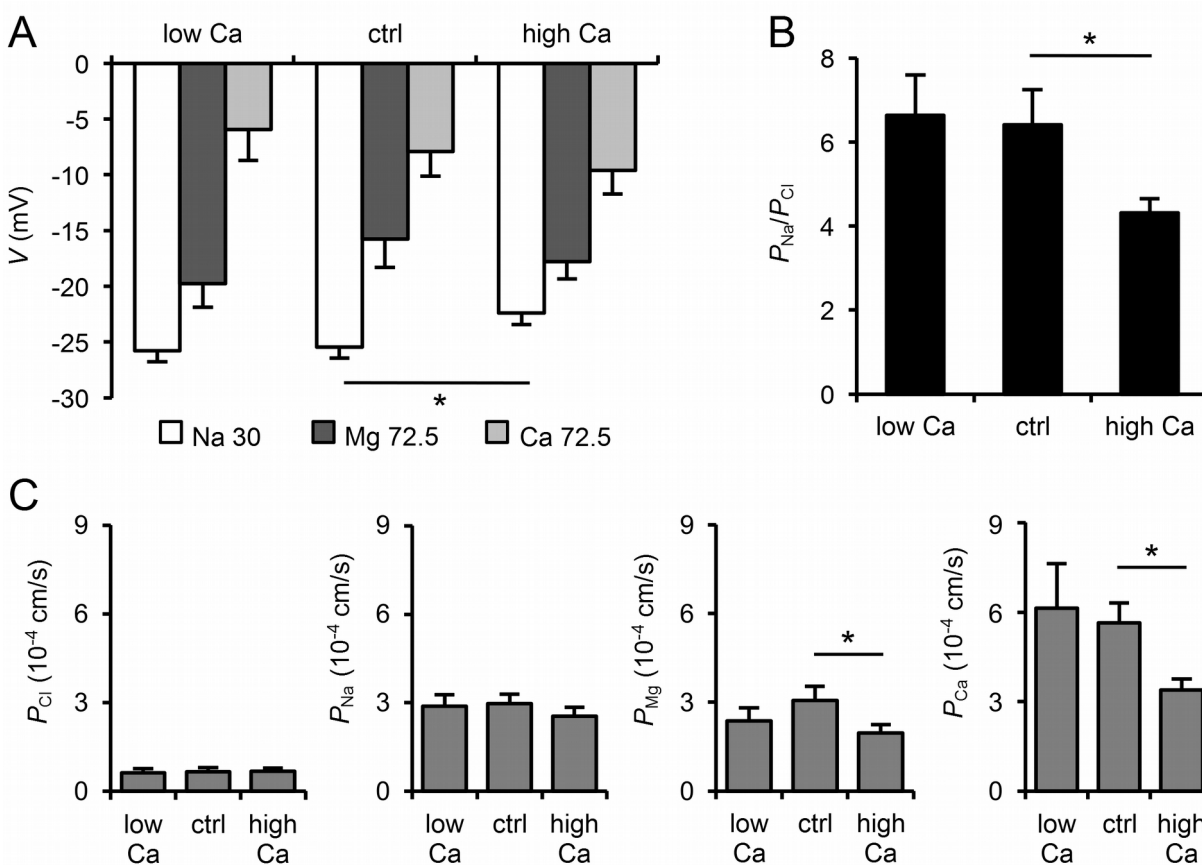


Figure 17: Ex vivo paracellular transport properties of microperfused TAL from the calcium diet groups after inhibition of NKCC2.

A) Diffusion potentials after replacement of the peritubular fluid with low-NaCl (Na 30), high-Mg²⁺ (Mg 72.5), and high-Ca²⁺ (Ca 72.5) solutions. B) Sodium-chloride permeability ratio as an indicator of the cation selectivity. C) Absolute paracellular permeabilities to Cl⁻, Na⁺, Mg²⁺ and Ca²⁺ (P_x). $n = 10-23$; *, $p < 0.05$

6.3.2. Dietary Mg²⁺ does not trigger regulation in the paracellular transport properties of the TAL

Mice were fed low and high magnesium diet to evaluate the possible physiological effect of magnesium on the paracellular pathway of cation reabsorption in the TAL.

Low and high-Mg²⁺ diets affected divalent cation metabolism

The mice tolerated the low-Mg²⁺ and control diets well. The animals on high-Mg²⁺ diet had soft stool, and were smaller and slimmer than the animals in the control group or in the low-Mg²⁺ diet group (Table 7).

Table 7: Metabolic parameters of mice on the magnesium diets

	low Mg ²⁺ diet (n)	control diet (n)	high Mg ²⁺ diet (n)
<i>body parameters</i>			
body weight, g	17.6 ± 0.4 (8)	16.8 ± 0.4 (8)	15.1 ± 0.5*(8)
body length, cm	8.8 ± 0.1 (8)	8.7 ± 0.1 (8)	8.4 ± 0.7*(8)
body mass index, kg/m ²	2.28 ± 0.04 (8)	2.20 ± 0.01 (8)	2.13 ± 0.04 (8)
<i>blood parameters</i>			
Na ⁺ , mM	152 ± 1 (8)	151 ± 1 (7)	150 ± 1 (8)
K ⁺ , mM	4.3 ± 0.1 (8)	4.3 ± 0.2 (7)	4.6 ± 0.1 (8)
Cl ⁻ , mM	110 ± 1 (8)	109 ± 1 (7)	106 ± 1 (8)
Ca ²⁺ , mM	2.30 ± 0.02*(8)	2.37 ± 0.03 (6)	2.12 ± 0.03*(8)
Mg ²⁺ , mM	0.53 ± 0.03*(8)	0.96 ± 0.03 (7)	2.20 ± 0.06*(8)
phosphates, mM	2.4 ± 0.1 (8)	2.50 ± 0.08 (7)	2.2 ± 0.2 (8)
urea, mM	10.9 ± 0.2*(8)	9.0 ± 0.6 (7)	9.82 ± 0.4 (8)
creatinine, μM	9.1 ± 0.3 (8)	8.5 ± 0.4 (7)	9.0 ± 0.5 (8)
hematocrit, %	46.5 ± 0.4 (8)	46.5 ± 0.7 (7)	44.5 ± 0.7 (7)
<i>fractional excretion</i>			
FE _{Na} , %	0.3 ± 0.1 (8)	0.3 ± 0.08 (4)	0.2 ± 0.03 (3)
FE _K , %	25 ± 3 (8)	17.3 ± 5.2 (5)	21.9 ± 5.4 (5)
FE _{Cl} , %	0.5 ± 0.2 (8)	0.3 ± 0.1 (4)	0.8 ± 0.1 (5)
FE _{Ca} , %	0.05 ± 0.01*(8)	0.7 ± 0.2 (5)	2.1 ± 0.3*(5)
FE _{Mg} , %	1.1 ± 0.2*(8)	17 ± 2 (5)	28 ± 4*(4)
FE _{phosphate} , %	24 ± 4 (8)	13 ± 4 (5)	^a 2.2 (1)
FE _{urea} , %	42 ± 4 (8)	42 ± 6 (5)	34 ± 5 (5)

^a Four of the urine phosphate concentrations were below detection limit (<9.6 mM). *, p < 0.05

Mg²⁺ and Ca²⁺ levels in the plasma were highly influenced by the diets (Table 7). The low-Mg²⁺ diet reduced the plasma concentration of both ions and increased plasma urea. As a result, the kidney reacted with a strong reduction of fractional excretion of Ca²⁺ and Mg²⁺. In the high-Mg²⁺

diet group, the plasma concentration for Mg^{2+} increased more than two folds, whereas a significant reduction in plasma Ca^{2+} was observed. Interestingly, the fractional excretion for these ions was augmented three times for calcium and around one and a half for magnesium.

Mg²⁺ diets caused no alterations in transepithelial transport and permeabilities of ex-vivo perfused TAL

Perfused TAL, enzymatically isolated from mice from the different diet groups, did not show any significant difference concerning the transport parameters transepithelial voltage, transepithelial resistance, and equivalent short circuit current (Figure 18). At the same time, inhibition with furosemide of the NKCC2 luminal co-transporter and subsequent dilution voltages did not lead to any differences in the extension of the diffusion voltages of Na^+ , or in the bi-ionic dilution voltages $Mg^{2+}-Na^+$, and $Ca^{2+}-Na^+$ compared to the control group (Figure 19, A). The tubules remain strongly cation-selective, with P_{Na}/P_{Cl} values higher than 4 (Figure 19, B). No differences were observed between the permeability ratios or absolute permeabilities to Na^+ , Cl^- , Mg^{2+} , and Ca^{2+} among TAL obtained from different diet groups (Figure 19, C); no matter that the kidney appear to be strongly working against the diets.

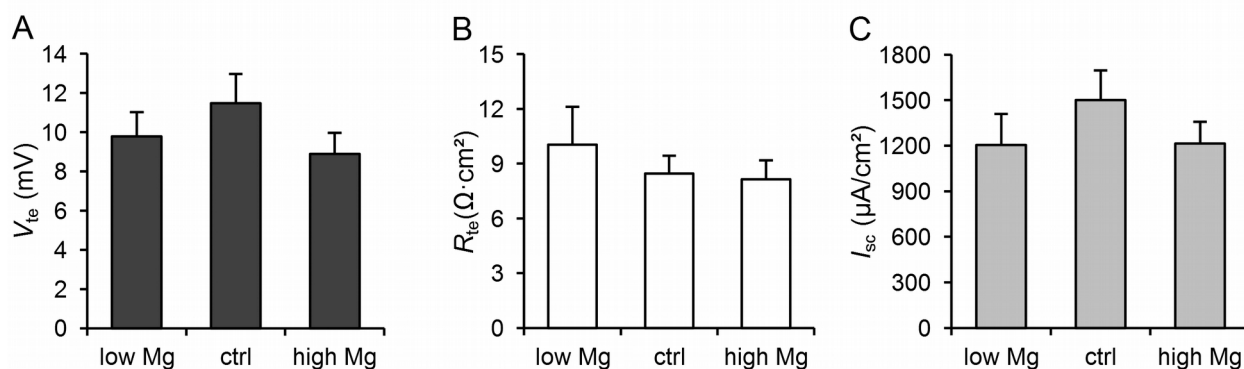


Figure 18: Transepithelial electrical properties determined on isolated and microperfused TAL of mice at control, low- Mg^{2+} , or high- Mg^{2+} diet.

A) Transepithelial voltage (V_{te}). B) Transepithelial resistance (R_{te}). C) Equivalent short circuit current (I_{sc}). $n = 17-23$; $p < 0.05$

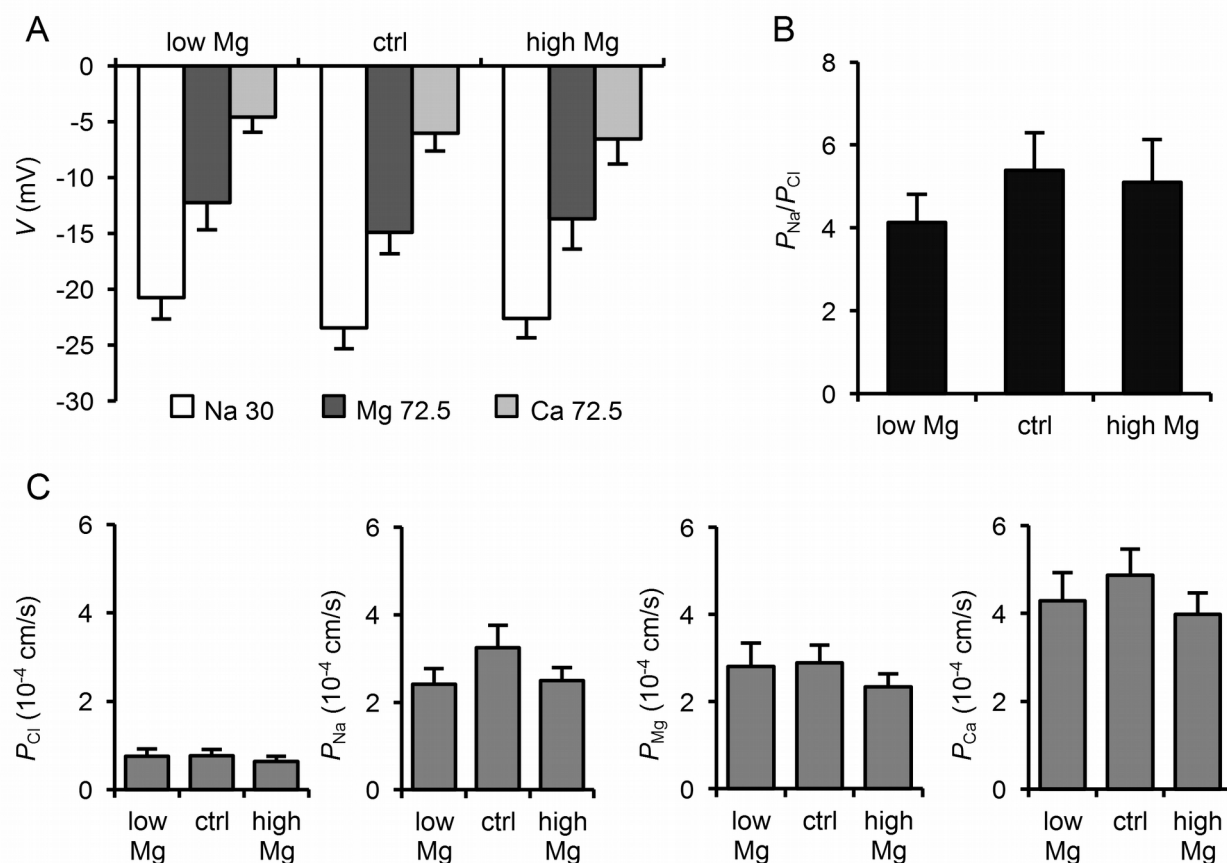


Figure 19: Ex vivo paracellular transport properties of microperfused TAL from the magnesium diet groups, after inhibition of NKCC2.

A) Diffusion potentials after replacement of the peritubular fluid with low-NaCl (Na 30), high-Mg²⁺ (Mg 72.5), and high-Ca²⁺ (Ca 72.5) solutions. B) Sodium-chloride permeability ratios (P_{Na}/P_{Cl}). C) Absolute permeabilities to Cl⁻, Na⁺, Mg²⁺, and Ca²⁺ (P_x). $n = 11-13$; $p < 0.05$

6.4. Inhibition of histone deacetylase with suberanilohydroxamic acid (SAHA) increases the paracellular cation conductance in the TAL

The calcium diet experiments showed an increase in Cld14 expression in the TAL as one of the physiological responses to high calcium intake under the chosen experimental conditions. Succeeding those experiments, and in collaboration with Professor Hou, electrophysiological measurements in freshly mechanically isolated TAL were performed to bring direct data to a novel regulatory pathway for Cld14 expression.

As previously mentioned Cld14 is a modulator of the paracellular permeability to cations in the TAL (see Introduction). Recent data revealed evidence for the existence of an epigenetic regulatory path for its expression (Gong *et al.*, 2012, 2014). It was shown that an increased expression of the micro RNA miR9 and miR374 reduced the expression of Cld14. This would result in an increased paracellular reabsorption to Ca^{2+} and Mg^{2+} , as Cld14 lowers the cation selectivity of the TAL tight junction due to its interaction with Cld16 (Gong *et al.*, 2012). On the other hand, the expression of miR9 and miR374 was up regulated in the presence of the HDAC inhibitor suberanilohydroxamic acid (SAHA). Furthermore, Gong *et al.* (2012) observed that SAHA affects the Ca^{2+} and Mg^{2+} excretion of mice: reduced fractional excretions compared to vehicle treated animals, together with increased plasma levels of Mg^{2+} , indicated that SAHA induced an increase in the reabsorption of divalent cations in the kidney.

To test the possible effect of SAHA on the TAL's paracellular permeability, the transport properties of TAL from wild-type C57BL6/J mice were studied after 4 hours of treatment with this inhibitor of the HDAC or vehicle. The transepithelial voltage was at the same magnitude in both, TAL from SAHA treated and vehicle treated animals, with values surrounding 14 mV (Figure 20). Equivalent short circuit current was also not significantly different between treatments, but a significant reduction of the transepithelial resistance (R_{te}) was a result of the SAHA treatment. Those results, in combination with the fact that V_{te} was completely suppressed by luminal furosemide, suggest that the transcellular transport was not affected by the treatments. R_{te} remained lower after the treatment with furosemide, and during the whole duration of the experiments, a clear indication that SAHA could have affected the TAL's paracellular properties. As a matter of fact, the paracellular permeability to Na^+ was highly increased in the tubules. No changes were detected regarding P_{Cl} , P_{Mg} , and P_{Ca} (Figure 20).

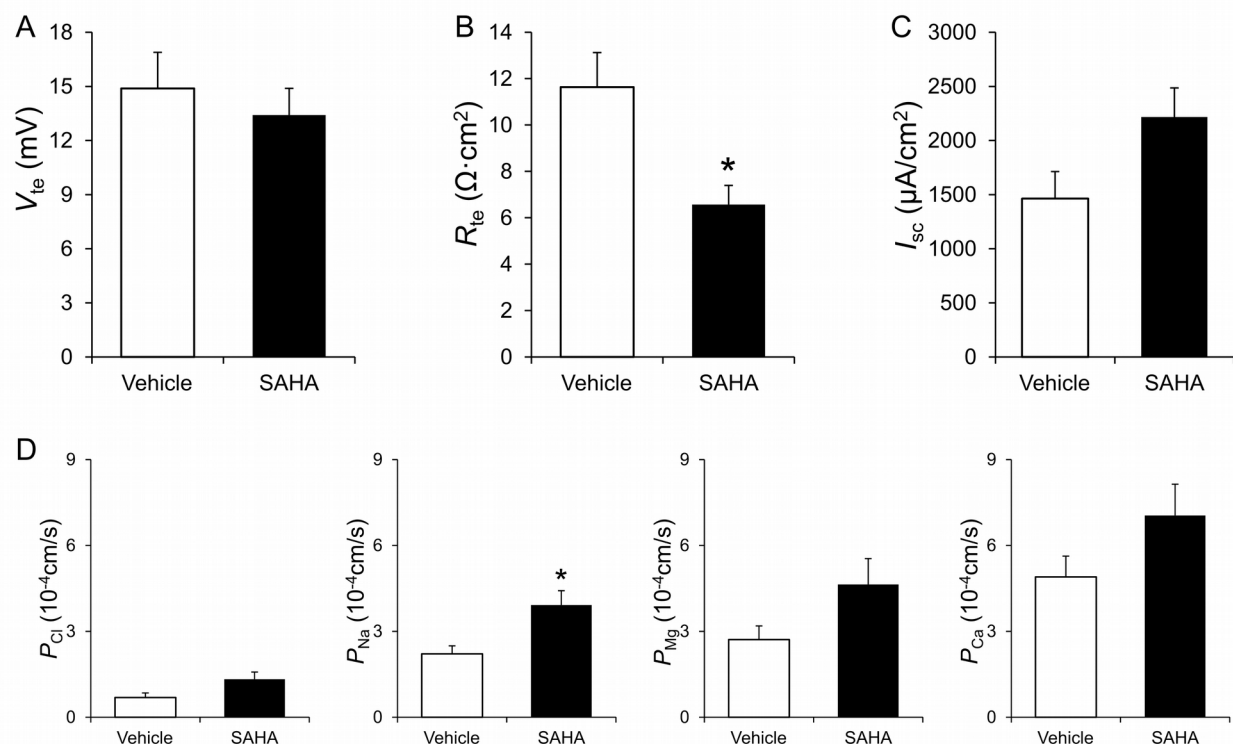


Figure 20: Properties of ex vivo perfused TAL tubules from wild-type mice after a four hour treatment with vehicle (left column) or SAHA (right column).

A) Transepithelial voltage (V_{te}). B) Transepithelial resistance (R_{te}). C) Equivalent short circuit current (I_{sc}). D) Paracellular permeabilities to Cl^- , Na^+ , Mg^{2+} , and Ca^{2+} (P_x , D). $n = 10-12$; *, $p < 0.05$

6.5. Regulation by arginine vasopressin of the tight junction's permeability in the TAL

In vivo model of high systemic arginine vasopressin (long-term)

To study a possible regulatory effect of arginine vasopressin (AVP) on the paracellular reabsorption of divalent cations in the TAL, young 8 to 10-weeks-old mice were fed with a water-restricted diet (WR) to induce high systemic AVP expression. A second group of mice was fed at the same time with a water-loaded diet (WL), as a reference for low AVP.

Mice receiving WR or WL treatments behaved and grew normally. The direct response to the treatments can clearly be illustrated by urine osmolality (Figure 21). Urine osmolality from WR animals was several times larger than of WL mice.

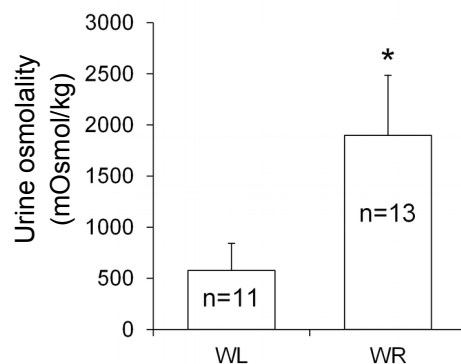


Figure 21: Urine osmolality of mice kept on water-loaded (WL) or water-restricted (WR) conditions for 5 days. n =11-13; *, $p < 0.05$

Freshly mechanically isolated mTAL from the WR group (n=20) displayed more active transport compared to the WL group tubules (n=15). They showed higher transepithelial voltage (V_{te}) and higher equivalent short circuit current (I_{sc}), whereas the transepithelial resistance (R_{te}) was lower (Figure 22). Diffusion voltages were also higher in the WR group, indicating a higher sodium-chloride permeability ratio (P_{Na}/P_{Cl}). Furthermore, a higher absolute permeability to sodium (P_{Na}) was observed in the TAL from WR compared to WL group (Figure 24).

No differences in the protein expression of Cldn10, Cldn16, Cldn19 or NKCC2 were observed by Western-blot (Figure 23).

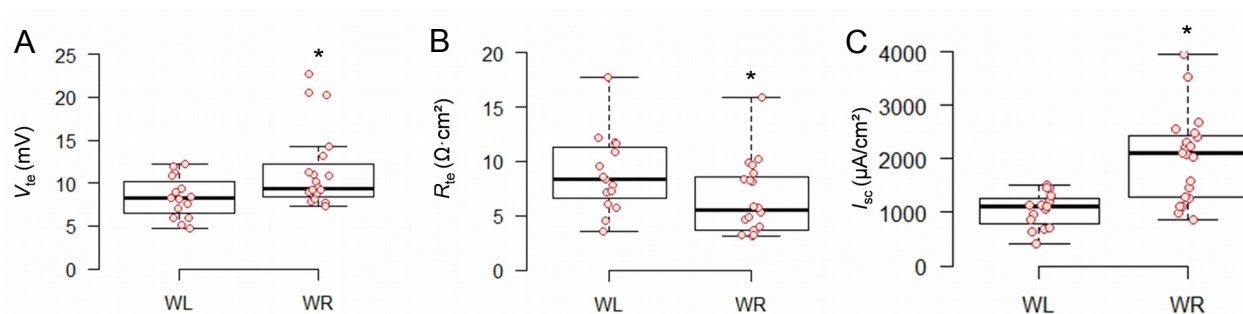


Figure 22: Transepithelial transport properties of mTAL from mice kept on water-loaded (WL) or water-restricted (WR) conditions.

A) Transepithelial voltage (V_{te}). B) Transepithelial resistance R_{te} . C) Equivalent short circuit current (I_{sc}). n = 15-20; *, $p < 0.05$

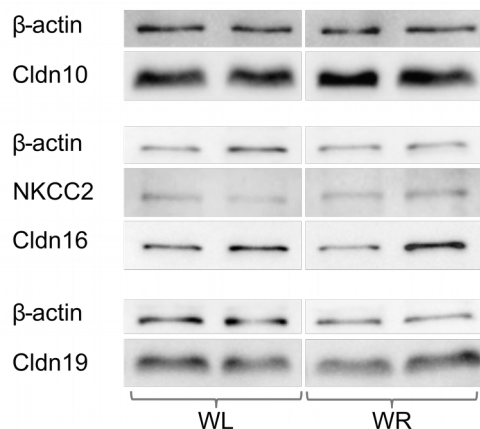


Figure 23: Expression of *Cldn10*, *Cldn16*, *Cldn19*, and *NKCC2* in TAL from mice under water-loaded (WL) or water-restricted (WR) conditions.

Samples from 2 mice are shown from each group, together with their correspondent β -actin expression as loading control.

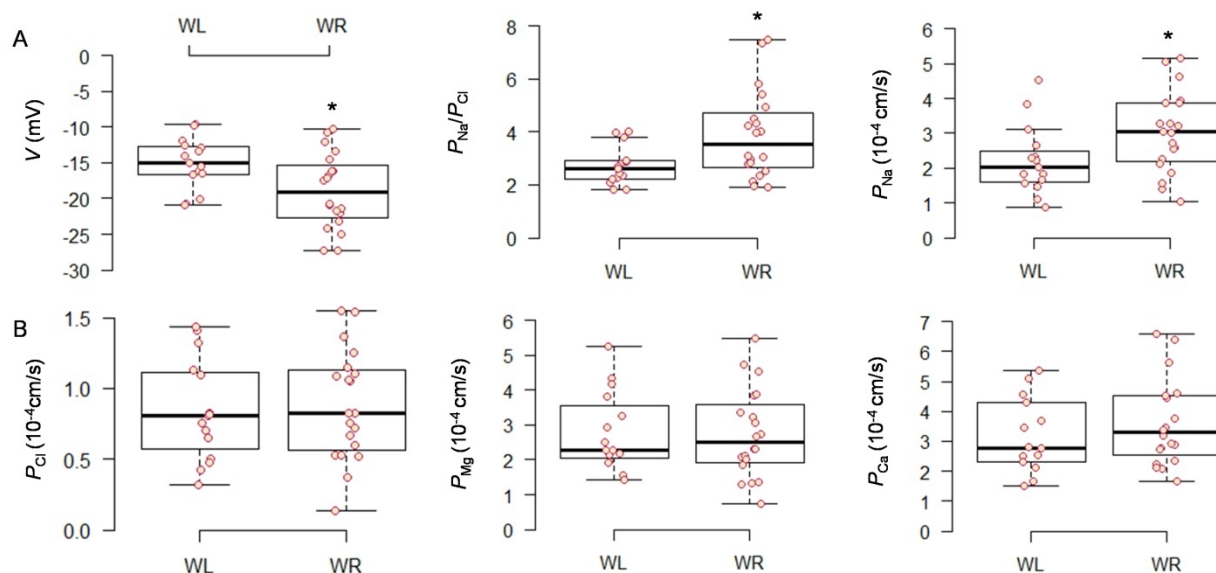


Figure 24: Paracellular transport properties of mTAL of mice on water-restricted (WR) and water-loaded (WL) conditions.

A) Diffusion potentials after replacement of the peritubular fluid with low-NaCl (V), sodium-chloride permeability ratio (P_{Na}/P_{Cl}), and absolute permeability to Na^+ . B) Absolute permeabilities to Cl^- , Mg^{2+} , and Ca^{2+} . $n = 15-20$; *, $p < 0.05$

Ex vivo stimulation of mTAL with AVP (short-term)

In order to test if short term stimulation with AVP in mTAL would affect the paracellular selectivity and the sodium permeability, a set of paired experiments was designed. In those

experiments, transepithelial transport and diffusion voltages from perfused freshly mechanically dissected mTAL were measured before and after stimulation with AVP (Figure 10). Time control experiments were conducted in parallel.

This *ex vivo* acute stimulation of mTAL ($n=6$) with AVP for 12 minutes increased the transepithelial transport and the selectivity for cations. I_{sc} and V_{te} increased when TAL were stimulated, whereas in the time control group I_{sc} and V_{te} decreased instead (Figure 25). At the same time, AVP induced more pronounced diffusion voltages leading to an increase in P_{Na}/P_{Cl} (Figure 26). This did not happen in the time control experiments. The absolute permeabilities to Na^+ and Cl^- showed a tendency to decrease with time.

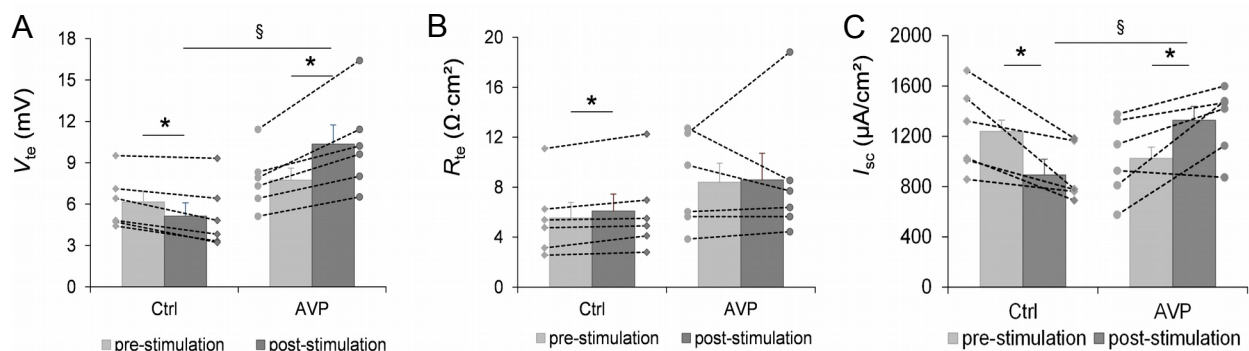


Figure 25: Transepithelial transport increases in presence of AVP.

A) Transepithelial voltage (V_{te}). B) Transepithelial resistance R_{te} . C) Equivalent short circuit current (I_{sc}). Individual data pairs are represented by dots linked with dashed lines. $n = 6$; *: pre- and post-stimulation comparison (paired), §: comparison with time control (unpaired), $p < 0.05$

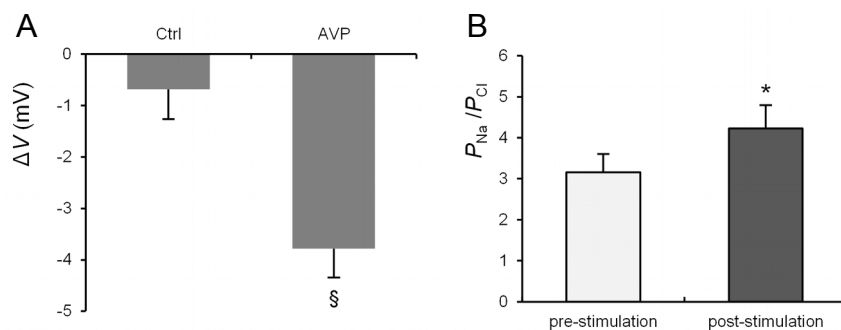


Figure 26: Selectivity for cations in freshly isolated mTAL after stimulation with AVP.

A) Diffusion voltage variation for time control and AVP stimulated TAL. B) Sodium-chloride permeability ratio (P_{Na}/P_{Cl}) in the tubules stimulated with AVP. $n = 6$; §: comparison with time control (unpaired), *: pre- and post-stimulation comparison (paired), $p < 0.05$

6.6. A constitutive high plasma aldosterone mouse model, had unaltered transport rates in the TAL compared to wild-type animals.

The transepithelial properties of a high-aldosterone mouse model were studied. This mouse model lacks the mineralocorticoid receptor in the principal cells of the collecting tubules ($MR^{AQP2Cre}$), thus creating a continuous stimulus for aldosterone production (Ronzaud *et al.*, 2007).

Enzymatically isolated mTAL from old $MR^{AQP2Cre}$ mice ($n = 15$) and their wild-type littermates (WT, $n = 14$) were microperfused in order to measure transepithelial and paracellular properties. No differences regarding the transport properties of the tubules were observed. The equivalent short circuit current (I_{sc}) as an indicator of the transepithelial transport was slightly but not significantly smaller in the TAL derived from the knock-out mice (Figure 27), which showed very similar transepithelial voltages and resistances. This implies that the transcellular transport machinery, the generator of the driving forces for the paracellular reabsorption of cations in these tubules, was not affected. In the same way, the paracellular permeabilities to Na^+ , Cl^- , Mg^{2+} , and Ca^{2+} were not altered in the knock-out mice compared to the WT animals (Figure 28). Apparently, aldosterone does not interfere with the TAL reabsorptive properties under the studied conditions.

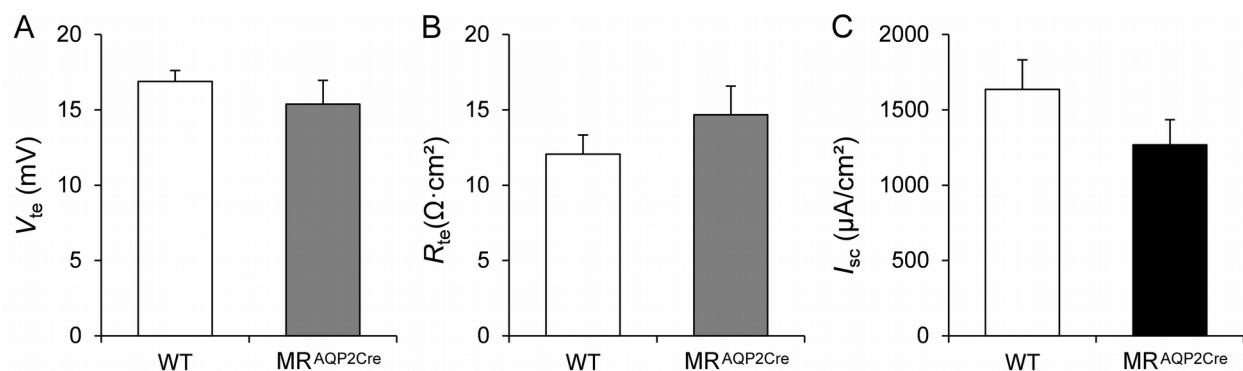


Figure 27: Transepithelial transport parameters in the TAL of wild-type (WT) mice and mineralocorticoid receptor-deficient ($MR^{AQP2Cre}$) mice.

A) Transepithelial voltage (V_{te}). B) Transepithelial resistance R_{te} . C) Equivalent short circuit current (I_{sc}). $n = 15-14$; $p < 0.05$

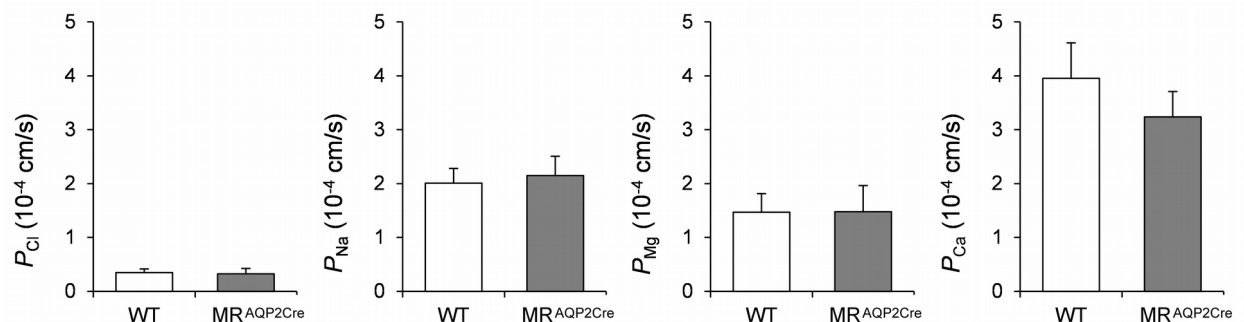


Figure 28: Paracellular permeabilities to Na^+ , Cl^- , Mg^{2+} , and Ca^{2+} (P_x) in TAL of mineralocorticoid receptor-deficient mice ($\text{MR}^{\text{AQP2Cre}}$) and litter-mate wild-type animals (WT). $n = 15-14$; $p < 0.05$

6.7. Inhibition of the deactivation of NKCC2 by treatment with the calcineurin inhibitor cyclosporin A

The transcellular pathway was challenged on a separated experimental line in collaboration with Dr. Kerim Mutig. Transcellular transport in the TAL depends on the activity of the NKCC2 cotransporter, whose activity is controlled in part by phosphorylation. In general, we propose that a regulatory mechanism exists that involves the sortilin-related receptor, L(DLR class) A repeats containing (SORLA) and calcineurin, for the control of NKCC2 function (Borschewski *et al.*, 2015).

It was shown that calcineurin $\text{A}\beta$ (Cn $\text{A}\beta$) interacts with NKCC2, and that the calcineurin inhibitor cyclosporine A (CsA) increases phospho-NKCC2 (pNKCC2) abundance, suggesting that Cn $\text{A}\beta$ may be involved in NKCC2 dephosphorylation. Likewise, Cn $\text{A}\beta$ was seen to interact with the SORLA's cytoplasmic tail. However, in SORLA knock-out mice ($\text{SORLA}^{-/-}$) an increase in Cn $\text{A}\beta$ abundance was observed, together with a reduction in the levels of pNKCC2. Therefore SORLA appears to interfere with the cellular trafficking and turnover of Cn $\text{A}\beta$. Here I show that inhibition of Cn $\text{A}\beta$ activity with CsA *ex vivo* partly prevented the decrease in activity of NKCC2 in wild-type mice but fails to do so in $\text{SORLA}^{-/-}$ mice.

To test the effect of CsA in the TAL's transcellular activity, tubules from $\text{SORLA}^{-/-}$ mice and wild-type Balb/c mice were isolated for microperfusion. We measured transepithelial voltage (V_{te})

and transepithelial resistance (R_{te}), and calculated the equivalent short circuit current (I_{sc}) as an indicator of NKCC2 activity (Greger *et al.*, 1983b; Greger, 1985). Measurements were performed on freshly isolated TAL (time 0h) and on tubules incubated for one hour with CsA or vehicle (Figure 29, A). As Cl^- affinity is the critical limitation for NKCC2 activity, and phosphorylation of NKCC2 at the SPAK/OSR1-dependent threonine (T96, T101) sites might have an effect on the NKCC2 affinity for Cl^- , measurements at low Cl^- concentration (30 mM Cl^- , luminal and basolateral) were performed in the same tubules in addition to measurements at a chloride concentration of 145 mM (Figure 29, B). At the high Cl^- concentration changes in I_{sc} were observed over time, treatment, and mouse strain (Figure 29, A). Those changes were caused by variations in R_{te} , whereas V_{te} remained the same. The transepithelial transport (I_{sc}) in tubules of WT mice was substantially reduced after one hour incubation with vehicle. After one hour of CsA-treatment, I_{sc} values in these tubules showed clearly a lower reduction in NKCC2 activity compared to vehicle. At the same time, transepithelial transport of freshly isolated TAL from *SORLA*^{-/-} mice (time 0h) were as low as almost half of the transport of TAL from WT mice in the same conditions. No changes were observed in tubules from *SORLA*^{-/-} mice after the one hour treatments, vehicle or CsA (Figure 29, A). Low Cl^- transcellular measurements in those tubules allowed us to set some information about Cl^- affinity. As expected V_{te} and I_{sc} respectively, of freshly isolated WT TAL was reduced to around 50% under the low Cl^- concentration used (Figure 29, B), corroborating it to be near the K_m value known from literature (Greger *et al.*, 1983b). 1h incubation led to a decrease in I_{sc} under low Cl^- to only 20% of the respective I_{sc} under high Cl^- . This decrease was partly prevented by CsA incubation, with 30% remaining I_{sc} under low Cl^- condition. In *SORLA*^{-/-} TAL I_{sc} under low Cl^- was always low, at around 20% of the respective value under high Cl^- , and did not change over time or by CsA. Thus, CsA prevents the natural deactivation of NKCC2 in TAL from WT animals under the studied conditions, but failed to do so in TAL isolated from *SORLA*^{-/-} mice.

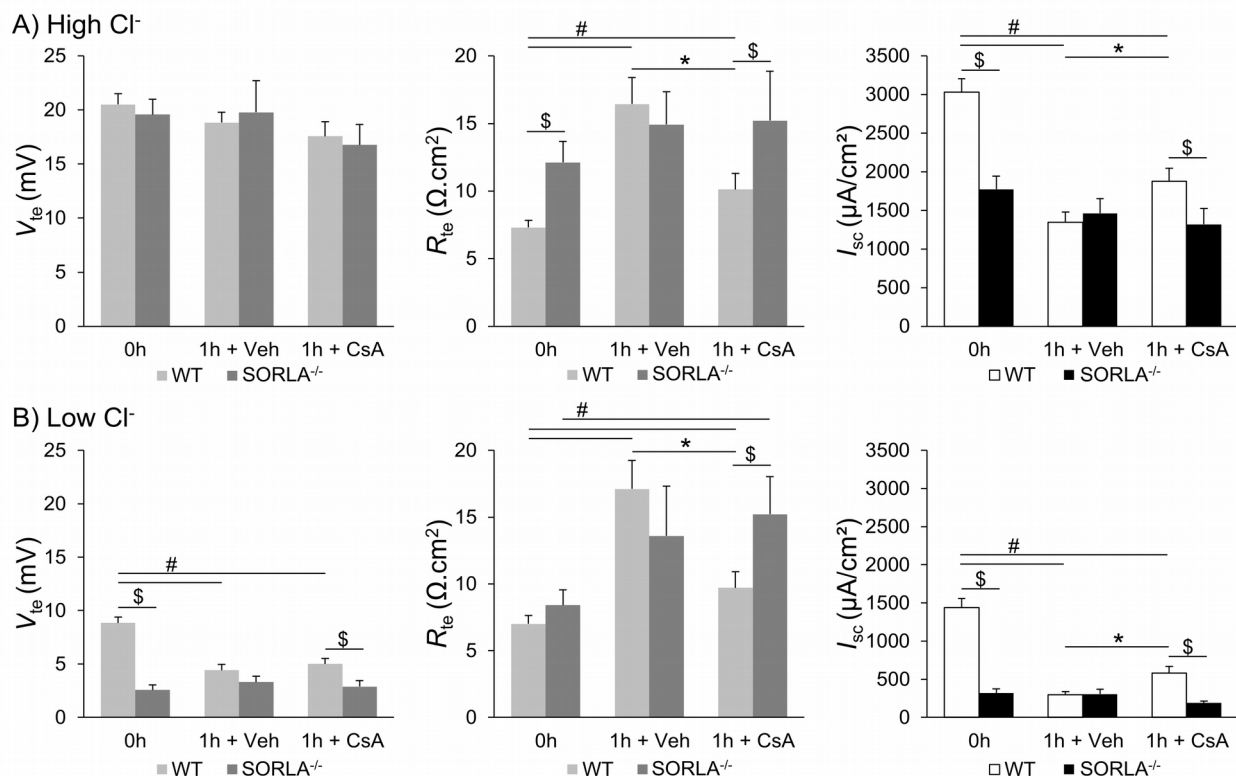


Figure 29: Response to one hour incubation with vehicle (Veh) or cyclosporin A (CsA) in TAL from wild-type mice (WT) or *SORLA*^{-/-} mice.

I_{sc} , equivalent short circuit current. V_{te} , transepithelial voltage. R_{te} , transepithelial resistance.

A) and B) Measurements conducted with NKCC2 working under high Cl⁻ (145 mM, V_{max}) and under low Cl⁻ (30 mM), respectively.

$n = 10, 8,$ and 7 for *SORLA*^{-/-} mice TAL. $n = 26, 16,$ and 13 for WT mice TAL. $p < 0.05$

\$: comparison between *SORLA*^{-/-} and WT at the same time.

#: observed differences among treatments and time 0 (0h).

*: significant differences between one hour of vehicle treatment (1h+Veh) and one hour of CsA treatment (1h+CsA).

6.8. Characterization of the TAL transport properties in Cld10/Cld16 double knock-out mice

A final approach to the regulation of the reabsorption of cations in the TAL to be presented in this dissertation, is the measurement of the transcellular transport and the paracellular properties of TAL from Cld10/Cld16 double knock-out mice (dKO), Cld16 knock-out (Cld16KO),

and Cld10 conditional knock-out animals (Cld10KO). This project was an attempt to elucidate the phenotypical differences observed in Cld10 and Cld16 knock-out mice models (Will *et al.*, 2010; Breiderhoff *et al.*, 2012), and to evaluate the functional interdependency between these two important claudins for the reabsorption of divalent cations in the kidney.

The animals were viable and grew well, without any obvious morphological deviation, but they showed metabolic impairment (Himmerkus *et al.*, manuscript in preparation). The dKO mice were polyuric and polydipsic. They showed a mild hypokalemia and a significantly larger urinary potassium excretion, accompanied with a reduced excretion of sodium compared to WT and single KO animals. Magnesium serum levels of dKO mice remained unchanged compared to the control group. Cld16KO mice were hypomagnesemic and Cld10KO mice hypermagnesemic in correspondence with previous results (Will *et al.*, 2010; Breiderhoff *et al.*, 2012). Importantly, calcium excretion in the dKO group was similar to the control group, whereas it was significantly higher in the Cld16KO group. Only the Cld10KO mice showed signs of nephrocalcinosis.

The mutations affected the electrophysiological properties of cortical and medullary TAL (cTAL and mTAL). Transepithelial voltages were higher in cTAL from Cld10KO animals compared to other groups including the control group; no significant differences were observed among measurements in mTALs (Figure 30). Transepithelial resistances (R_{te}) displayed different results: The R_{te} in the cTAL from dKO mice was almost twice as high as in the other groups, whereas in the mTAL all studied groups displayed larger resistances than the control group. This was accompanied by a lower transport rate (I_{sc}) in mTAL for all groups compared to control (Figure 30). In the cortical TAL the picture was completely different. In this case, I_{sc} in Cld10KO and Cld16KO were superior to the values obtained for the control group, indicating more net transport in those tubules.

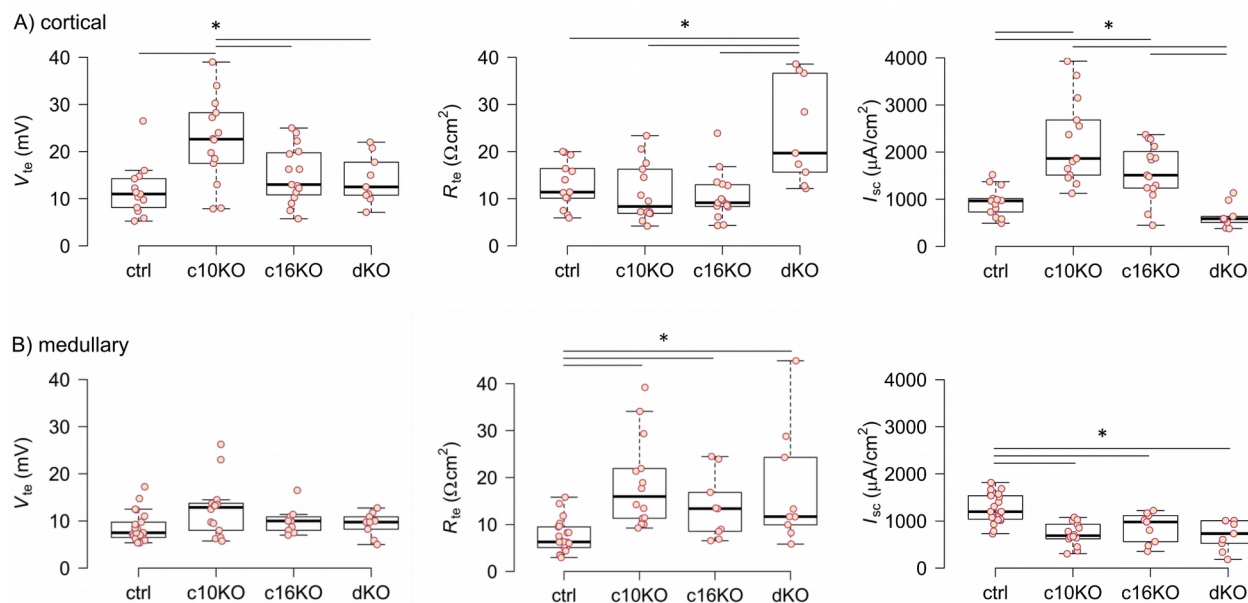


Figure 30: Transepithelial transport of cortical and medullary TAL in *CLd10*, *Cld16*, and *Cld10/Cld16* knock-out mouse models (*c10KO*, *c16KO*, and *dKO*).

A) and B) Transepithelial voltage (V_{te}), transepithelial resistance (R_{te}), and equivalent short circuit current (I_{sc}) of cortical and medullary TAL, respectively. $n = 9-22$; *, $p = 0.05$

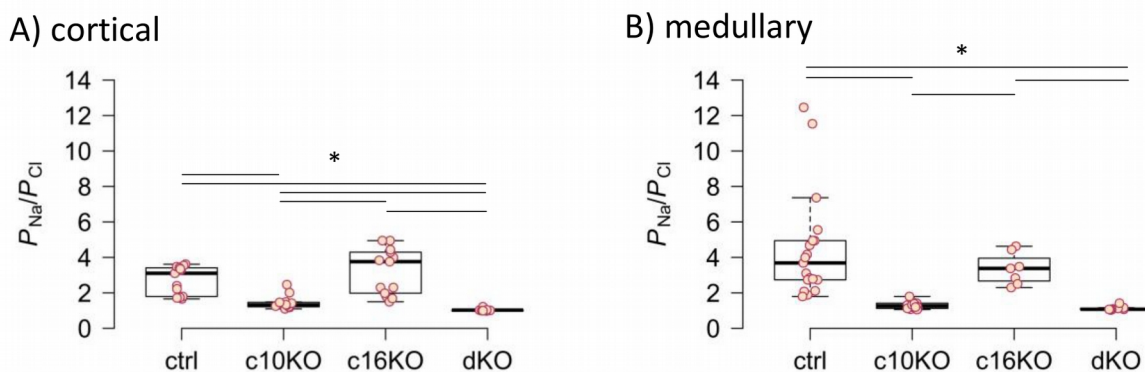


Figure 31: Sodium-chloride permeability ratios of cortical and medullary TAL from *Cld10* and *Cld16* knock-out, and double knock-out mice. $n = 9-22$. *, $p < 0,05$.

The analysis of the paracellular properties revealed that the selectivity for cations in the TAL was critically compromised in *Cld10KO* and in *dKO* mice in both, cortical and medullary tubules (Figure 31). Tubules from these two groups show hardly any selectivity, particularly in the TAL from *dKO* animals, where the P_{Na}/P_{Cl} was always very close to one. This effect was due to a

decrease in P_{Na} with no observed changes regarding P_{Cl} (Figure 32). The absolute permeabilities to Ca^{2+} and Mg^{2+} were in some extension also altered. None of the investigated groups showed differences in P_{Mg} compared to the control group, but cTAL from *Cld10*KO mice displayed a higher permeability than cTAL from the other two knock-out models (Figure 32, A P_{Mg}). Concerning P_{Ca} , only TALs from dKO mice were affected (Figure 32, A-B P_{Ca}).

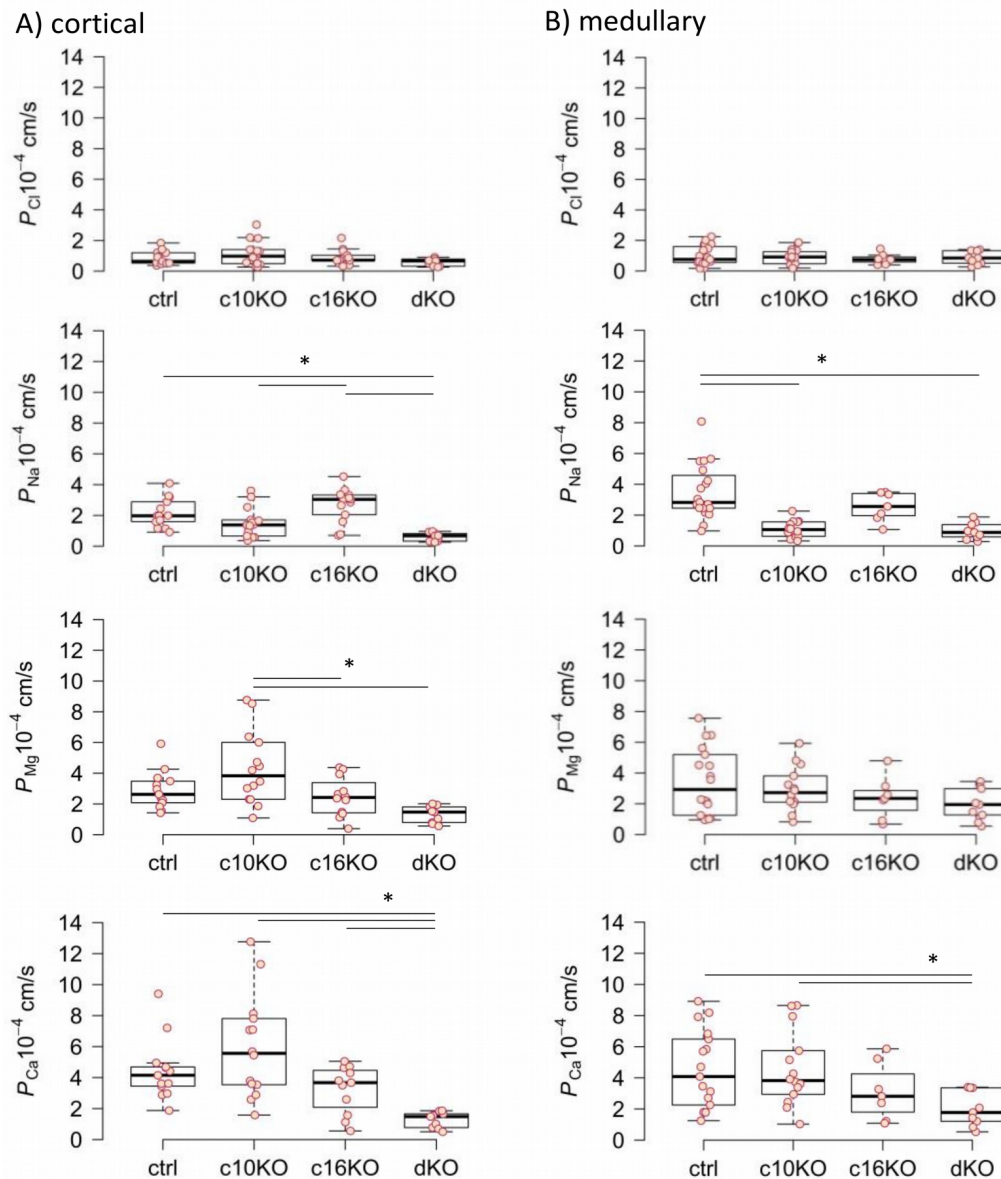


Figure 32: Absolute permeabilities to sodium, chloride, magnesium, and calcium of cortical and medullary TALs from *Cld10* and *Cld16* knock-out, and double knock-out mice. $n = 9-22$. *, $p < 0,05$.

7. Discussion

In the present dissertation I am particularly interested in possible regulatory pathways that affect the paracellular reabsorption of divalent cations in the TAL. To accomplish a variety of particular goals, wild-type mice were put on controlled diets aiming for a physiological response, or given a drug, like in the SAHA experiments. In other experiments isolated TALs were stimulated *ex vivo*, or specific knock-out mouse models were used to analyze their electrophysiological properties for reabsorption of ions.

7.1. Methodological discussion

Tubule isolation techniques

The mechanical dissection of renal tubules is the standard technique established for microperfusion or tubular isolation in general. But it has 2 main problems: first, as connective tissue grows with age among the kidney structures it is really difficult to dissect single tubules in mice older than 10-12 weeks; and second, it is not suitable in order to collect enough material for Western blot, PCR or any other molecular biology techniques.

The preparation of kidney slices with collagenase II as described in materials and methods solved in part both problems. It provided enough material from particular segments for molecular biology techniques. All of the nephron segments, from glomeruli to medullary collecting ducts, could be distinguished and were observed in abundance. Thin limbs, which were present, were more difficult to distinguish. TALs were present in a very high number, and at high quality. They were transporting actively and responded to solution exchanges and treatments like furosemide in the very same way as the mechanically dissected tubules. At times, due to partial digestion of the basement membrane collagen, enzymatically dissected TAL were softer and easier to blow up by over perfusion than the mechanically dissected ones. Care was taken to keep a working standard of low pressure for perfusion of enzymatically dissected

TALs. Even though, this method permitted the collection of good quality tubules from mice at any age. A disadvantage was that it was not possible to correctly determine the region in the kidney from where the perfused TAL came from. Most of the tubules obtained with this technique came from the cortex and outer stripe of the outer medulla, taking in account the residuals in the vial after the enzymatic procedure and the high amount of connective tissue in the papilla region. Some were also from the inner stripe of the outer medulla, as very long TALs still attached to a thin limb portion were visible.

In general, for TAL perfusion, the mechanical procedure was preferred over the enzymatic assisted, whenever possible, to meet the highest standards in localization and quality.

TAL perfusion

A modified version of the previously described perfusion system for *in vitro* perfusion of renal tubules (Burg, 1972; Greger & Hampel, 1981) was used. I did not make use of a pipette containing Sylgard 184 (a silicone oil) for sealing electrically the perfusion extreme as they describe. Instead, the electrical sealing was accomplished by the narrow construction of the constriction pipette. The constriction pipette was built to have internally the diameter of a TAL. When catching the tubule it was held in the constriction and then the perfusion was performed. This way, the walls of the tubule sealed against the constriction pipette, and most of the times it worked perfectly. In other cases, moving the perfusion pipette and sucking a bit more the tubule made it work.

For calculation of the absolute permeabilities the reverse of the TAL's transepithelial resistance (R_{te}) was used as equivalent to G_r . The resistance in the TAL has two main components: the transcellular component and the paracellular component. For an accurate estimation of the absolute paracellular permeabilities I used the resistance of the tubules calculated after blocking NKCC2 with furosemide, and with the same NaCl solution (control solution) present at the luminal and at the basolateral side of the membrane. This way, the main contribution to the tubule's transepithelial conductance is paracellular, since the conductance of the basolateral

membrane and thereby the transcellular component decreases as a consequence of the drop in cytosolic Cl^- in the presence of furosemide (Greger *et al.*, 1983a). Nevertheless, the effect of furosemide on R_{te} has several components which partially balance each other. On the one hand, the conductivity of Cl^- in the basolateral membrane goes down because of the decrease in intracellular Cl^- concentration. On the other hand, furosemide increases intracellular pH (de Bruijn *et al.*, 2015), a strong activator of the luminal K^+ channel (Bleich *et al.*, 1990), which increases the luminal conductivity. In summary, these effects could result in no change in R_{te} .

Western Blot

The Western blots resulted in clear bands easy to analyze, but I would like to discuss at this point a particularity related to the method and not to the results. As described in the materials and methods section, the samples were homogenized by counting the tubules included in each aliquot and by comparing the total amount with a defined guide, with the intention of having the same amount of tubules in the same volume in every sample. No protein determination was done for the difficulties of having not enough material. Sorted TALs, and not homogenized kidney tissue, were used for the electrophoresis run. Interestingly, the method of tubule counting was very precise and resulted in almost identical protein loads as visible from the β -actin band intensity. The advantage of using this method was the maximal background reduction by using only a single species of tubules instead of whole kidneys. In trials made before simultaneously with kidney homogenate and sorted tubules protein determination was done to guarantee the same amount of proteins in the homogenate samples. Those trials were performed to test the antibodies and the technique.

7.2. Influence of dietary intake of divalent cations on the TAL

Calcium diets

The study on the response to increased or reduced dietary intake of Ca^{2+} in young, female mice evidenced a regulation of the reabsorption of divalent cations in the TAL: High- Ca^{2+} diet caused a

reduction in both, the driving force and the permeabilities to Ca^{2+} and Mg^{2+} , and therefore reduced the capability for reabsorption of divalent cations in isolated TALs.

The calcium diets were well tolerated and the animals responded to the diets with adequate adaptation in their calcium and phosphate metabolism, like observed in similar studies (Brink *et al.*, 1992; Gorgels *et al.*, 2010; Dimke *et al.*, 2013). The animals put on the low-calcium diet displayed normal values for all measured blood parameters compared to the control group, but the 100% increase in the observed fractional excretion of phosphates reflects a response to the calcium reduction. It is clearly established that a reduction of calcium in the plasma leads to an increase of the secretion of the parathyroid hormone (PTH) controlling the intestinal absorption of Ca^{2+} , the renal reabsorption, and the release of Ca^{2+} from bones (Guyton & Hall, 2005; Boron & Boulpaep, 2009). PTH also increases renal vitamin D_3 production. In a similar diet experiment no permanent increase in PTH was observed for low-calcium diet mice, but a significantly larger abundance of plasma vitamin D_3 was detected (Dimke *et al.*, 2013). However, this could be the integrated signal of oscillating PTH concentrations, which in total have been higher than under control diet. Secretion of PTH by the parathyroids oscillates in a reversed function of the concentration of Ca^{2+} in plasma. The high excretion of phosphates in our study indicates that Ca^{2+} (together with phosphates) has been extracted from bones to sustain the normal calcium concentration in the plasma, as observed in these animals (Favus *et al.*, 2006; Renkema *et al.*, 2008). This is the expected effect of PTH. In kidney, PTH is described to increase renal Ca^{2+} reabsorption in the TAL and in the distal tubules (Tyler Miller, 2013; Houillier, 2014). Independent of PTH CaSR in the TAL has been shown to react to inhibitors increasing calcium reabsorption (Loupy *et al.*, 2012). This indicates that CaSR is a direct determinant of the calcium concentration in plasma. After 8 days of low calcium diet no clear effect was observed regarding the TAL's transport properties, but a tendency to a reduction of the fractional excretion of Ca^{2+} , indicating that there might be a reaction in the distal convoluted tubule.

The high-calcium diet, on the other side, proved to be a real challenge to mice by affecting their Ca^{2+} and phosphate values in the plasma, the fractional excretions of these ions, and their

reabsorption in the TAL. The increase of Ca^{2+} in the plasma inhibited the PTH secretion (data not shown), consequently vitamin D_3 is reduced (Dimke *et al.*, 2013). The small but yet significant increase of Ca^{2+} observed in the plasma is not sufficient to be considered as hypercalcemia and did not induce any appreciable symptom in mice, apart from the observed regulatory increase of calcium excretion and reduction of phosphate excretion. It is remarkable that the balance of NaCl transport and excretion in the kidney was not affected during the excretion of excess dietary Ca^{2+} .

The measurements of the TAL's transepithelial transport of ions and its paracellular permeabilities to sodium, chloride, magnesium, and calcium showed that the TAL reacts differently to low and high calcium intake. It was not significantly involved in the physiological response to Ca^{2+} shortage for 8 days, but it changed its reabsorptive properties when mice received high dietary Ca^{2+} . First of all, the transepithelial voltage generated by the active transepithelial transport of the TAL cells was lower in TALs from high-calcium diet mice in comparison to TALs from animals on control diet. Magnesium and calcium are exclusively reabsorbed in the TAL via the paracellular pathway and the tubule uses the generation of a transepithelial lumen positive voltage to favor their reabsorption. Therefore, the observed lower transepithelial voltage in tubules from high-calcium diet mice implies a reduction in the driving force that normally facilitates the reabsorption of divalent cations in the TAL. Additionally, extracellular basolateral calcium reduces the transcellular active transport of NaCl in the TAL, which is in complete concordance with this result. The interaction between Ca^{2+} and CaSR in the TAL has been previously proposed to reduce ROMK activity, and indirectly also NKCC2 activity by reducing the availability of K^+ in the lumen (Riccardi & Brown, 2010; Tyler Miller, 2013). However, there is controversy about this mechanism (Houillier, 2014) and the discussion has its focus on the prevention of kidney stone formation by diuretic effects of CaSR activation.

The data presented in this dissertation shows that a high-calcium diet for 8 days significantly reduced the paracellular permeabilities for Ca^{2+} and Mg^{2+} in the TAL, along with a reduction of the selectivity for cations. High-calcium diet has been shown to increase the renal expression of

Cld14 (Gong *et al.*, 2012; Dimke *et al.*, 2013). Over-expression of this claudin reduces the paracellular Ca^{2+} flux in cell cultures (Dimke *et al.*, 2013). Combined, these data show that it is possible to observe the effect of regulation in the paracellular pathway in *ex vivo* TALs under physiological stimulation. Furthermore, in parallel to the data presented here, our research group was able to show that the high-calcium diet mice displayed an increased mRNA expression for CLD10 and CLD14 genes, accompanied by an increase their protein expression in the TAL compared to the control group. Cld10 expression, determined by immunohistochemistry, was observed to be elevated in the TAL's tight-junction in the inner stripe of the outer medulla portion (ISOM). In the control animals the expression of Cld10 in the ISOM was rather low, allowing the comparison. On the other hand, the high expression of Cld10 observed within the cytoplasm and in the tight junctions in control and treated groups in the outer stripe of the outer medulla (OSOM) and the cortex, made it difficult to evaluate with this method if there were differences in the expression in those kidney portions among the groups. Cld14, which is generally expressed on very low levels in the kidney, was seen to be upregulated in the OSOM and in the cortex. The significant increase of the excretion of calcium observed for high-calcium diet mice can therefore be partly explained by the reduction of Ca^{2+} reabsorption in the TAL. This mechanism is probably controlled by a CaSR-independent response in the TAL and the expected reduction of PHT in the plasma due to the high Ca^{2+} concentration. Interestingly, the fractional excretion of Mg^{2+} did not change.

In conclusion, high-calcium diets induced a physiological response in the TAL. The TAL reduced the reabsorption of divalent cations by: reducing the driving forces that move them out of the tubular lumen; reducing the cation selectivity of the TAL's paracellular pathway; and effectively diminishing their paracellular permeability. These effects were in part a result of the increased expression of Cld14 and Cld10b in the TAL.

Magnesium diets

The high magnesium diet used in the magnesium experiments caused secondary effects in mice. The young female mice on high magnesium diet developed soft stool; and at the end of the 8

days on diet, they did not grow in body length nor gained weight in the same extension as the animals in control or low magnesium diet groups.

The animals in both, the low and the high magnesium diet groups, reflected the effects of their diets in their plasma composition and in their renal excretion compared to the mice of the control group. However, their TALs showed no alterations regarding any of the measured electrophysiological parameters. There are not many other studies on mice involving magnesium diet, but the fact that the animals on high magnesium diet had gastrointestinal side effects is a contradiction to a former study claiming that a high magnesium diet would aid a mouse model for β -thalassemia by correcting its hypomagnesemia and improving from anemia (De Franceschi *et al.*, 1997). Their control animals were 4 to 6 month old C57BL/6 mice that did not show any change in body weight during their 14 and 28 days of treatment. A noticeable difference, apart from the age, is that the additional Mg^{2+} was administered by gavage as a water solution of magnesium hydroxide (an additional 600 mg Mg^{2+} /kg body weight/day to the 400 mg present in their standard diet), whereas in the present study the additional Mg^{2+} was part of the food and was administered *ad libitum*, which resulted in a Mg uptake of 1,8 g Mg^{2+} /kg body weight/day in average. Our standard diet had instead 383 mg Mg^{2+} /kg body weight. In a more recent set of experiments, designed to study how to prevent vascular calcification in a mouse model for pseudoxanthoma elasticum, mice were fed using a similar procedure and with comparable amounts of magnesium in the diets as in this study (LaRusso *et al.*, 2009; Gorgels *et al.*, 2010). Again no soft stool or other affection was mentioned. Nevertheless, the occurring soft stool was somehow compensated as there was no disturbance concerning any other electrolyte but Ca^{2+} and Mg^{2+} .

The kidneys of animals on low magnesium diet reacted with a very low fractional excretion of Mg^{2+} , but this was not sufficient to balance out the reduced magnesium concentration in the plasma. Plasma magnesium values remained at about 50% of the value observed in control animals. Together with Mg^{2+} , the excretion of Ca^{2+} was affected approximately in the same extension, each of them being 15 and 14 times smaller than in the control group. This is clearly

different from the results of the calcium diet experiment, in which no differences regarding magnesium excretion were observed between low and high calcium diets. Interestingly, the calcium level in the plasma was also affected by the low magnesium diet showing a mild, but yet significant reduction. This particular result appears to be contradictory, as calcium in the diet was at the same level as in the control diet group, and if calcium excretion was reduced as discussed before it would be logical to expect an increased concentration in plasma. Therefore, although evidence is lacking, magnesium might be important for calcium absorption and assimilation. It has been described that low magnesium serum correlates with low vitamin D in humans, leading to problems with the intestinal absorption of calcium (Rude *et al.*, 1985; Deng *et al.*, 2013; Zittermann, 2013).

To this point it seems that kidneys, preventing Mg^{2+} from being excreted, affected Ca^{2+} excretion as well, indicating that those mechanisms might not be independent. This leads to the question what happens when dietary magnesium intake is increased?

The kidneys reacted with a very high fractional excretion of Mg^{2+} to the high magnesium diet. Again, this was not sufficient to balance the magnesium level in the plasma, which was still more than twice as high as the values observed in the control group. The high magnesium diet also affected the calcium homeostasis in a great extension. A very high calcium excretion was observed in those animals, three times the amount in control animals. The calcium fractional excretion of the mice on high magnesium diet was actually of the same extension as it was the fractional excretion of calcium in the mice on the high calcium diet compared to their controls. On the other hand, the plasma values for calcium on those animals were strongly diminished by the diet, when compared to controls. Ca^{2+} is going out of the extracellular liquids while the system works for controlling the increase in Mg^{2+} , with no extra calcium intake, resulting in plasma calcium reduction, and probably causing the growing problems observed in those mice. Turning now to the phosphates, only one value for fractional excretion of these ions is reported on the results section: a very low one. Another 4 analyzed urine samples had so low phosphate values that were below detection limit of the measurement procedure, so no fractional

excretion could be calculated. Then, considering these as very low excretion of phosphates, and taking in account that the presence of phosphates in those animals plasma did not differ from control, albeit it was slightly lower, it is possible to assume that likewise in the high-calcium diet phosphates and calcium have been recruited from serum to be stored at bones. The high plasma magnesium can activate the CaSR reducing the secretion of PTH in the parathyroid, which would result in bone formation and an increase excretion of Ca^{2+} and Mg^{2+} by the kidneys.

The kidneys, as seen, strongly reacted to both, low and high magnesium diets. I wanted to know whether the TAL's tight junction was subject of regulation or not, as it was observed in the high calcium diet. For this account I measured as before the TAL's transepithelial transport properties and the paracellular permeabilities for chloride, sodium, calcium and magnesium. The results in transepithelial resistance, transepithelial voltage, and the calculated equivalent short circuit current showed no differences between TAL from mice under control diet and the ones from mice under any of the magnesium diets. Surprisingly, there were also no differences in the paracellular permeabilities to Mg^{2+} , indicating that there were no changes in the magnesium reabsorption in those TAL. Conversely, Houillier (2014) refers that peritubular increase in magnesium concentration reduces the magnesium reabsorption in the TAL (Houillier, 2014), most likely as a response of CaSR.

As up to 70% of the filtered magnesium is reabsorbed in the TAL, an increase in reabsorption here during low magnesium diet might not be as effective as an increase in the reabsorption rates of Mg^{2+} in the distal convoluted tubules, since it might already be in saturation. In contrast, this would have been an expected point for regulation in response to high magnesium intake to favor the high excretion of Mg^{2+} that takes place in this conditions. It might be that the reduced Ca^{2+} in the extracellular liquids is a more prominent regulatory driver in the TAL than high Mg^{2+} ; further experiments would be needed to support this idea, or contribute with more information.

In conclusion, no matter that the kidneys and the mouse metabolism in general appear to be fighting against the diets, neither high nor low magnesium intake induced appreciable changes in the TAL electrogenic transepithelial translocation of ions.

7.3. Regulation by hormones and second messengers

Epigenetic down regulation of Cld14 expression by the HDAC inhibitor SAHA reduces cation selectivity in the TAL

Cld14 expression was one of the key points in the observed regulation in the TAL during the high calcium diet. The proposed epigenetic regulatory mechanism (Gong *et al.*, 2014) for Cld14 in the TAL involving the CaSR (Figure 33) added new insights to how high calcium could reduce cation reabsorption in the TAL. Furthermore, it contributed with a novel approach to the general understanding and possible handling of the calcium excretion.

SAHA administration in young male mice resulted in a reduction in the transepithelial resistance in the TAL and a clear increment in the TAL's paracellular permeability to Na⁺. Increases in the Na⁺ paracellular permeability would lead to an increase in the driving forces for reabsorption of Ca²⁺ and Mg²⁺ in the TAL. Taking into account that SAHA reduced the expression of Cld14 in the TAL (Gong *et al.*, 2014), this effect of SAHA favoring the cation selectivity in the TAL was then in consistence with Cld14 acting as a modulator of Cld16, and Cld16-Cld19 (Gong *et al.*, 2012).

The present data show a tendency to increase paracellular permeabilities to Ca²⁺ and Mg²⁺, but with a higher scatter. It might be that due to the variation presented in this results a bigger sample size would be require to make it clearer. On the other hand, it might well not be the case that Cld14 action on Cld16 directly affects the permeabilities to Ca²⁺ or Mg²⁺. Since the discovery of the link between Cld16, and later also Cld19, and FHHNC, the role of Cld16 in divalent cations reabsorption has been under study (Simon *et al.*, 1999; Hou *et al.*, 2005, 2008; Himmerkus *et al.*, 2008; Hou & Goodenoughb, 2010; Will *et al.*, 2010; Houillier, 2014), but no clear conclusions have been make yet. Cld16 appears to form heterodimers together with Cld19 that confer cation selectivity to the TAL's tight junction. The observed increase in permeability to Na⁺ when Cld16 was over-expressed and its almost exclusive expression in the cortical TAL in the kidney, led to the new theory that it might affect the divalent cation reabsorption by not directly influencing their permeabilities but by increasing the driving force (Houillier, 2014). The

discovery of Cld14 modulatory effects on Cld16 and now the regulatory pathway of Cld14 expression via sensing peritubular Ca^{2+} help to a better understanding of this mechanism.

Another important aspect to consider is that SAHA is not a specific inhibitor of a particular HDAC, and HDAC are considered global regulators. Nevertheless, inhibition of HDAC is described to silence only a 2% of transcribed genes (Van Lint *et al.*, 1996), and used in the very low concentrations that were used for the present study, adverse effects can be reduced (Gong *et al.*, 2014). In the kidney, inhibition of HDAC affected only the proposed miR-Cld14 regulatory pathway, with no other obvious interference in the electrolyte control by the kidney (Gong *et al.*, 2014).

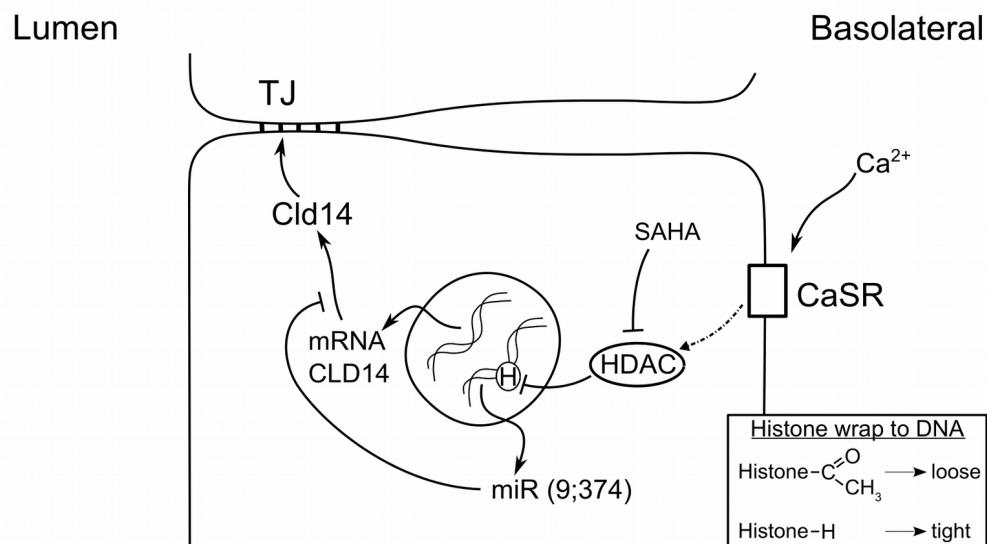


Figure 33: Epigenetic regulation of CLD14 expression.

The activation-deactivation of the genes coding for microRNA 9 (miR9) and microRNA 374 (miR374) controls the viability of mRNA CLD14 to be translated. Suberanilohydroxamic acid (SAHA) is a histone deacetylase inhibitor administered externally to test the model.

AVP

Vasopressin via interaction with the V2 receptor is known to increase cytoplasmic cAMP. In the TAL it increases the transcellular transport of NaCl and the activity of ROMK, causing a rise in the transepithelial voltage. The elevated transepithelial voltage implies an increase in the force that

drives the divalent cations to be reabsorbed through the tight junctions in the TAL. The present work presents a regulatory effect by AVP on the paracellular properties of the TAL that favors cation reabsorption.

Effect of water restriction in mouse TAL

Restriction in water intake triggers the secretion of AVP, raising urine's osmolality by increasing the water reabsorption in the kidneys. Conversely, excess in the water intake prevents the secretion of AVP, allowing the kidneys to waste water.

The urine osmolality of mice on water restricted and water loaded diets was used as a parameter of the efficiency of the method. Only one mouse from the water loaded group was not included in the analysis. This mouse urine osmolality value was comparable to the urine osmolality of the water restricted animals, and too high compared to the others in its group; so that, it was not considered to be “water loaded”.

The observed higher values in transepithelial voltage and in the transcellular transport (I_{sc}) in the freshly mechanically isolated mTAL from mice on water restricted conditions compared to the water loaded animals is in consistence previous reports of AVP activity in this tubular segment. Moderate water restriction has been described to increase NKCC2 abundance in rat mTAL after a 7-day treatment (Kim *et al.*, 1999). The stimulatory effect of AVP in the TAL has been linked to adenylyl cyclase IV, which enhance the protein expression and the phosphorylation of NKCC2 (Rieg *et al.*, 2013). They found the activation of NKCC2 via phosphorylation to be more sensible in the medullary portion, while its abundance increased in the entire segment. This is partly in correspondence to the finding that the AVP V_2 receptor is present vividly in the mTAL and in a weaker manner in the cTAL, except for the *macula densa* region (Mutig *et al.*, 2007). Nevertheless, no distinction in NKCC2 was found in the diets by Western Blot. The increase in membrane abundance of NKCC2 in presence of the AVP mimetic 1-desamino-8-D-Arg-vasopressin was described to be “moderate” compared to the more marked increases found in phospho-NKCC2 in single cTAL and mTAL (Mutig *et al.*, 2007). The lack of increase in the NKCC2

total expression in enzymatic isolated TAL, and the higher transepithelial transport rates in TAL from the WR group could speak in favor of the phosphorylation.

The effect of water restricted conditions on the paracellular properties of the TAL compared to the water loaded group suggests a regulation in this pathway by AVP. The increased selectivity for cations observed in mTAL from the WR group, at the expense of a raise in the permeability to Na^+ , balanced the overall raise in sodium-chloride reabsorption in this segment. Remember that approximately 50% of the Na^+ reabsorbed goes through the paracellular pathway, whereas the 100% of Cl^- is reabsorbed transcellularly. Under these circumstances, the kidney's medullary hypertonicity is increased, enhancing the water reabsorption and urine concentration in the medullary CD. The increased paracellular permeability to Na^+ in the tight junctions of mTAL can also enhance the reabsorption of divalent cations by increasing the driving force downstream in cTAL: the more the permeability to Na^+ in the mTAL, the less is the active concentration of Na^+ in the luminal fluid when it reaches the cortex in the cTAL. This situation would increase the chemical gradient for sodium, causing a higher diffusion of Na^+ back into the lumen, resulting in an enhanced lumen positive potential. Microperfusion of isolated cTAL would not add information to this particular, as it depends on the differential reabsorption that has taken place before. An increment in the transepithelial lumen positive potential could lead to a better reabsorption of divalent cations, even when the absolute paracellular permeabilities to these ions were not affected. Data from micropuncture studies would be needed to corroborate this idea. To this point, long-term treatment with DDAVP in DI rats was discussed not to have an effect in the Ca^{2+} or Mg^{2+} delivery to the TAL or in the percentage of fractional reabsorption of these ions in loops of Henle from medullary or superficial nephrons, but in reabsorption of Na^+ and Cl^- (Rouffignac *et al.*, 1991).

To try to find what could have been the change in the composition of the tight junction that favors the increase in P_{Na} , Western blots of the main claudins described to take part in cation permeability and selectivity of the TAL were performed. The total expression of Cld10, Cld16, or Cld19 was not changed. Increases in Cld10 abundance in the membrane are known to reduce

Na⁺ permeability, and make the tight junctions tighter. Cld16 and Cld19 interaction confers a high permeability to Na⁺ to the junction which is modulated by Cld14. Cld14 expression is too low to be nicely seen by Western blotting. In immunohistochemical observations (unpublished data) Cld10 have been seen to be highly present in intracellular compartments, very plausible in cytoplasmic vesicles. Cld10 membrane abundance could be changed by moving the cytoplasmic pool without needs of increase in the total expression, which is what was observed by Western blot. Even though, the abundance of Cld10 in the membrane observed by immunostaining in kidney from rats under similar conditions did not differ with the conditions. Further observations are needed, and possible post-transcriptional modifications (like phosphorylation) need to be evaluated.

Stimulation of freshly mechanically isolated mTAL with AVP

In order to examine the direct effect of acute stimulation with AVP on the paracellular properties of mTAL, paired experiments were performed. These experiments allowed the comparison between pre and post-stimulation with AVP of the transcellular and paracellular properties of TAL, but also with a time control series of experiments. I wanted to test the hypothesis that AVP not only activated the transepithelial transport, but also the paracellular permeability in the TAL. Therefore, only those tubules which showed an increase in V_{te} were included for the analysis, as they were considered to be successfully stimulated by AVP. The approximate 12 minutes time of stimulation after microperfusion and recovery from low sodium step was selected taking into account the dynamics of the transcellular transport simulation. At this time in most of the cases the increase in V_{te} had stabilized. AVP stimulation in those tubules increased the transepithelial transport or avoided decay. In contrast, the non-stimulated tubules had their transport rates reduced with time (Figure 25 C).

The changes observed in these acute experiments on the paracellular properties match the long-term experiments previously discussed with an increase in the cation selectivity of the tight junctions. Higher diffusion voltages after stimulation reflected an increased sodium-chloride

permeability ratio. This did not happen on the time control group, where diffusion voltages and permeability ratio were of the same magnitude. In this case an increase in P_{Na} was not observed.

Taken together, it is to this point not clear what the mechanism of action of AVP concerning the paracellular properties is. The long-term high systemic AVP induction reflected higher cation selectivity due to a higher P_{Na} , compared to control group. Nevertheless, no variations in total protein expression for the analyzed claudins were observed. In comparison, the *ex vivo* acute stimulation with AVP resulted also in an increase in cation selectivity, but due to variations in both Na^+ and Cl^- permeabilities, rather than a clear increase in P_{Na} . It is possible to conclude that long term *in vivo*, and acute *ex vivo* AVP stimulation modulate paracellular selectivity and permeability to cations in the mTAL. Further experiments are needed to explain the molecular nature of these effects.

7.4. Knock-out models

SORLA knock-out mouse model (SORLA^{-/-})

As discussed in the previous section, NKCC2 regulation defines the transcellular transport in the TAL, and the transcellular transport generates the transepithelial lumen-positive voltage typical for this tubular segment. It was shown that V_{te} was one of the key regulatory steps in the TAL: V_{te} was reduced as response to the high calcium diet and it was up regulated during stimulation with AVP or in a diet that was water restricted. V_{te} reflects the driving force for the paracellular reabsorption of divalent cations in the TAL.

Phosphorylation in the N-terminus of NKCC2 enhances its activity, thus increasing indirectly the V_{te} . As mentioned before, the processes that might reverse this mechanism are still under study. In our experiments with *SORLA^{-/-}* mice and the calcineurin $A\beta$ (CnA β) inhibitor cyclosporin A (CsA) we observed that there might be a regulatory pathway involving *SORLA* and CnA β for this particular dephosphorylation.

CsA partially prevents TAL from the loss of activity under control conditions. While after one hour incubation with vehicle the tubular transport rate declined, the extent of this phenomenon after one hour incubation with CsA was significantly smaller. The calcineurin inhibitor tacrolimus has been shown to increase the activity of the renal sodium-chloride cotransporter (NCC) in DCT by an increase in abundance of phospho-NCC (Hoorn *et al.*, 2011b). A different isoform, calcineurin A α , is important in the CD for the correct cellular trafficking of AQP2 (Gooch *et al.*, 2006; Fenton & Knepper, 2007). In the same line, the data presented here indicate that in the TAL CnA β is in part responsible for the deactivation of NKCC2.

When SORLA was not present, NKCC2 activity was considerably reduced. NKCC2 was probably working already at a minimum as transport did not decay with time. The normal phosphorylation pattern of NKCC2 might have been strongly affected. The same transport rates between TAL from SORLA^{-/-} mice after CsA incubation or after incubation with vehicle support this idea: if there is no correct phosphorylation, the inhibition of the phosphatase has no or little effect. Indeed, SORLA^{-/-} animals have very low baseline of pNKCC2 in comparison to WT animals (Borschewski *et al.*, 2015). There are two things to be considered here, first, the kinase activity that phosphorylates NKCC2 in SORLA^{-/-} mice could be affected. Previous descriptions show that SORLA is involved in the intracellular trafficking of OSR1/SPAK kinases. These kinases are involved in the activation of NKCC2, with WNK kinases as activator of SPAK (Reiche *et al.*, 2010; Hoorn *et al.*, 2011a; Gagnon & Delpire, 2012; Mount, 2014). So that, incorrect trafficking of the kinase could explain in part the reduced NKCC2 phosphorylation in SORLA^{-/-} mice. And second, we showed that in SORLA deficient mice the total abundance of the phosphatase CnA β was markedly higher than in WT mice, with a very high abundance near the apical membrane (Borschewski *et al.*, 2015). We also showed that there is an interaction between CnA β and NKCC2, and between CnA β and SORLA (Borschewski *et al.*, 2015). These indicate that CnA β might be the phosphatase responsible for the dephosphorylation of pNKCC2, and that SORLA could be involved in the normal intracellular trafficking of CnA β . Therefore, SORLA could be part in TAL cells internal control of the abundance of pNKCC2.

We propose an endogenous mechanism of control of the activation-deactivation of NKCC2 that involves SORLA (Figure 34). SORLA carries SPAK to the apical membrane where it can, when active, interact with NKCC2 (Reiche *et al.*, 2010; Ares *et al.*, 2011; Gagnon & Delpire, 2012). In parallel, SORLA might target CnA β to lysosomes, reducing its total abundance and presence in the proximity to the apical membrane when higher NKCC2 activity is needed, for example in the presence of AVP. This needs to be confirmed, but is in concordance with the mechanism of action of the Vps10p-domain receptor family, to which SORLA belongs (Hermeij, 2009), and with the described action of SORLA and Sortilin in regulating the abundance of neuronal membrane factors related to Alzheimer disease (Hermeij, 2009; Nykjaer & Willnow, 2012). According to those mechanisms (Hermeij, 2009), SORLA is capable of targeting internalized ligands from the membrane to lysosomes or convey a trans-Golgi network-to-endosome transport (Figure 34).

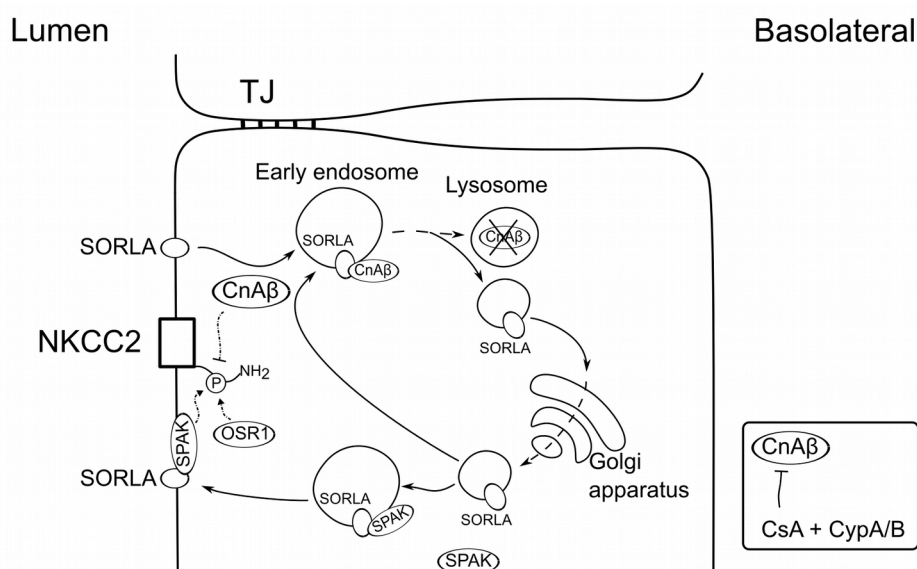


Figure 34: Proposed endogenous mechanism of SORLA as inhibitor of calcineurin A (CnA β).

The figure shows the described membrane-to-lysosome and the network-to-endosome mechanisms of action of SORLA. CnA β can be inhibited by addition of cyclosporin A (CsA) in the presence of the cytosolic proteins cyclophilin A and B (CypA/B).

In addition, the results here presented indicate that the phosphorylation state of NKCC2 changes its affinity of NKCC2 to Cl⁻. When the experiments at high and low Cl⁻ concentration are analyzed together, it is possible to observe that the activity of NKCC2 (using I_{sc} as an indicator) was

reduced to near 50% in WT animals at time 0h, a sign that the low Cl^- concentration was closed to the K_m . After one hour of incubation with vehicle, the tubule transport decreased to only 20% under low Cl^- conditions. Examining this two situations, and assuming that NKCC2 follows the kinetics described (Greger *et al.*, 1983b), we can interpret that the concentration of Cl^- at which NKCC2 reaches half of its activity has increased after one hour incubation *ex vivo*. After one hour incubation in the presence of CsA it was observed that I_{sc} under low Cl^- condition was only reduced to 30% of I_{sc} at high Cl^- . The affinity of NKCC2 for Cl^- after incubation with the CnA β inhibitor has to be therefore higher than the affinity of NKCC2 for Cl^- in TALs incubated in vehicle, and closer to its affinity at time 0.

The transport rates of TALs isolated from SORLA^{-/-} mice showed similar maximal activity at time 0, incubation in vehicle, or incubation with CsA. When the conditions were changed to low Cl^- , the activity was reduced to around 20% of the maximal value under all conditions, indicating a similar Cl^- affinity, comparable to that of NKCC2 in TALs from WT when incubated under vehicle conditions.

These results suggest that phosphorylation of NKCC2 influence its affinity for Cl^- .

MR^{AQP2Cre}

Although TAL is no classical aldosterone sensitive segment, there is literature on aldosterone and downstream targets that supported the hypothesis that high levels of Aldosterone might interfere with the segment. mRNA for MR was found in TAL of mouse and rats (Ackermann *et al.*, 2010), and the serum- and glucocorticoid-induced kinase-1 (sgk1) was also found in TAL from rats (Alvarez de la Rosa *et al.*, 2003). In parallel, some 11 β -hydroxysteroid dehydrogenase (11 β -HSD2), needed of aldosterone to act independently from cortisol, was reported to be present in the TAL (Farman & Bocchi, 2000). Aldosterone was found to have high stimulatory effect on TAL Na^+ transport (Work & Jamison, 1987), but this data is controversial and contrast to others which found no effect of aldosterone on the expression or activity of Na^+/K^+ -ATPase (Tsuruoka *et al.*, 1995). There are reports in cell culture that aldosterone might interfere with TAL function by

potentiating the action of vitamin D3 or by regulating the epithelial exchange of Na⁺ and H⁺ (Good *et al.*, 2003; Watts *et al.*, 2006). Even though, TAL from the high aldosterone mouse model (MR^{AQP2Cre}) did not show any difference in the transepithelial transport of ions compared to littermates under the conditions here used. A hypothetical function of MR in the TAL therefore remains unknown.

Cld10/Cld16 double knock-out mice

To better understand the paracellular properties of the TAL, knock-out mouse models of claudins have been developed. Claudin 16 (Cld16) and claudin 10 (Cld10) appear to be particularly important in the tight junction of the TAL, and their knock-out models have been well described in recent years.

Punctual mutations in Cld16, together with others in Cld19, have been identified as the genetic origins of the familial hypomagnesemia with hypercalciuria and nephrocalcinosis (FHHNC). The Cld16 knock-out mouse model (Cld16-KO) mimics part of the symptomatology of FHHNC, presenting high calcium excretion and low plasma magnesium, but no nephrocalcinosis (Will *et al.*, 2010). The Cld16-KO mice used in the present work have the same genetic background as those of Will *et al.* (2010), and accordingly the same symptoms. The higher transepithelial resistance and lower transport activity observed in mTAL from these animals, seemed to be a compensatory reaction, but no differences in the paracellular properties were found between this animals' TAL and TAL from wild-type mice (WT). In cTAL, while the transport rate was slightly but significantly higher, also neither the selectivity, nor the absolute permeabilities were affected compared with WT. This is in concordance with Will *et al.* (2010), were they also showed no differences in selectivity. Interestingly, in previous reports, with a Cld16 knock-down mouse model (Cld16-KD), the selectivity was found to be reduced in TAL from Cld16-KD (Himmerkus *et al.*, 2008; Hou & Goodenough, 2010). On the other hand, over-expression of Cld16 in LLC-PK1 cell cultures (a cell line with anion paracellular selectivity and no endogenous expression of Cld16, 14, or 19) reduces the transepithelial resistance and increased the selectivity for cations (Hou *et al.*, 2005; Gong *et al.*, 2012). In addition, all FHHNC disease

mutants of Cld16 strongly diminished P_{Na} , suggesting an additional function in the control of Na^+ permeability rather than directly in Ca^{2+} or Mg^{2+} (Hou *et al.*, 2005, 2013).

Cld10b is the splice variant expressed in the TAL. When expressed in MDCK or LLC-PK1 cell lines it provokes a substantial reduction in the transepithelial resistance, with an increased permeability to cations (Van Itallie *et al.*, 2006; Günzel *et al.*, 2009). Cld10 is thought to determine the paracellular permeability to sodium in the TAL tight-junction (Breiderhoff *et al.*, 2012). The kidney specific Cld10-KO mouse model was somewhat polyuric, hypermagnesemic, with acidic urine, and presented with nephrocalcinosis, as described by Breiderhoff *et al.* (2012). The imbalance created by the absence of Cld10 in those animals triggered the up and down-regulation of many other renal genes, involving calcium and potassium channels, calbindins, kinases, and interestingly up-regulation of Cld16, Cld14, and Cld19 (Breiderhoff *et al.*, 2012). Increases in the expression of Cld16 and Cld19 would increase the cation selectivity, but the simultaneous increment in Cld14 negatively modulates this effect (Gong *et al.*, 2012). Even though, the high plasma magnesium in these mice indicates a hyper-reabsorption of Mg^{2+} in the kidneys. In both, cTAL and mTAL, the selectivity was dramatically reduced compared to WT, together with a lower permeability to Na^+ in the mTAL. However, no differences in paracellular permeabilities to Ca^{2+} or Mg^{2+} were verified in those tubules.

In total, in the cTAL, the major site for reabsorption of Ca^{2+} and Mg^{2+} , it was possible to observe higher values for transepithelial voltage with a correspondent enlarged transport rate in the Cld10-KO animals compared to WT, while in mTAL a higher transepithelial resistance resulted in lower transepithelial transport. Then, this might affect the generation of the high osmolality gradient in the renal interstitium that helps to concentrate urine and reabsorb water.

Taken until this point, the data presented is consistent to the previous reports on this animal, and it is not yet clear what are the exact roles of Cld16 and Cld10. The total system is obviously affected and is not recovered by the genetic regulation of other claudins or transporters, neither in the TAL nor in other segments. The almost opposite symptomatology of Cld16-KO and Cld10-KO in terms of magnesemia, calcium excretion or presence of nephrocalcinosis apparently

indicates, at least indirectly, opposite effects of those claudins in the paracellular reabsorption of divalent cations. The simultaneous double knock-out of renal Cld16 and TAL-specific Cld10 (dKO) were expected to add information to this particular.

Those dKO animals are polyuric and polydipsic, with somewhat low urinary pH, but in contrast to Cld10-KO or Cld16-KO they show a normal magnesemia, no nephrocalcinosis, and normal excretion of Mg^{2+} and Ca^{2+} . Nevertheless, they are not healthy: they do not grow normally, they have low Na^+ excretion, and high excretion with low plasma values of K^+ (Himmerkus *et al.*, manuscript in preparation). This symptomatology was in part due to the high resistance of the TAL from these animals, with very low, close to 0, paracellular permeabilities to Na^+ and Ca^+ , compared to the values observed in the WT TAL. At TAL level, the dKO was more similar to the Cld10-KO, but for the particularity of the very low P_{Ca} . As a matter of fact, the Cld10-KO had a tendency to have higher paracellular permeabilities to divalent cations (Ca^{2+} and Mg^{2+}) in the cTAL than all the other groups studied.

It is surprising that the urinary excretion of Ca^{2+} in the dKO mice have values similar to WT mice. Our collaborators observed that several genes expressed in distal tubules were differentially regulated (data not published), suggesting further compensatory mechanisms in the distal nephron. The dKO seems to be impeded in paracellular reabsorption, hence compensatory mechanisms are necessary to balance the divalent cation reabsorption, probably at the expense of K^+ and Na^+ , and H^+ . The water regime is not balanced in those animals.

Taken all together, the absence of Cld16 and Cld10 at once, strongly affected the cation specific paracellular pathway in the TAL. This situation reversed the symptoms described for the single knock-out mouse models, but led to hypokalemia, polydipsia, polyuria, and problems with growth. Our results show a complementary function of Cld10 and Cld16 in the TAL regarding Ca^{2+} and Mg^{2+} paracellular reabsorption, and the importance of the TAL's paracellular pathway for the reabsorption of cations in the homeostasis of water and ions.

8. Conclusions

In the present study I introduced in detail a method for the calculation of the absolute paracellular permeabilities in the TAL. The accommodation of the experimental conditions permit us the use of this method to evaluate the regulation on the paracellular permeabilities of the TAL to Na^+ , Cl^- , Mg^{2+} , and Ca^{2+} . This method, together with the methodology for enzymatically and mechanically isolated renal tubules, and the other methods described, give us in our laboratory the tools to study the transepithelial and the paracellular properties of the TAL.

The study with calcium diets shows that the TAL adapts to high Ca^{2+} loads by reducing the driving force for Ca^{2+} and Mg^{2+} uptake and simultaneously reduces their paracellular permeability. This is supposed to be of high relevance for the maintenance of intact Ca^{2+} and Mg^{2+} metabolism and overall body function. Upregulation of Cld10b and Cld14 expression under high calcium diet might be involved in this response of the TAL. At the same time, the study shows that low calcium diet in mice for 8 days does not induce physiological responses in the transport of cations in the TAL.

Similarly, the overall metabolic response of mice to the Mg^{2+} diets suggests that magnesium might be important for calcium absorption and assimilation. Nevertheless, no matters that the kidneys and the organism in general appear to be fighting against the diet, neither high nor low magnesium intake induced appreciable changes in the TAL transepithelial translocation of ions.

When treated with SAHA, an inhibitor of HDAC the paracellular permeability to Na^+ is increased in the TAL and the transepithelial resistance reduced. These physiological responses to SAHA are supported by the previous observations that SAHA reduces Cld14 membrane expression in the TAL. It indicates that physiological activation and inhibition of HDAC can act as a regulator of the paracellular pathway in the TAL via epigenetic regulation of Cld14, an already known negative modulator of Cld16's Na^+ permeability.

In order to elucidate the effects of hormonal stimulation on TAL tight junction a high aldosterone mouse model and AVP were tested. AVP was tested via water restriction and acute stimulation. The high aldosterone mouse model (MR^{AQP2Cre}) did not affect the transepithelial transport in the TAL. Apparently aldosterone has no chronic effect in TAL.

Water restriction and AVP increase paracellular selectivity and permeability for cations in the TAL. Freshly isolated mTAL from the water restricted (WR) group maintain higher rates of transepithelial transport compared to tubules from the water loaded (WL) group. Diffusion voltages were larger in the WR group, resulting in higher P_{Na}/P_{Cl} , and higher P_{Na} compared to the WL group. As for the acute mTAL stimulation *ex vivo* with AVP, it increased transepithelial transport, with I_{sc} and V_{te} increased when stimulated; while in contrast, the time control group I_{sc} and V_{te} decreased over time. Besides, after AVP stimulation larger diffusion voltages took place and P_{Na}/P_{Cl} was increased. In conclusion, long term *in vivo*, and acute *ex vivo* AVP stimulation regulates paracellular selectivity and permeability for cations in the mTAL.

The paracellular reabsorption of divalent cations depends largely on the activity of the NKCC2. Inhibition of CnA β activity with CsA prevents partially the loss of activity of NKCC2 that normally takes place after one hour incubation, but no differences were observed in TALs from SORLA^{-/-} mice with this treatment. Changing from high Cl⁻ to low Cl⁻ conditions differences in the transport kinetics were observed in TAL from WT mice, but not in those from SORLA^{-/-} mice. These data indicate that CnA β is in part responsible in the TAL for the deactivation of NKCC2, and suggest that phosphorylation of NKCC2 influence its affinity for Cl⁻. SORLA might be involved in the intracellular trafficking of CnA β , and it could be partly used by TAL cells to control the abundance of pNKCC2.

The importance of the paracellular pathway for the reabsorption of divalent cations was evidenced with the characterization of the dKO mouse model. Our results show a complementary function of Cld10 and Cld16 in the TAL regarding Ca²⁺ and Mg²⁺ paracellular reabsorption: the absence of Cld16 and Cld10 at once, strongly affects the cation specific paracellular pathway in the TAL and the water and ion balance in general, but at the same time

dKO mice did not have the characteristic problems of any of the two single KO. In brief, both claudins are needed to be present in the tight-junctions of a healthy TAL to guarantee a proper homeostasis. When not present, the TAL's paracellular permeabilities to cations are extremely reduced, in particular in cTAL.

In summary, the tight junction in the TAL is an active and complex system that reacts to stimuli, and plays a key role in divalent cation homeostasis. This tight junction is involved in regulatory processes that respond to AVP or extracellular Ca^{2+} , and rely on the claudin expression to properly allow the transport of ions. Defects in claudin expression can be the cause of diseases. The data presented here are a further step in characterizing the paracellular pathway in the TAL and its regulation as a physiologically relevant mechanism in ion homeostasis. This opens new perspectives for research and disease treatment.

Publications related to the thesis

- 2015 Plain A, Wulfmeyer VC, Milatz S, Kliez A, Hou J, Bleich M & Himmerkus N (2015). Corticomedullary difference in the effects of dietary Ca(2+) on tight junction properties in thick ascending limbs of Henle's loop. *Pflugers Arch*; DOI: 10.1007/s00424-015-1748-7.
- 2015 Borschewski A, Himmerkus N, Boldt C, Blankenstein KI, McCormick JA, Lazelle R, Willnow TE, Jankowski V, Plain A, Bleich M, Ellison DH, Bachmann S & Mutig K (2015). Calcineurin and Sorting-Related Receptor with A-Type Repeats Interact to Regulate the Renal Na⁺-K⁺-2Cl⁻ Cotransporter. *J Am Soc Nephrol* 1–13.
- 2014 Gong Y, Himmerkus N, Plain A, Bleich M & Hou J (2014). Epigenetic Regulation of MicroRNAs Controlling CLDN14 Expression as a Mechanism for Renal Calcium Handling. *J Am Soc Nephrol* 26, 663–676.

Acknowledgments

I would like to thank my supervisor Prof. Markus Bleich for the opportunity to work in his group in this very interesting topic, and for all I have learned during this time by his side. I have no space enough to thank Nina Himmerkus for all her help, teachings and working time spend together; to Prof. Jens Leipziger for his good advises, and for receiving me and make me feel at home when I went to work to his lab; to Susanne Milatz for her invaluable help in writing, reviewing, translating, and editing; or to Sonja Reich for all the time spent proofreading this work. I thank Kerim Mutig, and Dorothee Günzel for their support to my work and nice discussions; and Prof. Jianghui Hou for all the material supplied.

Special thanks to Magda and Kerstin, it was a real pleasure to count with your friendship and your presence when I first arrived to Germany. I'd like also to specially thank Vera Wulfmeyer for the time working together, the talks, and the cookies (a very important point); and also to Wiebke, Svenja, Doro, Analisa, Adrian, Lieske, and Lara for the nice ambiance and good vibes.

I'm very grateful to Regina Lingg, Thomas Stegmann and Michaela Unmack for their technical assistance, and to Ingo Klein for is support with all my "electronic requests".

And last but not least I want to thank my family and friends that have been there to me, even when I disappeared for several months to live in the darkness (literally) for writing.

Erklärung

Hiermit erkläre ich an Eides statt, dass die vorliegende Dissertation, abgesehen von der Beratung durch meinen akademischen Lehrer, nach Inhalt und Form meine eigene Arbeit ist und ich keine anderen als die angegebenen Quellen und Hilfsmittel verwendet habe. Des Weiteren versichere ich, dass die vorliegende Dissertation weder im Ganzen noch zum Teil einer anderen Stelle im Rahmen eines Prüfungsverfahrens vorgelegen hat und unter Einhaltung der Regeln guter wissenschaftlicher Praxis entstanden ist.

Kiel, den 27. Oktober 2015

Allein Plain Reyes

References

- Ackermann D, Gresko N, Carrel M, Loffing-Cueni D, Habermehl D, Gomez-Sanchez C, Rossier BC & Loffing J (2010). In vivo nuclear translocation of mineralocorticoid and glucocorticoid receptors in rat kidney: differential effect of corticosteroids along the distal tubule. *Am J Physiol Renal Physiol* **299**, F1473–F1485.
- Alvarez de la Rosa D, Coric T, Todorovic N, Shao D, Wang T & Canessa CM (2003). Distribution and regulation of expression of serum- and glucocorticoid-induced kinase-1 in the rat kidney. *J Physiol* **551**, 455–466.
- Ares GR, Caceres PS & Ortiz PA (2011). Molecular regulation of NKCC2 in the thick ascending limb. *Am J Physiol Renal Physiol* **301**, F1143–F1159.
- Bachmanov AA, Reed DR, Beauchamp GK & Michael G (2002). Food Intake, Water Intake, and Drinking Spout Side Preference of 28 Mouse Strains. *Behav Genet* **32**, 435–443.
- Bleich M, Schlatter E & Greger R (1990). The luminal K⁺ channel of the thick ascending limb of Henle's loop. *Pflügers Arch Eur J Physiol* **415**, 449–460.
- Bleich M, Shan Q & Himmerkus N (2012). Calcium regulation of tight junction permeability. *Ann N Y Acad Sci* **1258**, 93–99.
- Boron WF & Boulpaep EL (2009). *Medical Physiology*, 2nd edn. Elsevier Saunders.
- Borschewski A, Himmerkus N, Boldt C, Blankenstein KI, McCormick JA, Lazelle R, Willnow TE, Jankowski V, Plain A, Bleich M, Ellison DH, Bachmann S & Mutig K (2015). Calcineurin and Sorting-Related Receptor with A-Type Repeats Interact to Regulate the Renal Na⁺-K⁺-2Cl⁻ Cotransporter. *J Am Soc Nephrol* 1–13.
- Breiderhoff T, Himmerkus N, Stuiver M, Mutig K, Will C, Meij IC, Bachmann S, Bleich M, Willnow TE & Müller D (2012). Deletion of claudin-10 (Cldn10) in the thick ascending limb impairs paracellular sodium permeability and leads to hypermagnesemia and nephrocalcinosis. *Proc Natl Acad Sci U S A* **109**, 14241–14246.
- Brink EJ, Beynen a C, Dekker PR, van Beresteijn EC & van der Meer R (1992). Interaction of calcium and phosphate decreases ileal magnesium solubility and apparent magnesium absorption in rats. *J Nutr* **122**, 580–586.

- de Bruijn PIA, Larsen CK, Frische S, Himmerkus N, Praetorius HA, Bleich M & Leipziger J (2015). Furosemide-induced urinary acidification is caused by pronounced H⁺ secretion in the thick ascending limb. *Am J Physiol Renal Physiol* **309**, F146–F153.
- Burg MB (1972). Perfusion of isolated renal tubules. *Yale J Biol Med* **45**, 321–326.
- Deng X, Song Y, Manson JE, Signorello LB, Zhang SM, Shrubsole MJ, Ness RM, Seidner DL & Dai Q (2013). Magnesium, vitamin D status and mortality: results from US National Health and Nutrition Examination Survey (NHANES) 2001 to 2006 and NHANES III. *BMC Med* **11**, 187.
- Dimke H, Desai P, Borovac J, Lau A, Pan W & Alexander RT (2013). Activation of the Ca²⁺-sensing receptor increases renal claudin-14 expression and urinary Ca²⁺ excretion. *Am J Physiol Renal Physiol* **304**, F761–F769.
- Engelund MB, Yu a SL, Li J, Madsen SS, Færgeman NJ & Tipsmark CK (2012). Functional characterization and localization of a gill-specific claudin isoform in Atlantic salmon. *Am J Physiol Regul Integr Comp Physiol* **302**, R300–R311.
- Farman N & Bocchi B (2000). Mineralocorticoid selectivity: Molecular and cellular aspects. *Kidney Int* **57**, 1364–1369.
- Favus MJ, Bushinsky DA & Jacob LJ (2006). Regulation of Calcium , Magnesium , and Phosphate Metabolism. In *Primer on the Metabolic Bone Diseases And Disorders of Mineral Metabolism*, pp. 76–83. American Society for Bone and Mineral Research.
- Fenton R a & Knepper M a (2007). Mouse models and the urinary concentrating mechanism in the new millennium. *Physiol Rev* **87**, 1083–1112.
- De Franceschi L, Brugnara C & Beuzard Y (1997). Dietary magnesium supplementation ameliorates anemia in a mouse model of beta-thalassemia. *Blood* **90**, 1283–1290.
- Gagnon KB & Delpire E (2012). Molecular Physiology of SPAK and OSR1: Two Ste20-Related Protein Kinases Regulating Ion Transport. *Physiol Rev* **92**, 1577–1617.
- Giebisch G (2001). Renal potassium channels: Function, regulation, and structure. *Kidney Int* **60**, 436–445.
- Giménez I & Forbush B (2003). Short-term stimulation of the renal Na-K-Cl cotransporter (NKCC2) by vasopressin involves phosphorylation and membrane translocation of the protein. *J Biol Chem* **278**, 26946–26951.

- Giménez I & Forbush B (2005). Regulatory phosphorylation sites in the NH₂ terminus of the renal Na-K-Cl cotransporter (NKCC2). *Am J Physiol Renal Physiol* **289**, F1341–F1345.
- Goldman DE (1943). POTENTIAL, IMPEDANCE, AND RECTIFICATION IN MEMBRANES. *J Gen Physiol* **27**, 37–60.
- Gong Y, Himmerkus N, Plain A, Bleich M & Hou J (2014). Epigenetic Regulation of MicroRNAs Controlling CLDN14 Expression as a Mechanism for Renal Calcium Handling. *J Am Soc Nephrol* **26**, 663–676.
- Gong Y, Renigunta V, Himmerkus N, Zhang J, Renigunta A, Bleich M & Hou J (2012). Claudin-14 regulates renal Ca⁺⁺ transport in response to CaSR signalling via a novel microRNA pathway. *EMBO J* **31**, 1999–2012.
- Gooch JL, Guler RL, Barnes JL & Toro JJ (2006). Loss of calcineurin Aalpha results in altered trafficking of AQP2 and in nephrogenic diabetes insipidus. *J Cell Sci* **119**, 2468–2476.
- Good DW, George T & Watts BA (2003). Aldosterone potentiates 1,25-dihydroxyvitamin D₃ action in renal thick ascending limb via a nongenomic, ERK-dependent pathway. *Am J Physiol Cell Physiol* **285**, C1122–C1130.
- Gorgels TGMF, Waarsing JH, De Wolf A, Ten Brink JB, Loves WJP & Bergen A a B (2010). Dietary magnesium, not calcium, prevents vascular calcification in a mouse model for pseudoxanthoma elasticum. *J Mol Med* **88**, 467–475.
- Greger R (1981). Cation Selectivity of the Isolated Perfused Cortical Thick Ascending Limb of Henle ' s Loop of Rabbit Kidney. *Pflugers Arch* **390**, 30–37.
- Greger R (1985). Ion transport mechanisms in thick ascending limb of Henle's loop of mammalian nephron. *Physiol Rev* **65**, 760–797.
- Greger R & Hampel W (1981). A modified system for in vitro perfusion of isolated renal tubules. *Pflügers Arch Eur J Physiol* **389**, 175–176.
- Greger R, Oberleithner H, Schlatter E, Cassola AC & Weidtker C (1983a). Chloride activity in cells of isolated perfused cortical thick ascending limbs of rabbit kidney. *Pflügers Arch Eur J Physiol* **399**, 29–34.
- Greger R, Schlatter E & Lang F (1983b). Evidence for Electroneutral Sodium Chloride Cotransport in the Cortical Thick Ascending Limb of Henle ' s Loop of Rabbit Kidney *. *Pflügers Arch Eur J Physiol* **308–314**.

- Günzel D & Fromm M (2012). Claudins and other tight junction proteins. *Compr Physiol* **2**, 1819–1852.
- Günzel D, Stuiver M, Kausalya PJ, Haisch L, Krug SM, Rosenthal R, Meij IC, Hunziker W, Fromm M & Müller D (2009). Claudin-10 exists in six alternatively spliced isoforms that exhibit distinct localization and function. *J Cell Sci* **122**, 1507–1517.
- Günzel D & Yu ASL (2009). Function and Regulation of Claudins in the Thick Ascending Limb of Henle. *Pflugers Arch* **458**, 77–88.
- Günzel D & Yu ASL (2013). Claudins and the modulation of tight junction permeability. *Physiol Rev* **93**, 525–569.
- Guyton AC & Hall JE (2005). *TEXTBOOK OF MEDICAL PHYSIOLOGY*, 11th ed. Elsevier Saunders.
- Halls ML, Cooper DMF, Rosenberg SS, Spitzer NC, Fearnley CJ, Roderick HL, Bootman D, Catterall W a, Dupont G, Combettes L, Gary S, Webb SE, Miller AL, Lewis RS, Hill-eubanks DC, Werner ME & Heppner TJ (2010). Regulation by Ca²⁺ -Signaling Pathways of Adenylyl Cyclases Regulation by Ca²⁺ -Signaling Pathways of Adenylyl Cyclases.
- Hermey G (2009). The Vps10p-domain receptor family. *Cell Mol Life Sci* **66**, 2677–2689.
- Himmerkus N, Shan Q, Goerke B, Hou J, Goodenough D a & Bleich M (2008). Salt and acid-base metabolism in claudin-16 knockdown mice: impact for the pathophysiology of FHHNC patients. *Am J Physiol Renal Physiol* **295**, F1641–F1647.
- Hodgkin A & Katz B (1949). The effect of sodium ions on the electrical activity of the giant axon of the squid. *J Physiol* **108**, 37–77.
- Hoorn EJ, Nelson JH, McCormick JA & Ellison DH (2011a). The WNK kinase network regulating sodium, potassium, and blood pressure. *J Am Soc Nephrol* **22**, 605–614.
- Hoorn EJ, Walsh SB, McCormick JA, Fürstenberg A, Yang C-L, Roeschel T, Paliege A, Howie AJ, Conley J, Bachmann S, Unwin RJ & Ellison DH (2011b). The calcineurin inhibitor tacrolimus activates the renal sodium chloride cotransporter to cause hypertension. *Nat Med* **17**, 1304–1309.
- Hou J & Goodenough DA (2010). Claudin-16 and claudin-19 function in the thick ascending limb. *Curr Opin Nephrol Hypertens* **19**, 483–488.
- Hou J, Paul DL & Goodenough D a (2005). Paracellin-1 and the modulation of ion selectivity of tight junctions. *J Cell Sci* **118**, 5109–5118.

- Hou J, Rajagopal M & Yu ASL (2013). Claudins and the Kidney Volume 75: Annual Review of Physiology. *Annu Rev Physiol* **75**, 479–501.
- Hou J, Renigunta A, Konrad M, Gomes AS, Schneeberger EE, Paul DL, Waldegger S & Goodenough DA (2008). Claudin-16 and claudin-19 interact and form a cation-selective tight junction complex. *J Clin Invest* **118**, 619–628.
- Houillier P (2014). Mechanisms and regulation of renal magnesium transport. *Annu Rev Physiol* **76**, 411–430.
- Van Itallie C, Rahner C & Anderson JM (2001). Regulated expression of claudin-4 decreases paracellular conductance through a selective decrease in sodium permeability. *J Clin Invest* **107**, 1319–1327.
- Van Itallie CM, Rogan S, Yu A, Vidal LS, Holmes J & Anderson JM (2006). Two splice variants of claudin-10 in the kidney create paracellular pores with different ion selectivities. *Am J Physiol Renal Physiol* **291**, F1288–F1299.
- Kahle KT, Macgregor GG, Wilson FH, Van Hoek AN, Brown D, Ardito T, Kashgarian M, Giebisch G, Hebert SC, Boulpaep EL & Lifton RP (2004). Paracellular Cl⁻ permeability is regulated by WNK4 kinase: insight into normal physiology and hypertension. *Proc Natl Acad Sci U S A* **101**, 14877–14882.
- Kim G-H, Ecelbarger CA, Mitchell C, Packer RK, Wade JB & Knepper MA (1999). Vasopressin increases Na-K-2Cl cotransporter expression in thick ascending limb of Henle's loop. *Am J Physiol Ren Physiol* **276**, F96–F103.
- Kimizuka H & Koketsu K (1964). Ion Transport Through Cell Membrane - Kimizuka-Koketsu.pdf. *J Theor Biol* **6**, 290–305.
- Konrad M et al. (2006). Mutations in the Tight-Junction Gene Claudin 19 (CLDN19) Are Associated with Renal Magnesium Wasting, Renal Failure, and Severe Ocular Involvement. *Am J Hum Genet* **79**, 949–957.
- LaRusso J, Li Q, Jiang Q & Uitto J (2009). Elevated dietary magnesium prevents connective tissue mineralization in a mouse model of pseudoxanthoma elasticum (Abcc6(-/-)). *J Invest Dermatol* **129**, 1388–1394.
- Lerolle N (2004). Angiotensin II inhibits NaCl absorption in the rat medullary thick ascending limb. *AJP Ren Physiol* **287**, F404–F410.

- Li J, Ananthapanyasut W & Yu ASL (2011). Claudins in renal physiology and disease. *Pediatr Nephrol* **26**, 2133–2142.
- Van Lint C, Emiliani S & Verdin E (1996). The expression of a small fraction of cellular genes is changed in response to histone hyperacetylation. *Gene Expr* **5**, 245–253.
- Loupy A, Ramakrishnan SK, Wootla B, Chambrey R, de la Faille R, Bourgeois S, Bruneval P, Mandet C, Christensen EI, Faure H, Cheval L, Laghmani K, Collet C, Eladari D, Dodd RH, Ruat M & Houillier P (2012). PTH-independent regulation of blood calcium concentration by the calcium-sensing receptor. *J Clin Invest* **122**, 3355–3367.
- Mount DB (2014). Thick Ascending Limb of the Loop of Henle. *Clin J Am Soc Nephrol* **9**, 1974–1986.
- Mutig K, Paliege A, Kahl T, Jo T, Mu W & Bachmann S (2007). Vasopressin V 2 receptor expression along rat, mouse, and human renal epithelia with focus on TAL. *Am J Physiol Renal Physiol* **293**, F1166–F1177.
- Nykjaer A & Willnow TE (2012). Sortilin: a receptor to regulate neuronal viability and function. *Trends Neurosci* **35**, 261–270.
- Ponce-Coria J, San-Cristobal P, Kahle KT, Vazquez N, Pacheco-Alvarez D, de Los Heros P, Juárez P, Muñoz E, Michel G, Bobadilla NA, Gimenez I, Lifton RP, Hebert SC & Gamba G (2008). Regulation of NKCC2 by a chloride-sensing mechanism involving the WNK3 and SPAK kinases. *Proc Natl Acad Sci U S A* **105**, 8458–8463.
- Reiche J, Theilig F, Rafiqi FH, Carlo A-S, Miltz D, Mutig K, Todiras M, Christensen EI, Ellison DH, Bader M, Nykjaer A, Bachmann S, Alessi D & Willnow TE (2010). SORLA/SORL1 functionally interacts with SPAK to control renal activation of Na⁽⁺⁾-K⁽⁺⁾-Cl⁽⁻⁾ cotransporter 2. *Mol Cell Biol* **30**, 3027–3037.
- Renkema KY, Alexander RT, Bindels RJ & Hoenderop JG (2008). Calcium and phosphate homeostasis: concerted interplay of new regulators. *Ann Med* **40**, 82–91.
- Riccardi D & Brown EM (2010). Physiology and pathophysiology of the calcium-sensing receptor in the kidney. *Am J Physiol Renal Physiol* **298**, F485–F499.
- Richardson C, Sakamoto K, de los Heros P, Deak M, Campbell DG, Prescott AR & Alessi DR (2011). Regulation of the NKCC2 ion cotransporter by SPAK-OSR1-dependent and -independent pathways. *J Cell Sci* **124**, 789–800.

- Rieg T, Tang T, Uchida S, Hammond HK, Fenton R a. & Vallon V (2013). Adenylyl cyclase 6 enhances NKCC2 expression and mediates vasopressin-induced phosphorylation of NKCC2 and NCC. *Am J Pathol* **182**, 96–106.
- Ronzaud C, Loffing J, Bleich M, Gretz N, Gröne H-J, Schütz G & Berger S (2007). Impairment of sodium balance in mice deficient in renal principal cell mineralocorticoid receptor. *J Am Soc Nephrol* **18**, 1679–1687.
- Rouffignac C De, Stefano A Di, Wittner M, Roinel N, Elalouf JM & Stefano ADI (1991). Consequences of differential effects of ADH and other peptide hormones on thick ascending limb of mammalian kidney. *Am J Physiol - Regul Integr Comp Physiol* **260**, R1023–R1035.
- Rude RK, Adams JS, Ryzen E, Endres DB, Niimi H, Horst RL, Haddad JG & Singer FR (1985). Low serum concentrations of 1,25-dihydroxyvitamin D in human magnesium deficiency. *J Clin Endocrinol Metab* **61**, 933–940.
- Salyer SA, Parks J, Barati MT, Lederer ED, Clark BJ, Klein JD & Khundmiri SJ (2013). Aldosterone regulates Na(+), K(+) ATPase activity in human renal proximal tubule cells through mineralocorticoid receptor. *Biochim Biophys Acta* **1833**, 2143–2152.
- Simon DB, Lu Y, Choate K a, Velazquez H, Al-Sabban E, Praga M, Casari G, Bettinelli a, Colussi G, Rodriguez-Soriano J, McCredie D, Milford D, Sanjad S & Lifton RP (1999). Paracellin-1, a renal tight junction protein required for paracellular Mg²⁺ resorption. *Science* **285**, 103–106.
- Tsuruoka S, Muto S, Taniguchi J, Suzuki M & Imai M (1995). Effects of glucocorticoid and mineralocorticoid on potassium transport in the rat medullary thick ascending limb of Henle's loop. *Kidney Int* **47**, 802–810.
- Tyler Miller R (2013). Control of renal calcium, phosphate, electrolyte, and water excretion by the calcium-sensing receptor. *Best Pract Res Clin Endocrinol Metab* **27**, 345–358.
- Watts BA, George T & Good DW (2006). Aldosterone inhibits apical NHE3 and HCO₃⁻ absorption via a nongenomic ERK-dependent pathway in medullary thick ascending limb. *Am J Physiol Renal Physiol* **291**, F1005–F1013.
- Will C, Breiderhoff T, Thumfart J, Stuiver M, Kopplin K, Sommer K, Günzel D, Querfeld U, Meij IC, Shan Q, Bleich M, Willnow TE & Müller D (2010). Targeted deletion of murine Cldn16

identifies extra- and intrarenal compensatory mechanisms of Ca²⁺ and Mg²⁺ wasting. *Am J Physiol Renal Physiol*; DOI: 10.1152/ajprenal.00499.2009.

Work J & Jamison RL (1987). Effect of adrenalectomy on transport in the rat medullary thick ascending limb. *J Clin Invest* **80**, 1160–1164.

Yu ASL, Cheng MH, Angelow S, Günzel D, Kanzawa SA, Schneeberger EE, Fromm M & Coalson RD (2009). Molecular basis for cation selectivity in claudin-2-based paracellular pores: identification of an electrostatic interaction site. *J Gen Physiol* **133**, 111–127.

Zittermann A (2013). Magnesium deficit - overlooked cause of low vitamin D status? *BMC Med* **11**, 229.

Curriculum Vitae

Personal information

Name Allein
Surname Plain Reyes
Date of birth 09.10.1980
Place of birth La Habana, Cuba
Nationality Cuban
Address Wilhelmshavener Str. 20, 24105 Kiel, Germany

Education

2011- current PhD Student, and research assistant, Institute of Physiology, Christian-Albrechts-University of Kiel
Supervisor: Prof. Dr. Markus Bleich
2005-2008 M.Sc. Animal Physiology, Universidad de La Habana.
M.Sc. Thesis: "Aging and its complexity: Heart Rate Variability"
Supervisor: Prof. Dr. José M. Nieto Villar
1999-2004 B.Sc. Biochemistry, Universidad de La Habana.
BSc Thesis Title: "Study Methods of Heart Rate Variability in Humans"
Supervisor: Dr. Andrés Machado García

Professional experience

2008-2010 Instructor Lecturer, Informatics' Group, School of Biology, Universidad de La Habana.
2004-2008 Scientific Trainee, Informatics' Group, School of Biology, Universidad de La Habana.
2003-2004 Student Trainee, Group of Animal and Human Physiology, School of Biology, Universidad de La Habana.
2002-2003 Student Trainee, Department of Molecular Biology, Center of Molecular Immunology (CIM), Ciudad de la Habana.

Thesis supervision

- 2005-2006 B.Sc. Biochemistry. "Influence of age and gender over Heart Rate Variability in Spinocerebellar ataxia". C. M. Díaz García, Universidad de La Habana. (co-supervisor)

Publications

- 2015 Plain A, Wulfmeyer VC, Milatz S, Kliez A, Hou J, Bleich M & Himmerkus N (2015). Corticomedullary difference in the effects of dietary Ca(2+) on tight junction properties in thick ascending limbs of Henle's loop. *Pflugers Arch*; DOI: 10.1007/s00424-015-1748-7.
- 2015 Borschewski A, Himmerkus N, Boldt C, Blankenstein KI, McCormick JA, Lazelle R, Willnow TE, Jankowski V, Plain A, Bleich M, Ellison DH, Bachmann S & Mutig K (2015). Calcineurin and Sorting-Related Receptor with A-Type Repeats Interact to Regulate the Renal Na⁺-K⁺-2Cl⁻ Cotransporter. *J Am Soc Nephrol* 1–13.
- 2014 Gong Y, Himmerkus N, Plain A, Bleich M & Hou J (2014). Epigenetic Regulation of MicroRNAs Controlling CLDN14 Expression as a Mechanism for Renal Calcium Handling. *J Am Soc Nephrol* 26, 663–676.
- 2008 Días CM, Coro F, Plain A, Machado A, Rodríguez E (2008). Efecto de la edad sobre la Variabilidad de la Frecuencia Cardiaca en individuos sanos. *Revista Cubana de Investigaciones Biomédicas*; 27(8).
- 2007 Tejera E, Plain A, Portelinha A, Cáceres JLH, Rebelo I, Nieto-Villar JM (2007). Heart rate variability complexity in the aging process. *Computational and Mathematical Methods in Medicine*; 8(4): 287-296.

Presentations and Posters at Scientific Meetings

- 2015 Himmerkus N, Borschewski A, Plain A, Bachmann S, Mutig K, Bleich M. Modulation of NKCC2 function by phosphorylation. Annual Meeting of the German Physiological Society, Magdeburg, Germany.
- 2015 Plain A, Marques R.D, Himmerkus N, Leipziger J, Bleich M. Regulation by AVP of the paracellular permeability in the thick ascending limb. Annual Meeting of the German Physiological Society, Magdeburg, Germany. (poster)

- 2015 Plain A, Marques R.D, Himmerkus N, Leipziger J, Bleich M. AVP-mediated regulation of the paracellular permeability in the thick ascending limb (TAL). Experimental Biology 2015. Boston. USA. (poster)
- 2015 Plain A, Himmerkus N, Bleich M. Stimulation of the paracellular transport in the TAL in presence of AVP. Kiel-Aarhus Renal Epithelial Physiology Workshop, Aarhus, Denmark. (oral presentation)
- 2014 Plain A, Himmerkus N, Bleich M. The influence of stimulation of the cAMP pathway on paracellular permeability in the thick ascending limb (TAL). Annual Meeting of the German Physiological Society, Mainz, Germany. (poster)
- 2013 Plain A, Wulfmeyer V, Hou J, Himmerkus N, Bleich M. Influence of calcium intake on the paracellular permeability of the thick ascending limb. Ostseephysiologen, Greifswald, Germany. (oral presentation)
- 2013 Wulfmeyer V, Himmerkus N, Hou J, Plain A, Bleich M. Segment specific tight junction pattern along the nephron. Annual Meeting of the German Physiological Society, Heidelberg, Germany. (poster)
- 2013 Plain A, Wulfmeyer V, Hou J, Himmerkus N, Bleich M. The influence of calcium intake on paracellular permeability and claudin expression in the thick ascending limb. Annual Meeting of the German Physiological Society, Heidelberg, Germany. (oral presentation)
- 2012 Plain A, Himmerkus N, Wulfmeyer V, Bleich M. Effect of Ca²⁺ and phosphate intake on TAL tight junction permeability. Sandbjerg Membrane Transport Meeting, Sandbjerg, Denmark. (poster)
- 2012 Himmerkus N, Plain A, Steinmeyer K, Bleich M. Phenotype of KCNT2 knockout mice. Annual Meeting of the German Physiological Society, Dresden, Germany.
- 2005 Machado A, Coro F, Rodríguez E, Plain A. Heart Rate Variability in healthy young humans from 18 to 25 years old, Commission of Bioinformatics, II Taller Nacional de Informática, Universidad de Ciencias Informáticas, Havana, Cuba.
- 2005 Plain A, Machado A, Coro F, Nieto JM. Non-linear methods in the Heart Rate Variability analysis, Commission of Bioinformatics, II Taller Nacional de Informática, Universidad de Ciencias Informáticas, Havana, Cuba. (oral presentation)

Teaching experience

- 2011-current Betreuung Physiologiepraktikum, Institute of Physiology, Christian-Albrechts-University of Kiel

- 2008-2010 Introduction to Informatics, 1st year Biology, Microbiology and Biochemistry, School of Biology, Universidad de La Habana: Lectures and Laboratory Lessons.
- 2004-2008 Informatics I, 1st year Biology, Microbiology and Biochemistry, School of Biology, Universidad de La Habana: Lectures and Laboratory Lessons.
Informatics II, 2nd year Biology, Microbiology and Biochemistry, School of Biology, Universidad de La Habana: Practical Lessons.
- 2002-2004 Assistant Student in the signature "Biochemistry" for the 3th year Microbiology students: Seminars.
- 2001-2002 Human Biology, to high school students. Lectures.